1985

Analytical applications of ultrasensitive polarization measurements

Donald Robert Bobbitt
Iowa State University

Bobbitt, Donald Robert

ANALYTICAL APPLICATIONS OF ULTRASENSITIVE POLARIZATION MEASUREMENTS

Iowa State University PH.D. 1985

Analytical applications of ultrasensitive polarization measurements

by

Donald Robert Bobbitt

A Dissertation Submitted to the
Graduate Faculty in Partial Fulfillment of the
Requirements for the Degree of
DOCTOR OF PHILOSOPHY

Department: Chemistry
Major: Analytical Chemistry

Approved:

Signature was redacted for privacy.

In Charge of Major Work

Signature was redacted for privacy.

For the Major Department

Signature was redacted for privacy.

For the Graduate College

Iowa State University
Ames, Iowa

1985

TABLE OF CONTENTS

CHAPTER I. POLARIZED LIGHT AS AN EXPERIMENTAL PARAMETER

> And God said: "Let there be light". And there was light. Genesis 1.3

Historical Perspective

Since the earliest recordings of history, man has been concerned with the interaction of light and matter. Reflection was probably the first of these interactions to be exploited as evidenced by the discovery of polished copper mirrors in Egyptian ruins. The field of optics really began in the period from the thirteenth to the seventeenth century. This period saw the beginning of corrected vision (eyeglasses) and the development of both the refracting telescope and the compound microscope. Galileo's discovery of the moons of Jupiter in 1610 with his hand-built telescope forever changed the way man thought about the earth and the stars. Early in the seventeenth century (1611) Willebrord Snell discovered and formulated the law of refraction. This work served as the beginning for the rapid optical developments of the eighteenth and nineteenth centuries, and this discovery is considered to be the beginning of modern applied optics (1).

Spectroscopy, that is, the study of the interactions of matter and light which involve the measurement of both the intensity and frequency of radiative energy had its conception in the late seventeenth century. It was during this period that Sir Isaac Newton first characterized dispersion, the separation of white light into a range of independent colors using a triangular glass prism. William Wollaston, and later Joseph Fraunhofer (1800s), discovered that the solar spectrum was com-

posed of narrow colored bands of light (spectral lines). Fraunhofer also was the first to use a grating for wavelength determinations.

Gustav Kirchhoff and Robert Bunsen in the mid nineteenth century were able to attribute characteristic spectral lines to individual atomic species. This was a landmark discovery and it served as the beginning of analytical atomic spectroscopy. Today, atomic spectroscopy is one of the most used methods for both qualitative and quantitative analysis of atomic species.

The understanding of the processes involved in the absorption and emission of radiation by atoms and molecules was greatly aided by the introduction and development of quantum mechanics in the early 1900s. The culmination of this theory was the work of Niels David Bohr in 1913. Bohr, using the hydrogen atom as an example, was able to predict the wavelengths of its emission spectrum. For the first time, a solid theoretical basis existed for the experimental observations of Wollaston and others over a century before.

Statement of the Problem

Over the past one-hundred years, much work has been directed toward the determination, in both a qualitative and quantitative sense, of molecular species in the condensed phase at room temperature (usual conditions for routine analysis). However, this determination is complicated by the fact that room temperature absorption spectra for condensed phase molecular species are broad and rather featureless. Usually in spectroscopic experiments, the wavelength and intensity of light

are varied, or recorded as the light interacts with matter. However, the broad nature of room temperature absorption profiles has necessitated that a separation step be included in the analysis. By isolating the species of interest, one can eliminate spectral overlap for similar molecules.

Since it usually is difficult to separate chemically similar molecules, several methods have been devised to permit analysis of similar molecular species in the presence of one another. These methods usually require the use of low temperatures (2), or special sample matrices (3,4). It would be preferable if, instead of altering the properties of the molecule of interest, one could exploit a property of light to impart selectivity to the spectroscopic analysis. One experimental parameter often overlooked is the extent, or change in polarization of light as it interacts with matter. Therefore, this thesis will describe experimental techniques which exploit the polarization properties of light to solve detection problems in chemical analysis.

First, the remainder of Chapter I will present a brief description of both the nature and preparation of polarized light, followed by a survey of several techniques which advantageously utilize polarized light as an experimental parameter. Chapters II through V will then describe several novel experiments which use polarized light to impart both selectivity and sensitivity to problems in spectroscopic analysis. Of particular concern will be the application of these methods to the detection problem in liquid chromatography where, for complicated samples, resolution of all of the components is rare or impossible.

Polarized Light

Light can be considered to be a supposition of time-varying electric and magnetic fields which propagate together while maintaining a constant 90° phase difference with one another. These fields are vectors (i.e., they have a direction associated with them) and their directions are usually perpendicular to each other and their direction of propagation (5). Because these two fields have a constant phase relationship, it is usually sufficient to describe the light wave using only one field. Most often the electric field is used because it interacts more strongly with matter than the magnetic field. Equation (1) describes the electric field strength, $E(z,t)$ of a time varying electric field with amplitude, E_0, at some position, z, and time, t.

$$E(z,t) = E_0 \cos(kz - \omega t + \phi) \qquad (1)$$

Here, k is known as the wavevector, ω is the angular frequency and ϕ is the relative phase of the disturbance. To describe the polarization properties of a light wave, therefore, one must consider how the electric field behaves as the wave propagates in space.

When the electric field vibrates in one plane in space (even though its magnitude and sign vary with time), the wave is said to be plane or linearly polarized. We can represent two harmonic light waves of the same frequency traveling through the same region of space by their orthogonal electric fields (6), that is

$$E_x(z,t) = \hat{i}\, E_{o,x} \cos(kz - \omega t) \qquad (2)$$

and

$$E_y(z,t) = \hat{j}\, E_{o,y} \cos(kz - \omega t + \phi) \quad . \qquad (3)$$

Here, ϕ as before, represents the relative phase difference between the two waves which are traveling in the z direction. The resultant for these two waves is, therefore,

$$E = (\hat{i}E_{o,x} \pm \hat{j}E_{o,y})\cos(kz - \omega t) \qquad (4)$$

where the sum represents the case when ϕ is an integral multiple of $\pm 2\pi$, and the difference occurs for odd integer multiples of $\pm\pi$.

Equation (4) represents a plane polarized wave with a fixed maximum amplitude ($iE_{o,x} \pm jE_{o,y}$). It also should be noted that the reverse of this process is also possible. That is, any plane polarized light wave can be resolved into two orthogonal components (Eqs. (2) and (3)). This point will be necessary for the understanding of the operation of calcite polarizing prisms, vida infra.

If the two orthogonal waves represented by Eqs. (2) and (3) have equal amplitudes, E_o, and if the relative phase difference between the two can be represented by $\phi = -\pi/2 + 2m\pi$ where $m = 0,\pm1,\pm2$, etc. Then, the two waves can be described by

$$E_x(z,t) = \hat{i}E_o \cos(kz - \omega t) \tag{5}$$

and

$$E_y(z,t) = \hat{j}E_o \sin(kz - \omega t) \quad . \tag{6}$$

The resultant wave is, therefore,

$$E = E_o[\hat{i} \cos(kz - \omega t) + \hat{j} \sin(kz - \omega t)] \quad . \tag{7}$$

Equation (7) represents a circularly polarized wave possessing a constant scalar amplitude (E_o) with an electric field whose orientation varies with time. As one observes the wave coming toward the observation point of reference, the electric field would appear to rotate in a clockwise manner with a frequency ω. Equation (7), therefore, is said to describe right circularly polarized light. For the case when $\phi = \pi/2 + 2m\pi$ ($m = 0,\pm1,\pm2$, etc.), Eq. (8) results giving

$$E = E_o[\hat{i} \cos(kz - \omega t) - \hat{j} \sin(kz - \omega t)] \tag{8}$$

which represents left circularly polarized light.

Just as a plane polarized light wave can be resolved into two orthogonal components, a plane polarized wave can also be thought of as being composed of equal amounts of left and right circularly polarized

light of equal amplitude. Specifically, if Eqs. (7) and (8) are algebraically combined, then one obtains

$$E = 2E_0\hat{i}\cos(kz - \omega t) \tag{9}$$

which is the equation for a plane polarized light wave with a maximum amplitude vector of $2E_0\hat{i}$ (7).

Actually, linearly and circularly polarized light are both specialized cases of elliptical polarization (7). For elliptically polarized light, the electric field vector will both rotate and change its magnitude as the wave propagates. The above statement is best illustrated by consideration of Eq. (10).

$$E = E_{0,x}[\hat{i}\cos(kz - \omega t)] + E_{0,y}[\hat{j}\cos(kz - \omega t + \phi)] \tag{10}$$

For the case when the phase difference, ϕ, is an integral multiple of π, Eq. (10) reduces to a form representing a plane polarized wave with a fixed maximum amplitude, but the amplitude's sign and magnitude change with time. For the situation where $E_{0,x} = E_{0,y}$, that is, when the amplitude is invariant with time and when the phase difference is a integral multiple of $\pi/2$, Eq. (10) will be reduced to a form which describes a circularly polarized wave. Finally, for those cases where the phase is an integral multiple of $\pi/2$ and the amplitude varies with time, Eq. (10) represents a state of elliptical polarization. That is, the elec-

tric field vector will both rotate and change in magnitude as the wave propagates. Figure 1 summarizes these various polarization states.

Production of Polarized Light

This section will briefly review three optical elements useful for the production of polarized light, that is, the Brewsters angle pile-of-plates polarizer, the Glan-Foucault polarizing prism and the Fresnel rhomb. Many other methods have been developed for the purpose of polarizing, or changing the state of polarization of light, and these methods have been discussed in great detail (8,9). However, only the above three are of consequence to the experiments to be described, vida infra.

When light is incident upon a plane boundary separating two different optical media, a portion of the light is reflected, and part is transmitted through the interface. Snell was the first to state the relationship between the incident and refracted waves.

$$\frac{\sin \theta}{\sin \phi} = n \tag{11}$$

Here, θ is the angle the incident wave makes with a plane normal to the boundary, ϕ is the angle of refraction and n is the ratio of the indices of refraction for the two media.

For the special case when the angle of reflection and refraction are orthogonal, Eq. (11) reduces to

$$\theta = \tan^{-1} n \tag{12}$$

Figure 1. Various polarization configurations corresponding to specific values of ϕ. Here E_x leads E_y by ϕ. The light would be circularly polarized when $\phi = \pi/2$ or $3\pi/2$ if $E_{o,x} = E_{o,y}$. Reprinted from reference 1

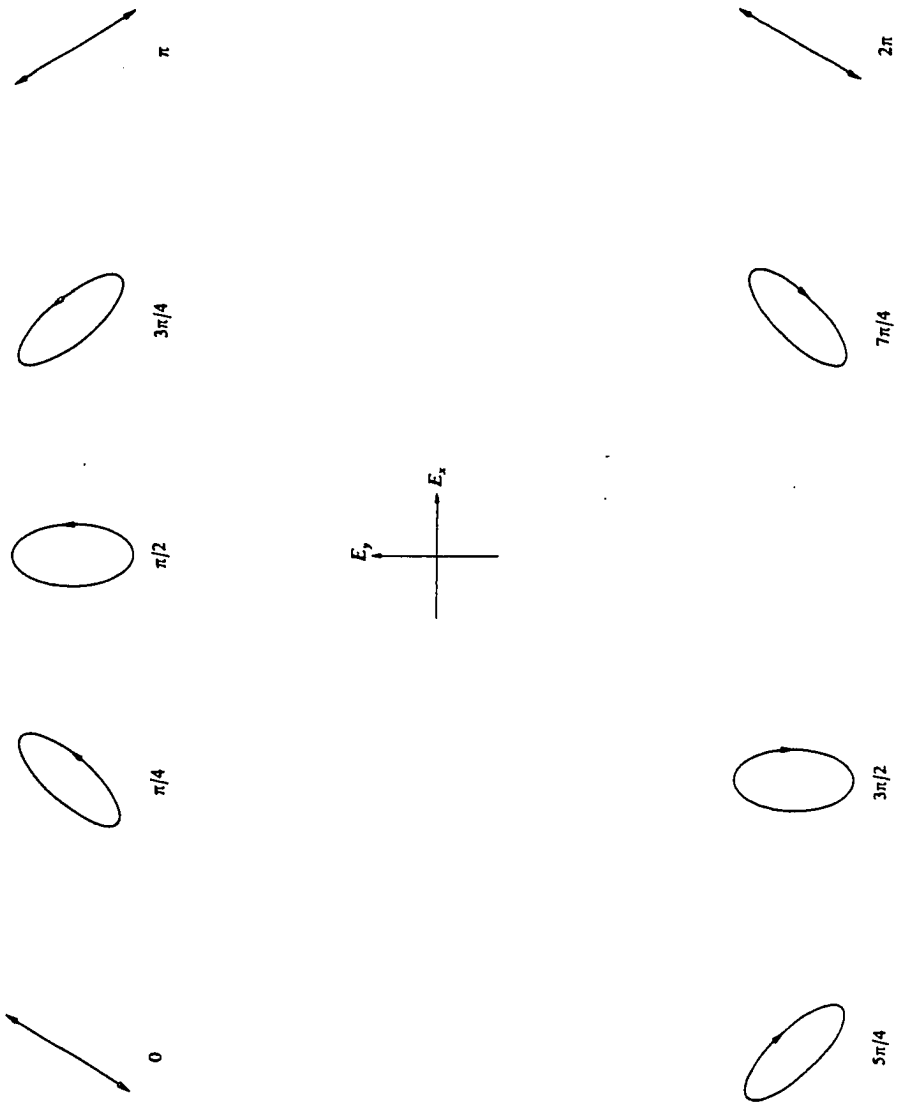
π
3π/4
π/2
π/4
0
E_y
E_x
2π
7π/4
3π/2
5π/4

This angle is known as the Brewster or polarizing angle. Using Eq. (12) and a value for n of 1.57 (common glass-air interface), one can calculate that the Brewster's angle is 57 degrees. If unpolarized light (which can be resolved into two orthogonal components of equal amplitude) is incident on a boundary at the Brewster angle, the reflected wave will be linearly polarized with the electric vector transverse to the plane of incidence. Since a portion of one polarization component has been removed by reflection, the transmitted wave will be partially polarized. However, because only about 15 percent of the one component is reflected, the process is not very efficient. If, instead of one interface, one has a series of interfaces at Brewster's angle, the degree of polarization of the transmitted beam can be made to approach 100%. This then is the basis for the pile-of-plates polarizer.

A pile-of-plates polarizer is useful for polarizing the output of high power lasers which might damage other optical elements. For example, a copper vapor laser produces 10 watts of unpolarized light in a beam of approximately one inch diameter. An economical polarizer capable of polarizing this large beam was constructed from a triangle of aluminum designed such that two sides were cut at Brewster's angle to a normal to the third side. A one inch aperture through the piece allowed the beam to pass unobstructed, while six glass slides (with two air-glass interfaces per slide) attached to each of the two Brewster's angle sides produced a beam which was approximately 95 percent plane polarized.

A more efficient way to plane polarize light is to use a uniaxial-birefringent crystal such as calcite ($CaCO_3$). Crystals of this type have their atoms arranged so that light propagating in one particular direction will encounter an asymmetric structure. The optic or transmission axis is, therefore, the only direction for which the atoms are arranged symmetrically.

Uniaxial crystals, because of their unusual structure, possess two principal indices of refraction for the ordinary (parallel to the optic axis) and extraordinary (perpendicular to the optic axis) rays, respectively. This property can be exploited to separate light into two plane polarized orthogonal components.

The Glan-Foucault polarizer is constructed of two 90° triangular pieces of calcite which are in optical contact at their respective hypotenuses. An incident light ray will encounter the first calcite surface normally and its electric field can be resolved into two orthogonal components, one of which is parallel to the optic axis while the other perpendicular. Since calcite possesses different refractive indices for the two orthogonal components, by judicious choice of the angle of the hypotenuse, one component will be totally internally reflected while the other component will pass into the second calcite piece undeviated. The difference in refractive indices for the two components is

$$\Delta n = (n_e - n_o) \tag{13}$$

which is a measure of the birefringence. For calcite, Δn is -0.172 which is a very large difference (compare to quartz where Δn = 0.009). The net result of this is that Glan-Foucault polarizers can be constructed which can plane polarize light to a very high degree (1 part in 10^{10}). This high degree of polarization, that is, the ability to reject light of the improper polarization relative to the desired plane is the basis for the polarimetric experiments to be described in the following chapters.

Both of the previous two methods dealt with ways to prepare plane polarized light. In some experiments, it is useful to convert plane polarized light into its circularly polarized analog. One way to accomplish this is to use a quarter wave plate specially constructed for this purpose (10). However, wave plates are designed such that they have their maximum efficiency at one particular wavelength. This can be a problem for experiments which involve scanning the light source over the spectral region of interest.

During the process of internal reflection, the components parallel and perpendicular to the plane of incidence are shifted in phase relative to each other. To impart a phase shift of 45° in glass (n = 1.57), the light must strike the glass-air interface at 54.6°. It is easy to see that two such reflections will cause a total phase shift of 90° to occur. Referring to the previous section (Eq. (10)), a phase shift of $\pi/2$ corresponds to elliptical polarization. If the electric field vectors are equal for the two orthogonal components, the requirements for circular polarization will exist.

The optical element which accomplishes the conversion of linear to circularly polarized light by the process of internal reflection is known as the Fresnel rhomb. Light enters normal to the face with the electric field vector linearly polarized 45° to the plane of incidence. This assures that $E_{\parallel}$ and $E_{\perp}$ will initially be equal. Therefore, after two reflections in the rhomb, the two components will have undergone a 90° phase retardation relative to each other, and since $E_{\parallel}$ is equal to $E_{\perp}$ for the resultant wave, the conditions for circular polarization exist. The advantage to the Fresnel rhomb is that since the retardance is almost independent of wavelength over a large spectral range, the Fresnel rhomb can, therefore, function as an achromatic 90° retarder.

Experimental Applications of Polarized Light

The most obvious use for polarized light involves the investigation of optically active systems via their birefringence. The fact that optically active molecules rotate the plane of polarization of plane polarized light has been known for over 170 years. This important topic will be discussed in detail in a following section. However, what is not as obvious is the fact that optically active molecules also possess different absorption coefficients for left and right circularly polarized light (11). Circular dichroism (CD) is the term used to describe the measurement of this differential absorption of incident left and right circularly polarized light. The theory and necessary instrumentation have been extensively reviewed (11,12).

From an analytical perspective, most applications of CD involve the qualitative aspects of this technique. This is because circular dichroism is a spectroscopic technique that is very sensitive to the primary, secondary and tertiary structures of biological systems (13). For this reason, CD has been used for the determination of the conformation of polypeptides (14-16) and A- and B-type DNA (17). Additionally, CD has been applied to the identification and quantitation of alkaloids in a variety of complex matrices, including nicotine in tobacco leaves (18), cocaine (19), heroin (20) and others (21-23). The advantage inherent to circular dichroism over simple absorption measurements lies in the selectivity particular to the CD technique.

This property was exploited in the application of CD detection to the effluent from a liquid chromatograph (24,25). The selectivity of CD minimizes the requirements of the liquid chromatograph to separate all of the many components present in a complicated sample matrix such as encountered in natural-product extracts or biological fluids (25). Further extension of this concept has resulted in the development of a functioning CD detector for gas chromatography (26).

In two photon fluorescence, two photons with a combined energy equal to an excited atomic or molecular state are absorbed enabling the species to reach an excited fluorescing state. This process is already quite selective. However, different transition probabilities govern the process when the exciting and fluorescence photons have various combinations of polarization (27,28). Thus, proper choice of polarization conditions will increase the selectivity of this technique further.

A different two-photon technique has been used to investigate sodium transitions in the vapor phase (29). When the 3s-5s two photon transition of sodium is probed with two circularly polarized photons, selection rules are such that the two absorbed photons must have opposite senses of circular polarization. Therefore, if one of these two fields is plane polarized while the other is circularly polarized, the circularly polarized field will only affect one of the two circularly polarized components of the plane polarized field. The result is a simple rotation of the direction of polarization of the plane polarized field.

Similar techniques have been developed to obtain high resolution spectra of atomic systems. In Doppler-free laser polarization spectroscopy (30), a circularly polarized field resonant with a particular absorption induces changes in the absorption coefficients and refractive indices of the atoms it interacts with. A second counter-propagating plane polarized field probes these induced changes which results in the rotation of the probe beams direction of polarization. Since the two fields are counter-propagating, they interact with atoms that have essentially zero axial velocity. This decreases the Doppler contribution to the line width. Recently, this technique has been applied to the determination of sodium and barium at trace level concentrations (31). This technique was able to suppress background contributions from flame luminescence and particle scattering.

A technique similar to the above is polarization labeling spectroscopy (32). Here, a light-induced anisotropy is used to label a molecu-

lar ground-state level with the result that only those optical transitions which share this common level are detected. This labeling technique can result in substantial simplification of molecular spectra.

Other work in polarization spectroscopy has developed the theoretical groundwork for the investigation of relaxation processes (33). Experimental utilization of polarization spectroscopy for this purpose was performed on the picosecond time scale in the condensed phase (34). Additional work has centered on the improvement of the sensitivity of this technique using optical heterodyne detection (35), and in the application of polarization spectroscopy as a probe of Raman optical activity (36). Clearly, the sensitivity and selectivity of this technique has contributed to its many applications.

Another technique which has benefited from the judicious choice of polarization conditions is light scattering. In light scattering, the depolarization ratio is dependent on the scattering particles' size and shape (37). This can add to the information available when applied as a detector for LC (38). Further, by proper choice of experimental conditions, one cannot only obtain particle size information, but one can also derive information concerning the molecular conformation, weight and rotations of eluting molecules or distributions (39).

Finally, there are several advantages to the use of polarized light in Raman measurements. It is known that Raman cross sections are usually different for same-sense versus opposite-sense circularly polarized light. This is the basis for the nonlinear Raman technique known as the Raman induced Kerr effect (RIKE), which will be discussed in Chapter V.

However, conventional Raman spectroscopy can also utilize polarized light to provide additional information, particularly with respect to the conformation of polymers (40). For example, Raman polarization measurements have been used to determine the degree of order of polymer systems (41), the effect of aqueous solutions on the polymer conformation (42), and to follow the effects of mechanical stress induced by drawing (43,44).

In summary, the work surveyed here demonstrates the breadth of different experiments which benefit from polarized light. It is evident that the property of polarization can be an important experimental parameter in many spectroscopic techniques resulting in both improved selectivity and sensitivity. This point will be developed further in the next section where a discussion of polarimetric methods of analysis will be presented.

The Nature and Detection of Optical Activity

From a historical perspective, the first recognition of optical activity as a unique phenomenon was made by Dominique F. J. Arogo in 1811. He discovered that the plane of vibration of a beam of plane polarized light underwent a rotation as it propagated along the optic axis of a piece of quartz (6). Jean Baptiste Biot made similar observations seven years later for both condensed and gaseous phase molecules such as turpentine and other natural substances (45). Biot also was the first to differentiate between right- and left-handed rotation. The

common designation now is to describe clockwise rotation as dextrarotatory (d), and counter-clockwise rotation as levorotatory (ℓ).

In 1822, Sir John F. W. Herschel recognized that the ℓ and d rotations caused by different pieces of quartz corresponded to two different crystalline structures. Louis Pasteur, in 1848, continued the understanding of the structural requirements necessary for optical activity when he was able to physically separate tartaric acid crystals into their ℓ and d forms (46). Even with this discovery, almost thirty years passed before Jacobus van't Hoff and Joseph Le Bel, working independently, established that every organic compound known at that time possessing optical activity contained at least one asymmetric carbon atom (i.e., a carbon atom bonded to four different univalent groups) (47). Presently, this concept has been modified only slightly, and the necessary condition for expressing optical activity is now known to be the nonsuperimpossibility of a species and its mirror image.

Much work has involved a theoretical understanding of the nature of optical activity (48-53). Although many elegant theoretical explanations have evolved from these studies, a more practical explanation was advanced by Fresnel in 1825. Fresnel stated, quite simply, that optically active materials possess different refractive indices for left and right circularly polarized light. As demonstrated earlier, plane polarized light can be considered to be composed of equal amounts of opposite sense circularly polarized light. Upon passage through an optically active material, one circular component will be retarded in phase relative to the other. The result of this is that the emerging plane polar-

ized wave will have had its electric field vector rotated. The term used to describe such materials which possess two indices of refraction is known as circular birefringence (54). Equation (14) presents the relationship between the amount of rotation (α) experienced by a plane polarized light wave upon passage through an optically active medium, and the difference in the two indices of refraction ($\Delta n = n_L - n_R$)

$$\alpha = \frac{\pi d}{\lambda_o} (n_L - n_R) \tag{14}$$

where d is the thickness of the medium, λ_o is the vacuum wavelength of light probing the medium, and n_L and n_R are the indices of refraction for left and right circularly polarized light, respectively. By convention, if $n_L > n_R$, the rotation is described as d-rotatory and, if $n_R > n_L$, ℓ-rotatory.

Because optical activity is sensitive to the arrangement of atoms at and near the optically active center, much qualitative structural information can be elucidated from a determination of a molecule's rotational properties. In addition, it is possible to use optical activity to obtain quantitative information using the relationship between the specific rotation of a substance, $[\alpha]$, and various experimental parameters

$$[\alpha]_\lambda^t = \frac{\alpha}{C \cdot \ell} \tag{15}$$

Here, α is the observed rotation in degrees, C is the concentration of rotating substance in grams per milliliter and ℓ is the length of material traversed by the probe beam (conventionally designated in decimeters). The quantitative aspects of polarimetry will be addressed more fully in Chapter III. However, it should be pointed out that the specific rotation of a substance is a unique physical constant, as are a molecule's boiling point, refractive index, molecular weight, etc. As such, the specific rotation provides information useful not only for identification, but it also can be used to determine the enantiomeric purity of a substance.

The instrumentation necessary to measure the amount of rotation induced by an optically active substance is schematically represented in Fig. 2. Since the amount of rotation, like refractive index, is dependent upon wavelength, a source of plane polarized monochromatic light is needed. This can either be supplied by a metal vapor lamp and filter (for example, the sodium D line) typical of nonscanning instruments, or a monochromator can be used to select a wavelength of interest from a polychromatic lamp. The monochromatic light source is then rendered plane polarized by a polarizer before interacting with the sample. To determine the extent of rotation, another polarizer is placed after the sample with its transmission axis oriented so that the minimum amount of light reaches the photodetector in the absence of any rotation. When the plane of polarization is rotated, the electric field vector is no longer parallel to the point of minimum transmission defined by the second polarizer and some light will pass through it to the detector.

An excellent review of the experimental techniques and physical optics inherent to polarimetric measurements is available (55). Commercially, several manufacturers offer polarimetric equipment including O. C. Rudolph and Sons, Bendix, Carl Zeiss, The Perkin-Elmer Corp., Japan Spectroscopic Co. (JASCO), and the Cary Instrument Co. However, even the best instruments available do not have the requisite sensitivity to detect, or measure optical rotations for substances present at trace-level concentrations. For example, a Bendix-NPL automatic polarimeter equipped with a 110 μℓ flow cell produced a full scale deflection corresponding to 0.01° at a signal to noise ratio of four (56). This shows that the detectability, in terms of degrees of rotation, is in the range of 5×10^{-3}. This is insufficient for trace applications. Many attempts to adapt commercial instrumentation to uses such as detectors for liquid chromatographic effluents have resulted in poor detection limits. This restricts the usefulness of polarimetric detectors (24,25,57-60). Clearly, a new design will be necessary to extend the scope of polarimetric measurements.

Relevant Laser Properties

Since the first demonstration by T. H. Maiman in 1960 (61), the laser has revolutionized the field of optical spectroscopy. The laser possesses several unique characteristics which have made possible many elaborate analytical experiments including the development of liquid chromatographic detectors based on new detection principles. These properties have been discussed in detail for both conventional (62) and

microbore (63) chromatography. This section will review those properties of the laser which make it an ideal source for polarimetric measurements.

Monochromaticity/power

One of the unique characteristics of the laser is its ability to deliver a large photon flux in a narrow spectral region. For discrete line lasers, as in for example an argon ion laser, the output can be extremely monochromatic. Tunable dye lasers lase over a relatively large spectral region (~80 nm), however, dye laser cavities have such high gain that various optical elements can be introduced into the laser cavity to produce single frequency operation while still maintaining relatively large output powers.

Since optical activity is dependent on the wavelength of light used to probe it, the monochromatic nature of the laser is a direct benefit for polarimetric experiments. In addition, it has recently been reported (64) that monochromatic light improves the accuracy of polarimetric measurements because of the wavelength dependence of the specific rotation.

Tunability

The recording of optical activity versus wavelength generates optical rotatory dispersion (ORD) curves. These spectra are characteristic for different optically active materials. Since the curves are broad and rather featureless, the high monochromaticity possible with single-frequency dye lasers is not useful. However, the tunability of the dye

laser adds another dimension to the analysis permitting ORD spectral analysis if desired. This is not possible with either discrete line lasers or atomic vapor lamps as sources.

Spatial coherence

The highly collimated nature of the laser beam is the most important property contributing to the success of the experiments to be described in the next section. It is the unique characteristic of the laser cavity that contributes to the well-defined cross-sectional intensity distribution of most lasers. A laser cavity possesses standing waves which can be thought of as a series of transverse electric and magnetic (TEM) modes. The lowest order of these modes is known as TEM_{00}, and it is the most efficient for focusing to a small area. In comparison, conventional spatially-incoherent light possessing many TEM modes cannot be focused without sacrificing power.

If one looks at a cross-sectional slice of a TEM_{00} laser beam, the intensity distribution across the slice is Gaussian in appearance. That is, the most intense portion occurs at the center of the beam and the intensity distribution decreases from the center with a Gaussian dependence (65). At the focal point, the beam cross section would still be Gaussian, but the width of the Gaussian curve would be much narrower.

As a consequence of the inherent low divergence of the laser, laser beams can be propagated over relatively large distances while still maintaining the spatially coherent nature of the beam. This has direct benefit to polarimetry where it is necessary to locate favorable regions

on the polarizer and analyzer even though they may be spaced more than one meter apart. Since these favorable regions are spatially small, the focusing properties of the laser beam are advantageous (66). In addition, highly focused laser beams permit the construction of micro-volume detection cells for liquid chromatographic applications. Finally, the highly collimated laser beam permits extensive spatial filtering resulting in substantial discrimination against stray or scattered light.

Polarization

Most lasers are either plane polarized by virtue of the stimulated process, or are made to be polarized by virtue of the optical components inside the laser cavity. Whereas a conventional light source will only have half of its available power in one polarization plane, a laser polarized to 1 part in 1000 (typical for an argon ion laser) will have 99.9% of its power in the desired plane. This will have direct benefit to detection schemes based on the polarization of light.

Since extinction ratios of 1 part in 10^{10} are possible with selected polarizer/analyzer pairs, it is not immediately obvious as to the advantage of a laser beam polarized to the extent of only 1 part in 10^3. However, the standard mount for the calcite polarizing prisms used for these experiments eliminates the rejected beam (incorrect polarization) by a black coating surrounding the prism. Naturally, the more light which is rejected (i.e., of the incorrect polarization), the more light will be incident on and absorbed by this black coating. The result of this is that large amounts of rejected light can cause heating of the

prism, which may result in a degradation in the extinction ratio. Therefore, the more polarized the probe beam is to begin with, the better the chance of maintaining the extinction ratio for a polarizer/analyzer pair.

Laser-Based Polarimeter

In 1980, Yeung and co-workers demonstrated a novel laser-based polarimeter (67). This polarimeter was able to achieve a rotational detectability at least two orders of magnitude better than previous designs. This detectability is necessary to properly apply polarimetric detection to liquid chromatography. The laser-based polarimeter, with a 200 μℓ flow cell was used to detect carbohydrates in urine (68), free and esterfied cholesterol in blood (69) and optically active components in shale oil extracts (70).

At a signal to noise ratio of three, Yeung and co-workers could detect rotations as small as 5×10^{-5} degrees with a flow system. For a compound such as raffinose ($[\alpha] \cong 100°$), this translates into a mass detectability of 250 ng, assuming a peak volume of 500 μℓ. The instrumental and experimental parameters upon which these results are based have been extensively reviewed (67,71). This section will summarize those factors which are common to the experiments described in Chapters II-V.

The success of polarimetric experiments is usually dependent on the quality of the polarizers used to plane polarize light and determine its plane of orientation. To differentiate these functions, the polarizer

is considered to plane polarize the light source, while the analyzer serves to define the point of minimum transmission from which changes in the plane of polarization will be measured. The critical parameter for a given polarizer/analyzer pair is known as the extinction ratio, and it is defined as the amount of light transmitted of the incorrect polarization (along the extinction axis) versus the amount of light of the proper polarization incident on the analyzer.

The highest quality polarizers available are of the Glan-Thompson design. These prisms are constructed of calcite and fastened together with a cement such as Canada balsam possessing a refractive index in between n_e and n_o. These high quality prisms (Karl Lambrect Corp., Chicago, IL #MGT-25E8-45) are guaranteed to have an extinction ratio of at least 10^{-6}. However, the limitation to better extinction was found to be due to crystalline defects in the calcite itself (66,72). Therefore, localized regions can be found that have much better polarizing properties. By proper selection of the polarizer/analyzer pair, extinction ratios of approximately 10^{-10} can routinely be found.

The laser provides several key advantages which make this experiment possible. First, the collimated nature of a laser beam means it can be tightly focused without sacrificing power. This simplifies the process of locating favorable regions even though the polarizer and analyzer may be some distance apart. Second, because the polarizer and analyzer can be separated without deterioration of the extinction ratio, stray light can be spatially filtered much more effectively. Third, the laser has high pointing stability. Therefore, once a favorable subre-

gion is found, the beam will not wander from that location. Any change in position of the beam would most likely mean a change in the extinction properties at that new location. This would result in increased background light to the detector.

Once an extinction ratio of 10^{-10} has been obtained, it is important to minimize mechanical vibrations which can alter the alignment of the analyzer with respect to the polarizer. This is accomplished by mounting each prism in a rigid translational stage (Aerotech Inc., Pittsburgh, PA, model #STS-30/R). Another cause of extinction degradation is birefringence introduced into the system. One source of birefringence is the windows used on the detection cell which must be placed within the polarizer/analyzer cavity. Window birefringence is minimized by using very thin #1 glass coverslips as window material. By careful selection, windows can be found that maintain the extinction ratio.

In any detection scheme, it is always preferable to make the measurement in an AC versus DC mode (73). In order to use phase sensitive detection, the signal must be modulated in some manner. For polarimetric experiments, one efficient way to accomplish this is to modulate the plane of polarization of the light in the polarizer/analyzer cavity. That is, the plane of polarization is periodically rotated away from the point of maximum extinction, and the analyzer converts this polarization modulation into intensity modulation. This periodically varying light intensity is then detected by a photodetector and demodulated by a lock-in amplifier to give the resulting DC signal.

When plane polarized light passes through a light transmitting medium in a direction parallel to the lines of force of an applied magnetic field, the polarization plane of the light is rotated. This is known as the Faraday effect, which is named after its discoverer, Michael Faraday. The angle (in minutes of arc) through which the plane of polarization is rotated is given by (44)

$$\alpha = V \cdot B \cdot L \tag{16}$$

where V, the Verdet constant, is in units of minutes of arc gauss^{-1} cm^{-1}, B is the magnetic field strength (in gauss) and L is the length of the medium (in cm). V is dependent on the nature of the medium, the temperature and the wavelength of light. For a fixed length, the amount of rotation is determined strictly by the medium and the applied magnetic field. The field strength, in turn, is controlled by the current passing through the magnetic coil.

Since extraneous birefringence must be kept to a minimum, the first Faraday rotators were based on air as the active medium. However, since the Verdet constant of air is small, relatively large currents were needed to effect a reasonable modulation (i.e., $\sim 10^{-3}$ degree). A better design using a liquid-based Faraday cell followed which greatly reduced the constraints on the switching electronics. The key point is that the modulation must be stable to the same extent as the rotations one is measuring. This is not a problem with modern transistor technology.

For rotation away from minimum of an amount α, the Law of Malus states that

$$I_{trans} = I_o \sin^2\alpha \tag{17}$$

where I_{trans} is the light passing through the analyzer and I_o is the maximum intensity transmitted when $\alpha = 90°$. Since the light beam is modulated from an angle α to $-\alpha$, if an optically active component is present which causes a rotation of δ, the lock-in signal will be proportional to

$$I = I_o[\sin^2(\alpha + \delta) - \sin^2(\alpha - \delta)] \quad . \tag{18}$$

For $\delta = 0$, the lock-in signal will be zero. For small α and δ, Eq. (18) can be reduced to (71)

$$I = 4 I_o\alpha\delta \tag{19}$$

which shows the value of using as large a modulation as possible.

Figure 2 schematically summarizes the different components of the polarimeter. The coil attached to the DC power supply serves as an internal standard. By knowing the current passing through the coil and the Verdet constant of the medium, one can calculate the amount of rota-

Figure 2. Simple polarimeter schematic

SR	Light source
P	Polarizer
A	Analyzer
M	Modulation solenoid
C	Cell
DC	DC solenoid and power supply
REF	Reference waveform
PMT	Photomultiplier tube
LI	Lock-in amplifier
DISP	Display

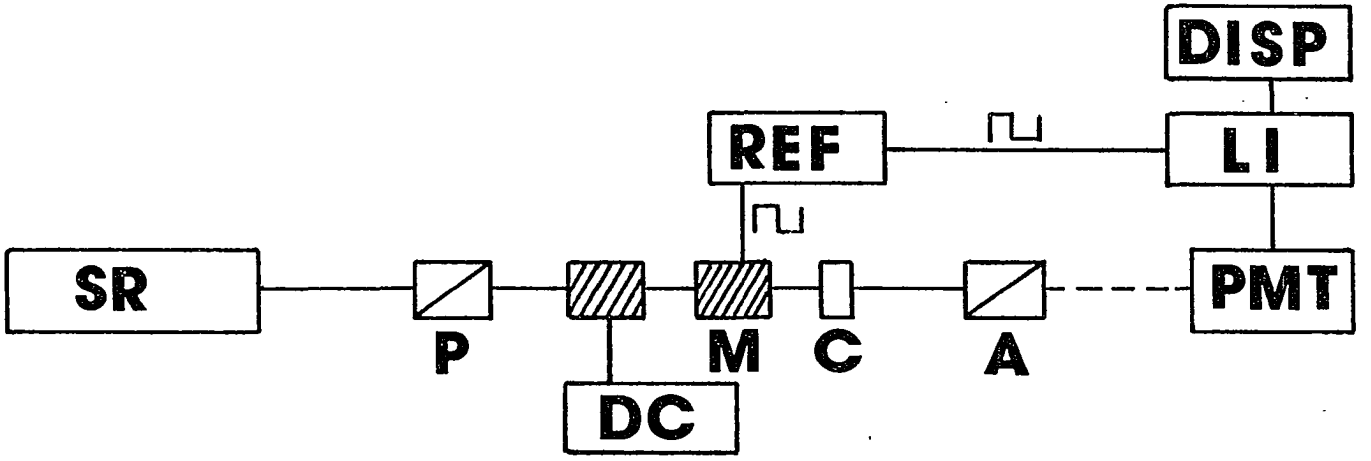
DISP
REF
LI
SR
P
M
C
A
PMT
DC

tion induced by this coil. By applying a field to this DC coil, the system can periodically be calibrated against a known rotation.

In summary, a functioning state-of-the-art polarimeter based on an argon ion laser has been described. It is also possible to obtain similar detectabilities using a less expensive helium-neon laser (74). Clearly, the system is not dependent on any laser for its success.

Before the system could be improved further, it was necessary to model the polarimeter to determine which were the critical parameters contributing to the success of this instrument. A computer was used to calculate the signal to noise ratio of the system while such factors as extinction ratio, source flicker noise, source power, electrical noise, stability of modulation, depth of modulation and amount of stray light reaching the detector were varied (75). This modeling showed that the flicker noise of the laser was the dominant source of noise in the system, and this was substantially minimized by the 10^{-10} extinction ratio. Therefore, unless the laser can be stabilized further (76), the favorable extinction ratio must be maintained in order to achieve 10^{-6} degree detectability.

The results of the computer study also helped in designing modifications which resulted in a functioning micropolarimeter with a 1 $\mu\ell$ flow cell (Chapters III and IV). For example, the modeling showed the importance of stray light on the S/N as the polarizer/analyzer cavity was shortened. Therefore, spatial filtering became very important to the success of these experiments. Further, the 10^{-10} extinction ratio

will be shown to be of advantage in a polarization sensitive Raman technique, the Raman induced Kerr effect presented in Chapter V.

CHAPTER II. ANALYSIS OF EXTRACTS OF COALS AND COAL-DERIVED PRODUCTS BY LIQUID CHROMATOGRAPHY WITH OPTICAL ROTATION DETECTION

Introduction

The characterization of coal and coal-derived products is of great importance from both a scientific (geological information) and practical (monetary, environmental) perspective. Given has eloquently stated the practical benefits which would be realized by a thorough understanding of the geochemistry of coal (77,78). Briefly, proper utilization of coal requires that readily evaluated parameters be correlated with process response, that is, with end product use (79,80). Therefore, the differences in flora, the environment of deposition, and the temperature, time and pressure of transformation all influence the chemical properties of the product coal. To properly apply a coal to a particular end use and to assure the optimum conditions for its efficient utilization requires a knowledge of these characteristics.

Chemical fossils (81) are those organic compounds present in the geosphere whose carbon skeleton suggests an unambiguous link with a known natural product. Chemical fossils, also known as biological markers, and their stereochemistry (82,83) are being used to gain geochemical information on coal and other fossil fuels (84). Specially, several biomarkers have been identified in coal process liquids including simple acyclic isoprenoids (85-88), the more stereochemically rich cyclic terpenoid hydrocarbons (89-91) and various polar, oxygen containing biomarkers (90). Currently, biomarkers are identified and quantitated using the combined techniques of gas chromatography and mass spec-

trometry (GC-MS). However, this technique can only observe the chirality indirectly by inferring this property from a structural determination.

Optical activity in fossil materials is a consequence of the remnants of molecules that were present in the source organisms. The coalification process would be expected to destroy, or at least modify any chemically reactive chiral centers present in these molecules. However, certain chiral centers, particularly those involving only C-C and C-H bonds may be stable enough to survive the coalification process unmodified. Therefore, the study of the chiral material in coals and coal products should be useful in determining the biogenetic origin of coals and to assess the severity of the coalification process.

Bulk optical rotation measurements have been reported for various fossil fuels including lubricating oils (92), petroleum distillates (93), and shale oil (94). For coal-derived materials, Zahn and coworkers found optical activity in many of the fractions of coal tars and synfuel liquids (95,96). This study was in addition to earlier reports of optically active materials in peat (97), lignite (98,99), European brown coal (92,93) and coal process liquids (100,101). A recent study (85) has confirmed these observations.

Because of the complex nature of coal and other fossil materials (102,103), much work has been done to develop useful analytical procedures for its proper characterization (104-111). Recent work has concentrated on the chromatographic aspect of the coal analysis problem (112-114). However, since it is doubtful that chromatographic separa-

tion efficiencies will ever reach the point where baseline resolution of all of the thousands of different components present in a coal sample will be achieved (115), there is a need to develop more selective detectors to simplify the analysis.

Since optical activity is usually an indication that the material under study has a biotic origin, and since most compounds are not optically active, an optical rotation detector would meet the requirements for selectivity outlined above. That is, an optical rotation detector will respond only to chiral materials (achiral materials will be transparent to the detector) and, therefore, the analysis of complicated samples will be simplified by application of this detection scheme. Another advantage to the application of optical rotation detection to the analysis of coal liquids is that biomarkers, whose crucial characteristic is chirality would be observed directly. Figure 3 lists some of the steps necessary to isolate biomarkers in coal liquids. Direct observation would save substantial amounts of preparation time since the tedious separation and concentration procedures necessary to isolate biologically interesting molecules for achiral detection would be avoided. However, even with a selective optical rotation detection system, a coal liquid still contains too many compounds to analyze directly without separation. Additionally, since coal liquids contain both levorotatory and dextrorotatory components, partial cancellation of the rotation would be observed during any bulk measurement on the coal liquid. Bulk rotation measurements, therefore, only demonstrate the minimum amount of chiral material present. However, this cancellation

Figure 3. General procedure for biomarker isolation and identification

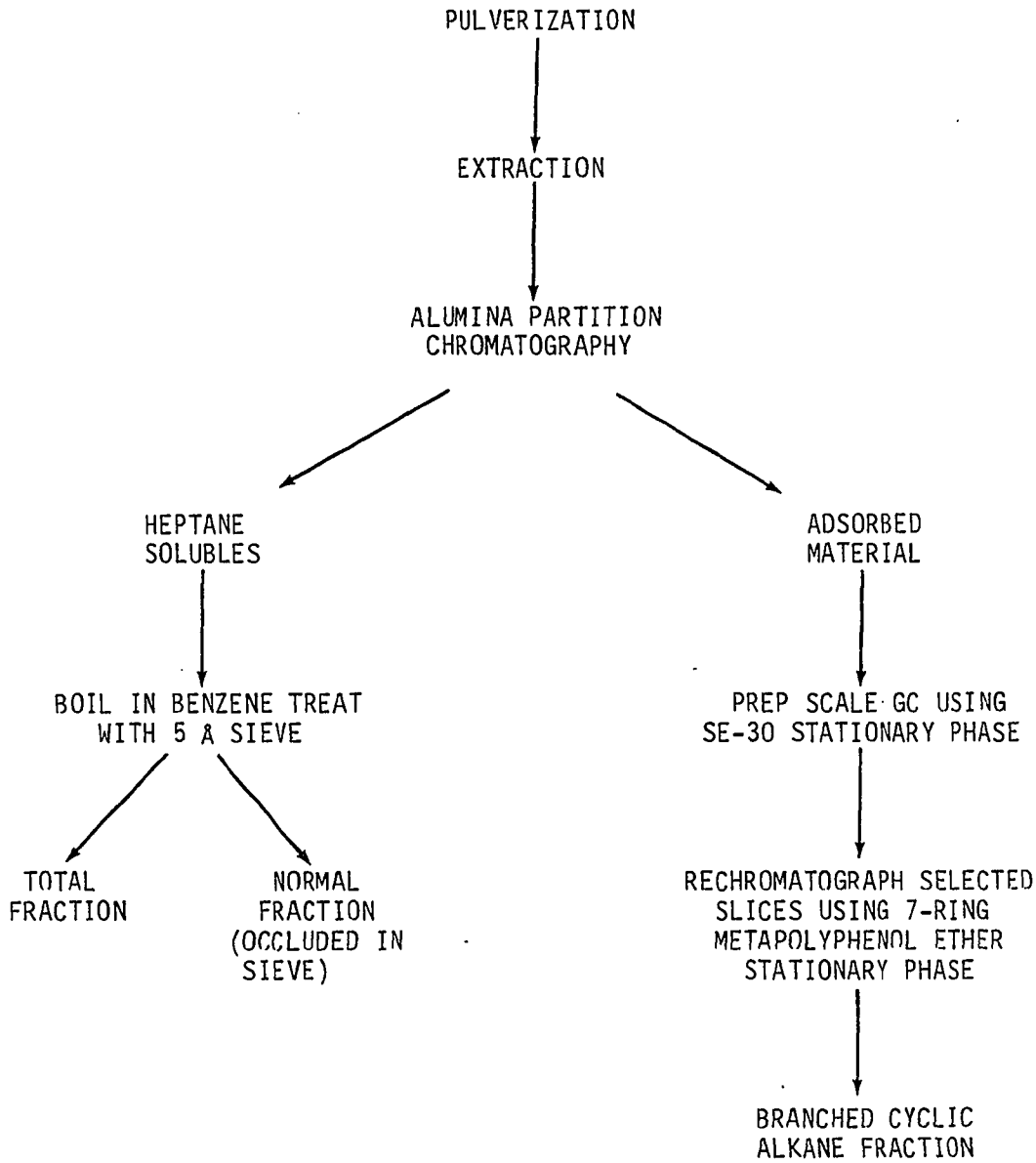

FURTHER SEPARATION OF FRACTIONS BY GAS CHROMATOGRAPHY WITH MASS SPECTROMETRIC IDENTIFICATION

can be minimized if the coal liquid is first subjected to a chromatographic separation step before analysis. Therefore, the combination of liquid chromatography with optical rotation detection (LC-ORD) is a useful system for the analysis of chiral materials in coal and coal-derived liquids.

This chapter will present the results of the application of LC-ORD to the analysis of several coal samples (116,117). First, the experimental parameters necessary to obtain useful information will be discussed, and then the results of several investigations involving coal samples from widely differing geographical locations, as well as samples from similar regions will be presented.

Experimental

The first part of this study involved the analysis of four coals from different geographical areas. The purpose was to determine if the technique of LC-ORD could show differences in the chiral fingerprints of these coals. The second part involved a suite of Illinois No. 6 coals, including samples taken across one particular seam. It was hoped that this would demonstrate the sensitivity of the technique to subtle changes in formation conditions.

Materials

The coals for the first study were obtained from the Ames Laboratory Coal Library (Ames, Iowa), which contains at present nine coals representative of all ranks from subbituminous to lvb. Samples were rigorously protected from air from the time of collection, crushed under

CO_2, riffled and stored under nitrogen until used. The coals were Dietz No. 1 and No. 2, Decker Mine, Bighorn County, MT; Illinois No. 6, Captain Mine, Randolph County, IL; and Kittanning, PBS Mine, Somerset County, PA. The solvent-refined coal (SRC) used was a sample of Pamco (Fort Lewis, WA) SRC, provided by Dr. T. F. Yen of the University of Southern California. Details of the other properties of this SRC have been reported earlier (118). The elemental analysis of the samples is given in Table 1.

Samples of the ground coal and synfuels were Soxhlet-extracted with benzene for 20 hours. The benzene was then removed by evaporation and the residue extracted with pentane. The pentane fraction was freeze-dried to produce the starting materials. Weighed amounts of the resulting materials were dissolved in acetonitrile for injection into the liquid chromatograph. Three separate extractions were performed on each of the coals to minimize problems with heterogeneity. Only one extraction was performed on the synfuel sample because it was expected to be homogeneous. The efficiency of the extraction procedure for each sample is shown in Table 2.

Coal tar was generated by heating a thin bed of coal rapidly (<30 s) to 500°C between two 44 μm mesh electrically heated stainless steel screens under vacuum (33 Pa). Tar was collected on the water-cooled walls of the vessel, while volatiles not condensed on the walls were collected in a liquid nitrogen trap. Toluene extracts of Illinois No. 6 coal at 290° and 420°C were obtained at 21 MPa using a hot tube reactor.

The suite of Illinois No. 6 coals were obtained from the Penn State Coal Bank (College of Earth and Mineral Sciences, Coal Research Section, University Park, PA). These samples were protected from air and stored under nitrogen as described previously. Table 3 lists the eight coal samples analyzed as well as a brief description of each. The Illinois No. 6 coal samples were Soxhlet-extracted with a benzene-methanol mixture (75:25) for 24 hours and then the solvent was removed by evaporation. The residue was then extracted with pentane. The freeze-dried pentane fraction was dissolved in acetonitrile using ultrasonic agitation. Table 4 lists the amounts extracted for each of the eight Illinois No. 6 samples. As before, at least two replicate analyses of each sample were made to insure reproducibility.

Chromatography

Separations were performed on a 25 cm x 4.6 mm C_{18} reverse-phase HPLC column packed with 10 μm particles (Alltech Associates, Arlington Heights, IL). The mobile phase for the first study was 100% acetonitrile, while for the Illinois No. 6 coals, a mixture of acetonitrile and water (95:5) was used. All chemicals were reagent grade (Fisher Scientific, Fair Lawn, NJ). The solvent delivery system was either a reciprocating piston pump (Micromeretics, Norcross, GA, model 750) or a constant flow syringe pump (ISCO, Lincoln, NE, model 314). The pump was coupled to the system via a conventional injection valve with a 100 μℓ injection loop (Rheodyne, Berkeley, CA, model 7010). A flow rate of 0.6 ml min^{-1} was used for all these studies.

Table 1. Elemental analysis of coal samples (wt %)[a]

	Illinois No. 6	Kittanning	Dietz	W. Kentucky
C	80	92	75	80
H	5.5	4.5	5.3	5.7
K	2.4	2.5	1.7	1.8
S	1.6	0.1	0.3	4.4
Cl	0.0	0.1	0.1	--
O	10.6	0.7	17.8	8.0

[a] D_{mmf} (dry, mineral matter free) calculated according to Given, P. H. and Yarzab, R. F. (Ref. 108, Vol. II, Chapter 20).

Table 2. Extraction efficiencies

	Extracted Yield (mg)	(wt %)
Illinois No. 6 coal	40	1.4
Kittanning coal	60	2.9
Dietz coal	2	0.1
Pamco SRC	700	23
Illinois No. 6, 290°C	17	3.3
Illinois No. 6, 420°C	88	17.5
Illinois No. 6 tar	30	7.5
Illinois No. 6 volatile fraction	30	7.5

Table 3. Illinois No. 6 coals used in this study

PSOC #	Description
1188	Perry Co., IL; whole channel sample
1189	Perry Co., IL; upper 30 inches of PSOC-1188
1190	Perry Co., IL; next 31 inches of PSOC-1188 to a 1 inch blue shale parting
1191	Perry Co., IL; bottom 9 inches of PSOC-1188 between blue shale parting and floor of seam
1098	Saline Co., IL; whole channel sample
1323	Vermillion Co., IL; whole channel sample
1317	Macoupin Co., IL; whole channel sample
1318	Knox Co., IL; whole channel sample

Table 4. Extraction efficiencies for Illinois No. 6 coals

PSOC #	Wt. Pentane Extract[a] (mg)
1188	44.8
1189	58.4
1190	49.2
1191	49.3
1098	76.3
1323	75.9
1317	55.7
1318	35.5

[a]From 1.00 gram coal sample.

Detection

The optical rotation detector used is described in detail in Chapter I. A commercial refractive index (RI) detector (Waters Associates, Milford, MA, model R401) was connected in series after the optical rotation detector. The outputs of both the ORD and RI detectors were connected to two digital voltmeters (Keithley, Cleveland, OH, model 160B), the analog outputs of each voltmeter were in turn interfaced to a computer (Digital Equipment, Maynard, MA, model PDP 11/10 with LPS-11 laboratory interface). The computer stores information every 1 s and allows normalization with respect to laser power and sample amounts injected. The laser power and overall instrumental response of the ORD system can be accounted for by recording the response to a known amount of optical rotation generated by a DC solenoid.

Results and Discussion

General considerations

The purpose of this study was to compare chromatograms obtained using optical rotation detection for various coal-derived materials. With that in mind, a final extraction step using pentane was chosen for each sample so that similar fractions would be isolated from each of the materials. Pentane possesses two characteristics which made it the solvent of choice. First, pentane extraction is a standard technique for the isolation of highly saturated hydrocarbons. As mentioned previously in the introduction to this chapter, saturated hydrocarbons are the substances in which unmodified chiral centers would most likely be

found. Second, because pentane possesses a low boiling point (<30°C), removal of the pentane solvent prior to analysis is easily accomplished without the risk of losing the more volatile components of the coal-derived material.

Chromatographic considerations (choice of column, eluent, etc.) were based on previous studies of similar materials (70). The flow rate (0.6 ml min^{-1}) and eluent (acetonitrile) allowed most of the injected material to be eluted in a reasonable period of time, while still providing enough chromatographic efficiency to allow easily resolvable features for interpretation. Since the pentane extract of each sample was freeze-dried and redissolved in acetonitrile (the chromatographic eluent) prior to analysis, no large artificial peaks indicative of large refractive index changes are evident. These RI peaks, usually present when the sample solvent and chromatographic eluent are different, can obscure early eluting components. The conditions for these studies, therefore, preserved all the chromatographic information.

In order to compare chromatograms from different coals and coal-derived materials, it is necessary to be able to calibrate each chromatogram with respect to the amount of material injected. However, since extraction efficiencies and solubilities can be expected to vary substantially from one material to the next, normalization based on prepared concentrations would be difficult for several reasons. First, since only small amounts of materials are present in the final extract, weighing of these small quantities of material would be unreliable. Second, since many of the extracted compounds are sparingly soluble in

acetonitrile, slight changes in storage conditions can cause these components to precipitate from solution. Third, any volatile components present in the sample may be lost during a drying process.

A better method is to normalize the data for each sample with respect to the area of the refractive index chromatogram obtained simultaneously with the optical rotation information. Since the refractive index of acetonitrile is quite low (n_D^{20} = 1.3442), most eluting compounds would be expected to have refractive indices greater than acetonitrile. The RI chromatogram, therefore, provides a good first approximation to the amount of material injected. A more accurate, but complicated procedure has recently been developed (119,120) based on the refractive index detector. However, for these studies, the simpler approximation is sufficient.

The optical rotation detector is susceptible to laser power fluctuations. That is, the sensitivity of the detector changes with the laser power, as well as with changes in the switching and detection electronics. However, overall system performance can be accounted for by calibrating the data against the known rotation induced by a standardizing DC solenoid. A check of system performance was made in this manner at the beginning and end of each chromatographic run. The data, therefore, are consistent for each study after being normalized for amount injected and detector sensitivity.

Finally, since the chiral materials become quite diluted during the extraction and chromatographic procedure, it is useful to consider at

what concentration level materials will be detectable with this system. The optical rotation detector used in this work has a detectability of $\approx 1 \times 10^{-5}$ degrees of rotation. If we assume a component has a specific rotation ($[\alpha]_D^{25}$) of 10 degrees in a 1 dm cell, then the 1×10^{-5}° detectability implies that the concentration at the detector must be 1×10^{-7} g ml^{-1}, or greater. Assuming a peak volume of 500 µℓ and a chromatographic dilution factor of 20, the mass which must be injected of any particular chiral component is calculated to be 10 µg. Since a 100 µℓ injection loop was used for these studies, a chiral component must be present at the 100 µg ml^{-1} concentration level (100 ppm) in the extract before injection to be detected. This, then, is the minimum detectable concentration useful with the optical rotation detector.

Study I: Geographically variant samples

The chromatograms for the three coal extracts and the solvent refined coal (SRC) extract are shown in Fig. 4. The optical rotation (OR) and refractive index (RI) data were obtained simultaneously. To facilitate comparison of the OR chromatograms, the data have been normalized to the same RI integrated area. The truncation evident in several of the peaks is an artifact of both the plotting program used and the constant vertical scales. Therefore, all data are within the digitization range of the data sampling system and the integrated areas are meaningful. The first peak in the OR chromatogram for the PAMCO SRC corresponds to a rotation of 3.8×10^{-4} degrees in a 10 cm cell, while the first feature in the respective RI chromatogram corresponds to a refrac-

Figure 4. Chromatograms of coal extracts: l.h., optical rotation chromatograms; r.h., refractive index chromatograms. Eluent: 100% acetonitrile; flow rate: 0.6 ml min^{-1}

(A) Illinois No. 6, Randolph County, IL, Captain Mine
(B) Kittanning, Somerset County, PA, PBS Mine
(C) Dietz, Bighorn County, MT, Decker Mine
(D) PAMCO SRC, Fort Lewis, WA

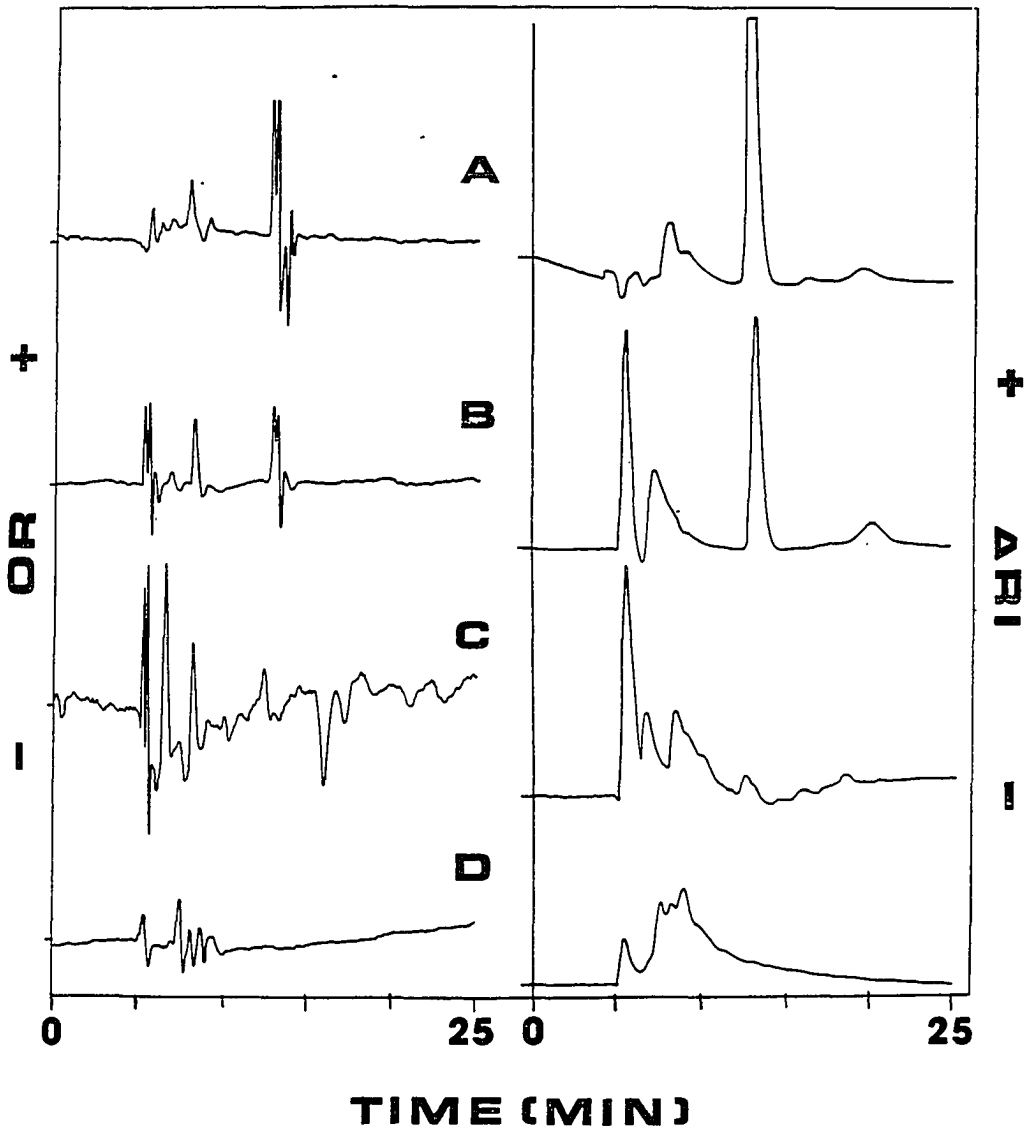
A
B
C
D
+
OR
I
+
ARI
I
0
25
0
25
TIME (MIN)

tive index change of 1.3×10^{-5} units. All chromatograms have been confirmed by multiple extractions of each sample, and multiple injections of the same extract. Therefore, the features shown are reproducible.

From inspection of Fig. 4, several observations can be made concerning the chromatograms. First, the optical rotation chromatograms are rich in structure showing the wide diversity of chiral materials present in the parent coal. Second, since complete chromatographic resolution of the components was not achieved in these studies, the chromatograms are, therefore, indicative of the minimum number of optically active species. Even so, the differences in the four OR chromatograms suggest that optical rotation is capable of providing chromatograms which should be useful for the fingerprinting of coals and coal-derived materials. Third, comparison of the RI and OR chromatograms underscores the fact that even when the chromatographic resolution is poor, as evidenced by the RI chromatograms, the selective nature of optical rotation detection can provide useful information. Finally, it is evident from the Dietz coal chromatograms that the OR detector is more sensitive than the RI detector. Two features are visible in the OR chromatogram at approximately sixteen minutes, while the RI detector hardly shows a deflection from baseline. Clearly, the features represent at least two compounds which are fairly optically active but present in the parent coal in only small amounts.

The optical rotation chromatograms show features which are dextrorotatory as well as levorotatory. This points out the importance of

chromatography in conjunction with OR measurements as a means of revealing chiral features hidden by inadvertent mutual cancellation. Since the chromatography only provides the minimum amount of chiral material, some mutual cancellation may be still occurring for coeluting substances. Therefore, moderate increases in chromatographic resolution will most likely provide dramatic increases in the number and amount of chiral materials detectable.

The integrated areas for the optical rotation chromatograms based on both the algebraic (with regard to sign) and absolute sum are presented in Table 5. The algebraic sum is an indication of the optical activity measurable for a bulk analysis, while the absolute sum is a better indication of the chiral content of the materials. For the Dietz coal extract in Table 5, the algebraic sum shows there to be little chiral material in the Dietz coal. In fact, the OR chromatogram shows this not to be true, and the absolute sum collaborates this fact. Specifically, the chiral content is larger by a factor of 12 (2.00 versus 0.16) than would be assumed from a bulk measurement of a Dietz coal extract. The difference will become greater as the chromatographic resolution improves.

There are distinct differences in the optical rotation chromatograms for the various coal extracts. Although it will be necessary to study the variations among extracts of the same coal from different mines and a suite of coals representing different seams to learn the significance of differences among extracts of these coals, the results here show qualitatively that the OR chromatograms are useful for coal

Table 5. Integrated optical activity of extracts

	Absolute Sum[a]	Algebraic Sum[b]
Illinois No. 6 coal	0.85	0.54
Kittanning coal	0.51	0.18
Dietz coal	2.00	-0.16
Pamco SRC	0.65	-0.08
Illinois No. 6, 290°C	0.81	-0.21
Illinois No. 6, 420°C	0.73	-0.32
Illinois No. 6 tar	0.72	-0.49
Illinois No. 6 volatile fraction	0.37	0.21

[a]Integrated areas of chromatograms using absolute values of measured optical rotation, in arbitrary units.

[b]Integrated areas of chromatograms using signed values of measured optical rotation, in the same units as (a).

characterization. The integrated absolute OR given in Table 5 shows that the Dietz coal extract has the largest fractional content of chiral materials, followed by the extracts from the Illinois No. 6 coal and Kittanning coal. This is consistent with the fact that the H/C ratio is the highest for the Dietz coal and the lowest for the Kittanning coal. The presence of chirality is more probable in saturated molecules than in unsaturated ones. The trend is also consistent with the fact that the Dietz coal is the youngest of the three, while the Kittanning coal is the oldest. The longer a coal is subjected to transformative processes, the more the chiral materials in the coal would be expected to be modified or destroyed.

Besides the obvious differences in the coals, there are similarities among the extracts of the coals, especially the Illinois No. 6 and the Kittanning. Since geochemical studies have shown that certain potentially chiral systems (e.g., steranes, hopanes and other isoprenoid skeletons) are ubiquitous in fossil fuels (84), it is not surprising to find related patterns of optical activity in these two Carboniferous coals.

To determine how processing affects the optically active components, the results of a study of extracts from the same Illinois No. 6 coal are plotted in Fig. 5. Two of the chromatograms represent high temperature extractions (290 and 420°C, respectively); one represents a tar formed from the Illinois No. 6, while the last chromatogram was obtained from the volatile fraction collected in a dry ice/acetone cold

Figure 5. Chromatograms of various extracts of Illinois No. 6 coal: l.h., optical rotation chromatograms; r.h., refractive index chromatograms. Eluent: 100% acetonitrile; flow rate: 0.6 ml min^{-1}

(A) Toluene extract of Illinois No. 6 coal, 300 psi, 290°C
(B) Same as (A), 420°C
(C) Tar of Illinois No. 6 coal
(D) Volatile fraction deposited in liquid nitrogen trap during tarring process

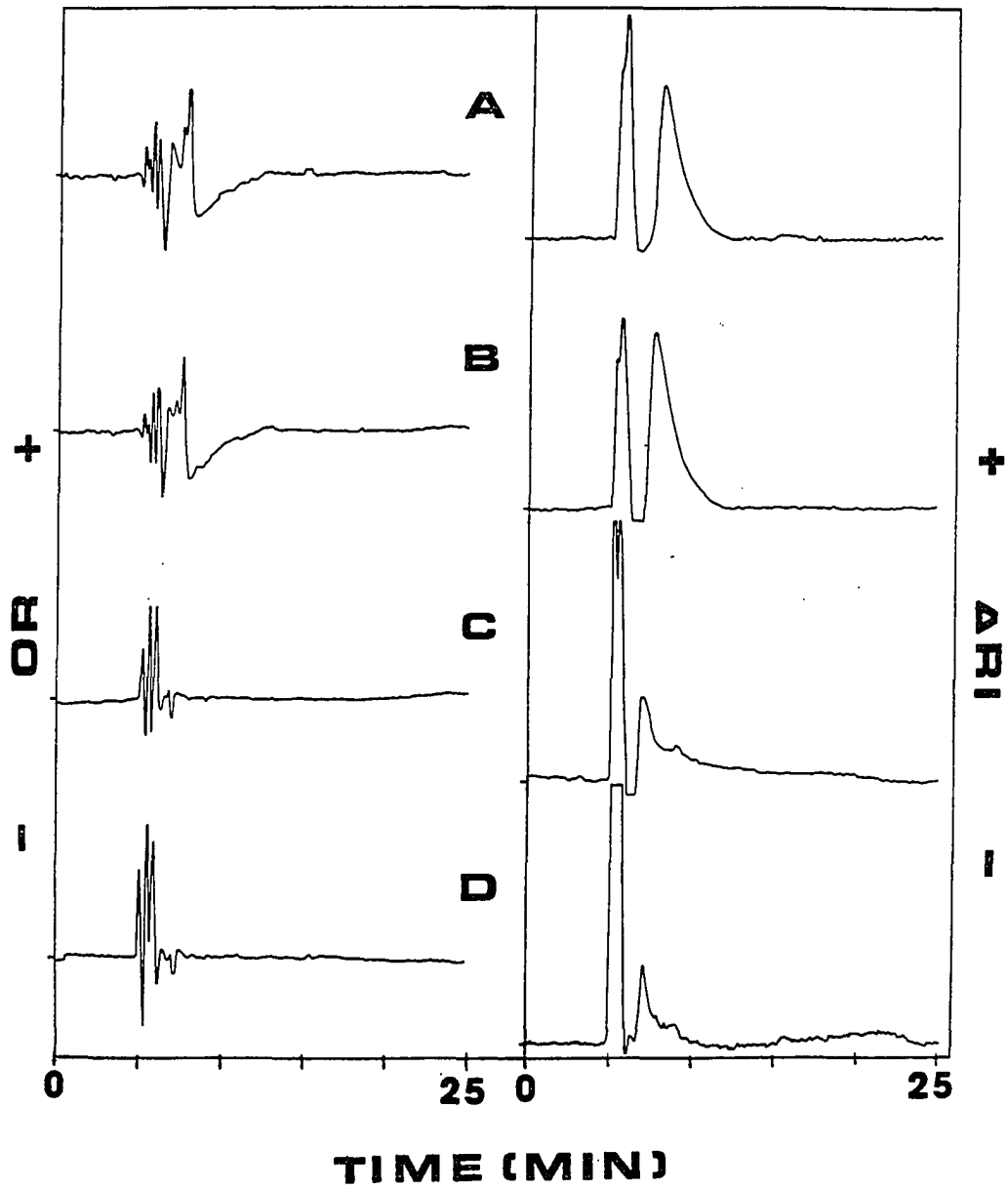
A
B
C
D
+
-
OR
+
-
ARI
0
25
0
25
TIME (MIN)

finger during the tarring process. The chromatographic conditions and the vertical scales are identical to those used in Fig. 4.

The great differences between the room temperature extract of the Illinois No. 6 coal and the samples from high-temperature extraction or pyrolysis is not surprising, for at least two reasons. First, a substantially greater fraction of the coal is represented by the high-temperature extracts and tar, and second, it is likely that the increase in yield on raising the temperature is due in part to the rupture of some covalent bonds. When weak covalent bonds are cleaved thermally, the structures in coal may be expected to generate materials closely related to the trapped molecules extractable at room temperature. However, the relative proportions of different functional classes may be very different. With this in mind, further study is needed to address the chromatography used in this study. The chromatographic conditions were chosen to maximize the information in the room temperature extracts. It will be necessary to develop other chromatographic conditions to better resolve the early eluting features to learn more about the similarities and differences of the high temperature extracts.

An inspection of Table 5 also leads to the conclusion that some thermal chemistry - fragmentation or racemization - takes place for the high-temperature samples. The chiral content decreases in the order Illinois No. 6 coal >290°C extract >420°C extract > tar > volatiles, confirming the gradual degradation of the chiral information with the degree of processing. The Pamco SRC originated from a similar coal and

shows about the same degradation as the high-temperature benzene extracts.

The fact that the algebraic sum of optical rotations changes sign for some extracts from the same source materials is not particularly significant, since it is well established that subtle changes in structure remote from the centers of dissymmetry can change the sign of rotation at a given wavelength (121). In a simple example (122) related to fossil fuels, phytane produced from 3R, 7R, 11R-1-phytanyl iodide by reduction has a specific rotation of +3.9°, while 1-phytene produced from the same starting materials by elimination has a specific rotation of -5.0°.

$$R\text{-}CH_2CH_2I \xrightarrow{LiAlH_4} R\text{-}CH_2CH_3 \qquad R\text{-}CH_2CH_2I \xrightarrow{KOH} R\text{-}CH{=}CH_2$$

$$R = (CH_3)_2CH\,[\text{-}CH_2CH_2CH_2\underset{\displaystyle CH_3}{\underset{|}{CH}}\text{-}]_3$$

To better determine the nature of some of the eluting compounds detected in this study with respect to their chromatographic properties, samples of pristane ($C_{19}H_{40}$) and phytane ($C_{20}H_{42}$) were injected into the liquid chromatograph. The observed retention times under identical chromatographic conditions as used in these studies were 79 and 99 min, respectively. This is well beyond the 25 min monitored in the chromatograms of Figs. 4 and 5. Therefore, it is clear that either the extracted molecules are hydrocarbons of much lower molecular weight than pristane and phytane, or the molecules are polar compounds that elute

faster than would be predicted from their molecular weights. The later seems more likely, and the detected molecules are probably fairly large hydrocarbon-like molecules with polar moieties which have a pronounced effect on their chromatographic behavior. This last point of uncertainty demonstrates the need for further investigation of not only the optimum chromatographic conditions, but it also shows the need to isolate and identify some of these optically active components.

Study II: Illinois No. 6 samples

From the results of the first study, it is clear that LC-ORD is capable of detecting differences in the distribution of chiral materials in coals from very different geographical areas. The purpose of this second study was to ascertain if differences can be detected in a series of coals representing the same general geographical region, but from different mines. Table 3 lists the coals which were studied along with their Penn State Coal Bank identification number (PSOC#) and a brief description. Note that five different counties of the Illinois coal field are represented including a series of samples from Perry county taken across the coal seam.

A preparation study was undertaken to determine the best method for the extraction of chiral material from coal. Table 6 lists the results of twelve samples of PSOC #1188 coal and the extraction yields for the different methods. Clearly, a benzene/methanol extraction yields the most amount of material. However, what is somewhat surprising is the yield obtained for the 45 minute extraction using ultrasound. Two-

Table 6. Preparation study for Illinois No. 6 coal. Sample: PSOC-1188; pentane soluble fraction

Sample #	Approximate wt. Extracted (mg)	Nature of Procedure
1	1.8	Quick prewash with pentane
2	63.9	24 hr ØH/MeOH extraction
3	4.6	24 hr ØH/MeOH extraction of residue from #2
4	28.7	45 min ØH/MeOH extraction with ultrasound followed by 500 ml pentane elution from silica column
5	41.5	45 min ØH/MeOH extraction with ultrasound
6	21.9	45 min ØH/MeOH extraction with ultrasound of residue from #5
7	2.2	Next 300 ml pentane elution of #4
8	11.0	72 hr ØH extraction
9	59.4	72 hr ØH/MeOH extraction of residue from #1
10	42.7	72 hr ØH/MeOH extraction of PSOC-1188 dust
11	5.5	168 hr pentane extraction
12	17.7	72 hr tetrahydrofuran extraction

thirds of the material extractable in a twenty-four hour Soxhlet extraction was obtained in only 45 minutes using ultrasonic agitation. Analysis of the extracted material showed the distribution and relative amounts of chiral materials to be almost identical to the twenty-four hour sample. Therefore, future studies should utilize this method which will result in substantial savings in sample preparation time.

Figure 6 presents the chromatograms for a series of samples taken across a coal seam. As in the previous study, all chromatograms have been normalized to the same integrated RI area and corrected for OR system sensitivity. Additionally, all previous statements about the chromatographic nature (i.e., fairly polar) of the eluting components applies to this study also. From inspection of Fig. 6, it is apparent that the OR chromatograms from the top and middle of the seam are almost identical. However, it is interesting to note that the OR chromatogram from the bottom 9 inches appears somewhat different than the other two. This part of the seam was separated from the rest by a layer of blue shale. Geologically, this shale parting signifies a drastic change in the local conditions in the area from the time the 9 inches was formed till deposition commenced again. Therefore, the OR chromatograms are consistent with this picture.

For such similar samples as these, the differences in the OR chromatograms appear in the relative amounts of very similar components. This can be compared to the previous study where differences in the types of components eluting from the LC were easily seen. Even though more study is needed to evaluate the significance of these differences,

Figure 6. Chromatograms of Illinois No. 6 coal: l.h., optical rotation chromatograms; r.h., refractive index chromatograms. Eluent: 95:5 acetonitrile:H_2O; flow rate: 0.6 ml min^{-1}

(WHOLE) Whole channel sample
(TOP) Top 30 inches
(MID) Middle 31 inches to blue shale parting
(BOTT) Bottom 9 inches from blue shale parting to seam floor

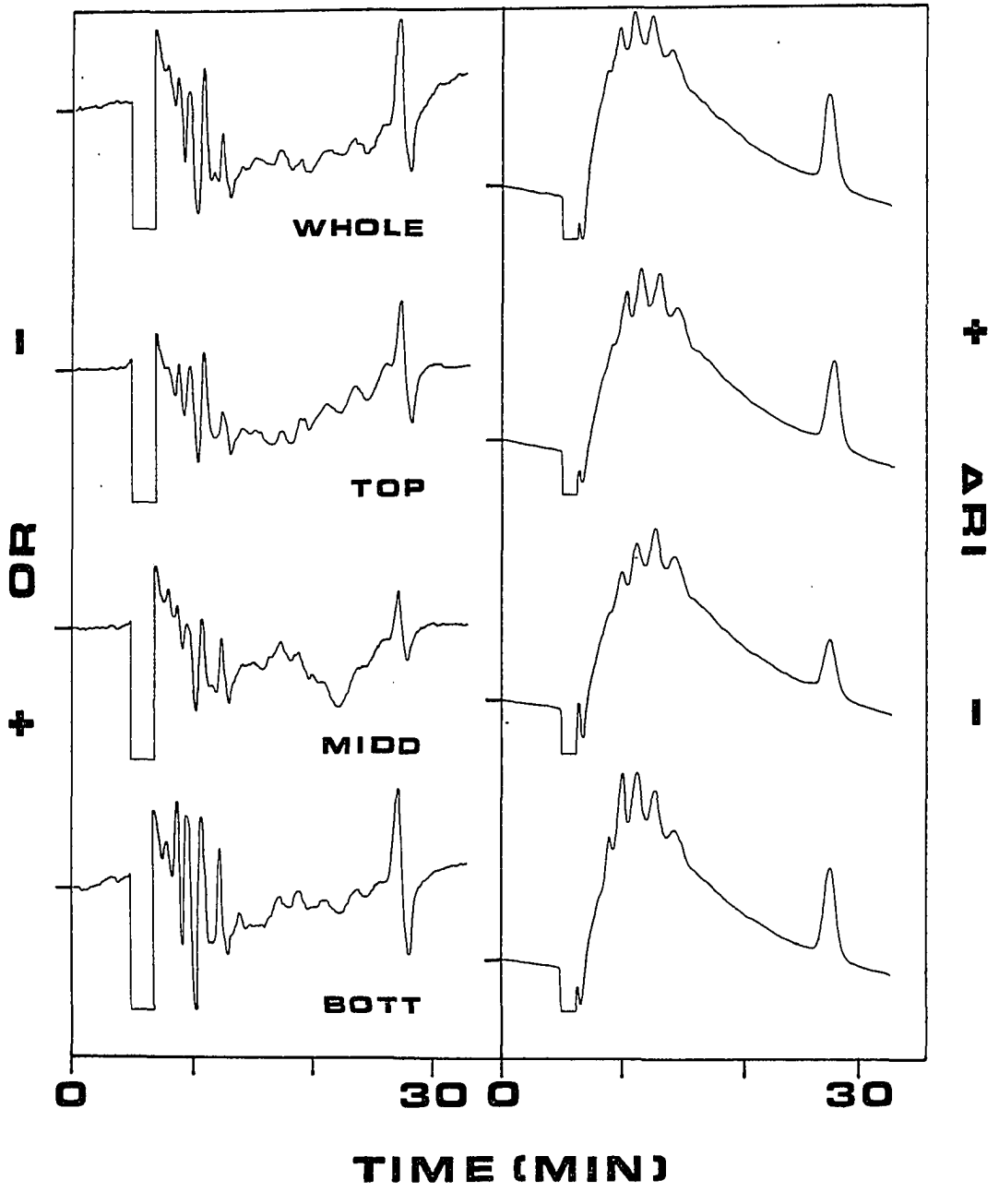
WHOLE
TOP
MIDD
BOTT
I
OR
+
+
ARI
I
0
30
0
30
TIME (MIN)

the results presented here were reproducible for these samples. It should also be pointed out that very little information is obtainable about these samples from the RI chromatograms. Therefore, selective OR detection is a better technique for chiral fingerprinting of similar coal samples.

Figure 7 is a map of the state of Illinois showing the location of the mines from which the five samples were taken. Each mine is identified by the county in which it is located. Figures 8 and 9 present the RI and OR chromatograms, respectively, for these five samples.

As before, the RI chromatograms in Fig. 8 are very similar and it would be very difficult to attempt to draw any conclusions based on this data alone. However, the OR chromatograms (Fig. 9) show several striking differences. First, OR chromatograms for coal samples from the three counties located in the southern-half of the state (Saline, Perry and Macoupin counties) show many similarities. For example, there is a large feature at approximately 10 minutes which is the start of a series of three features. The differences in the chromatograms appears to be in the amounts of the three components found in the different coals. Second, OR chromatograms for coal samples from the two northern-half counties appear quite different, not only when compared to each other, but also when compared to chromatograms from the southern three. The sample from Vermillion county is the best example of this with many more eluting components evident than for any of the other four coals.

The combined technique of LC-ORD appears to be useful for the differentiation of similar coal materials. For samples taken across a

Figure 7. Map of the State of Illinois

(KNO) Knox County
(VER) Vermillion County
(MAC) Macoupin County
(PER) Perry County
(SAL) Saline County

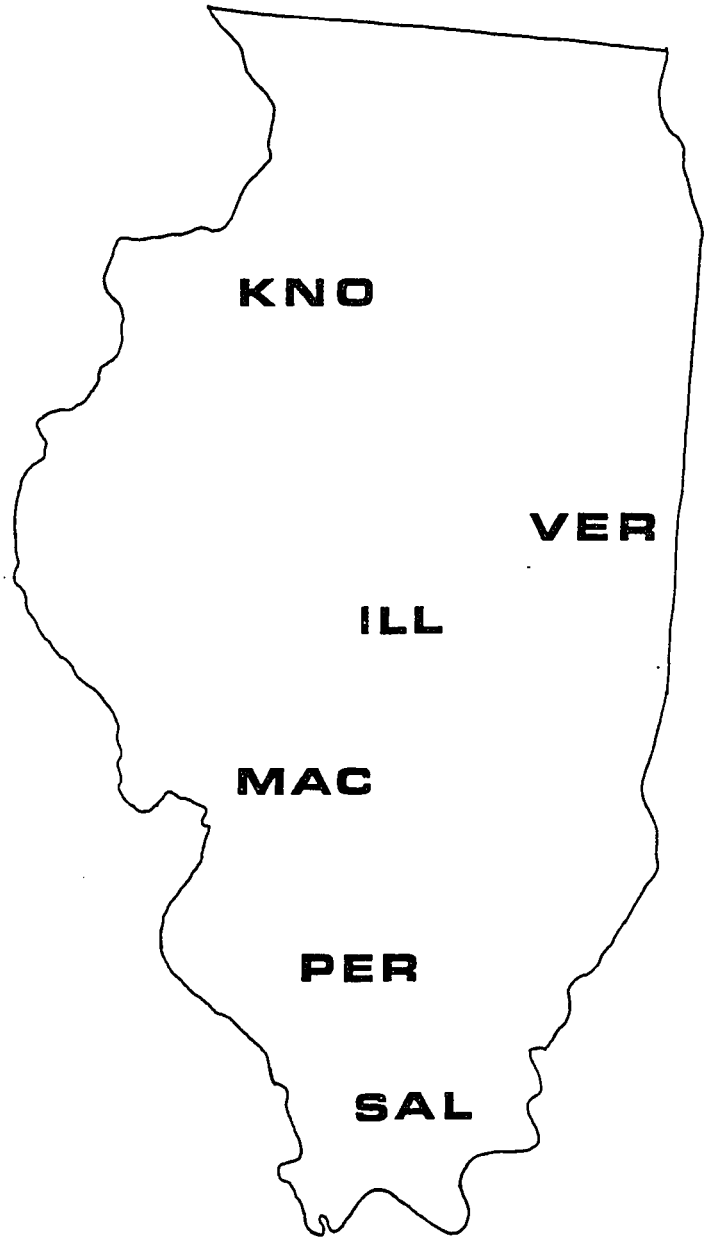
KNO
VER
ILL
MAC
PER
SAL

Figure 8. Refractive index chromatograms of selected Illinois No. 6 coals. Eluent: 95:5 acetonitrile:H_2O; flow rate: 0.6 ml min^{-1}

(SAL) Saline County
(VER) Vermillion County
(MAC) Macoupin County
(KNO) Knox County
(PER) Perry County

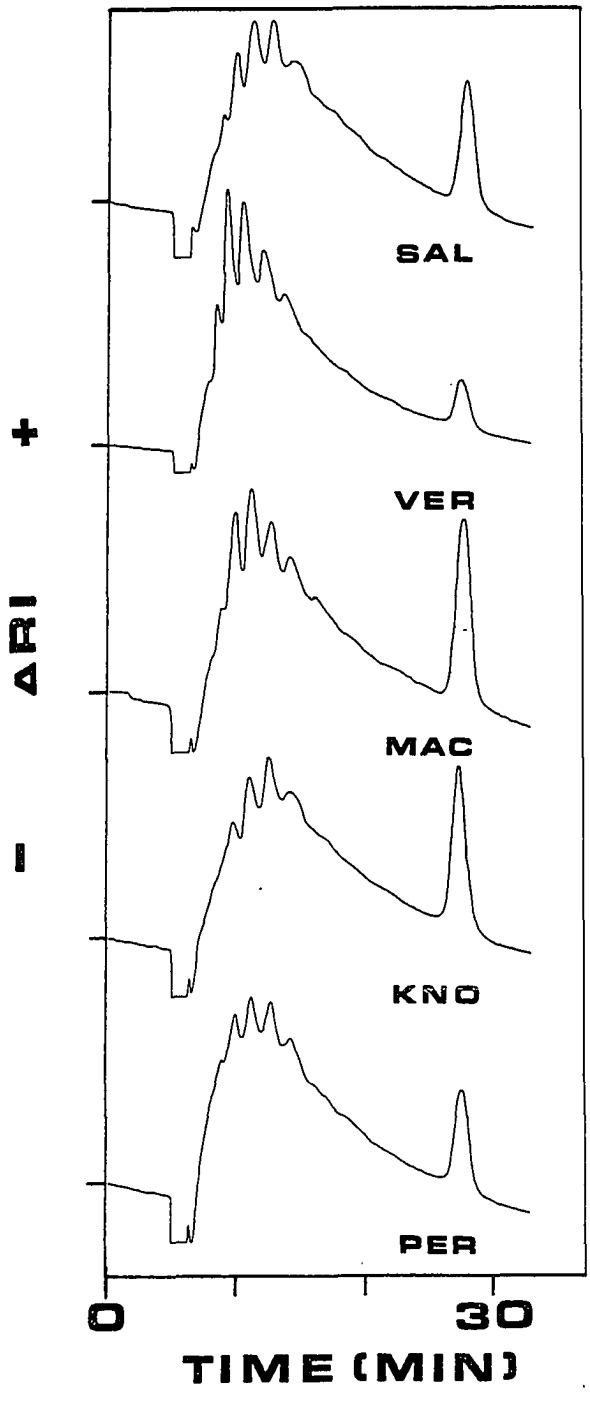
SAL
VER
MAC
KNO
PER
- ΔRI +
0
30
TIME (MIN)

Figure 9. Optical rotation chromatograms of selected Illinois No. 6 coals. Eluent: 95:5 acetonitrile:H_2O; flow rate: 0.6 ml min^{-1}

(SAL) Saline County
(VER) Vermillion County
(MAC) Macoupin County
(KNO) Knox County
(PER) Perry County

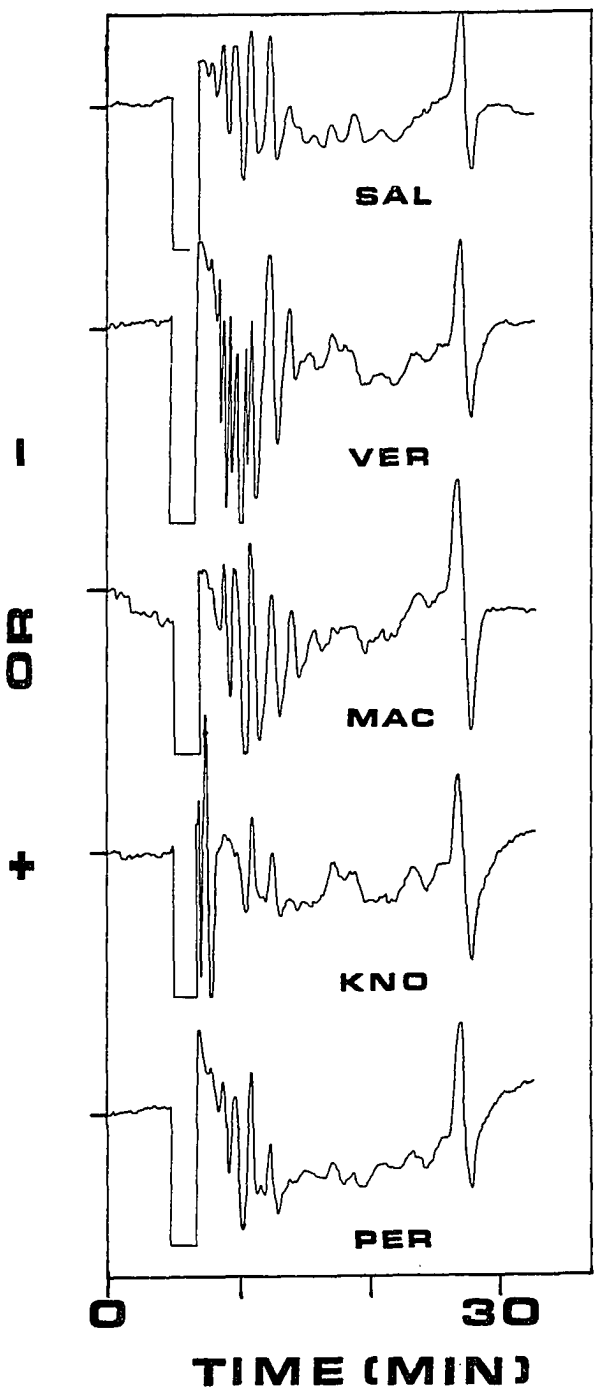
SAL
VER
MAC
KNO
PER
I
OR
+
0
30
TIME (MIN)

seam, the main difference is in the relative quantity of the different optically active materials, rather than in the types of materials present. This is substantiated by the fact that the same peaks are evident in the different chromatograms, but the peaks are present in different ratios. A clear example of this can be seen in comparing the layer protected by the shale to the results for the middle or top portion of the seam.

The samples from the five different counties again produce OR chromatograms rich in structure. Differences not only in the ratios, but also in the distribution of components, were seen. This result was surprising considering the geographical proximity of the five mines, and it demonstrates the sensitivity of the ORD system to small changes in origin conditions for similar biogenetic materials.

Conclusions

In the present work, the first profiles of the optically active components in coal extracts and various coal-derived products have been obtained using optical rotation detection. The technique of LC-ORD is useful for the characterization of closely related materials of different biological origins, and the information can be used to monitor the severity of processing of fossil fuels.

CHAPTER III. DIRECT AND INDIRECT POLARIMETRY FOR DETECTION IN MICROBORE LIQUID CHROMATOGRAPHY

Introduction

A recent development in the field of liquid chromatography (LC) has been the trend toward smaller columns (123,124). Microbore LC utilizes columns of 1 mm internal diameter or less, and column packing technology is such that 1 mm columns are commercially available. Microbore columns possess several advantages over conventional 4.6 mm LC columns. First, from an economic standpoint, microbore columns require less packing material and eluting solvent than conventional columns (125). That is, because microbore columns typically require flow rates of approximately 20 μℓ/min, more exotic eluents can be used at about the same cost as conventional solvents with standard 4.6 mm columns. Second, 1 mm columns can be connected together in series without loss of resolution (126,127). Recently, one million theoretical plates were generated by coupling twenty-two 1 m columns together (128). Although the retention times and pump pressures were excessive, this certainly points to the possibility of coupling several columns together to achieve the necessary plate count for a difficult separation. Third, microbore columns can be packed more efficiently than larger diameter columns resulting in increased efficiencies.

To maintain the high efficiency of the microbore column, detection cells must have volumes 5-10 times less than the peak volumes. This corresponds to cell volumes of 1 μℓ for a typical 1 mm i.d. column.

Laser-based LC detectors lend themselves well to miniaturization due to the highly collimated nature of the laser beam. Recent work has demonstrated the utility of small volume, laser-based detectors using thermal lens calorimetry (129-131), fluorescence (132-134), and simultaneous monitoring of refractive index, absorption and fluorescence (135).

Optical activity would be a useful parameter to monitor because it is usually an indication of biological activity, past or present. For this reason, optical rotation detection is very selective. Several recent attempts to couple conventional polarimetric instruments to the effluent from a liquid chromatograph has not met with much success (136-139). Sensitivities are usually greater than 10^{-4} degrees, and mass detectabilities were shown to be no better than the refractive index detector (136).

A laser-based polarimeter utilizing intercavity quenching of the laser gain produced impressive results (140). However, the experimental details and results were sparse, it was not demonstrated on a flowing stream and the authors did not attempt to address the problem of detection cell window birefringence. Conceptually, a similar laser-based polarimeter was presented (141). The authors did a thorough theoretical study of different cavity configurations, however, they did not show any experimental results. Zapapsskii (142) used 250 mW of argon ion laser power and low drift bridge photodetectors to obtain an impressive 2 x 10^{-7} degree rotational sensitivity. However, except for a description of the detectability of the system, the experimental details were sparse. As before, detection cell birefringence was not addressed. For

the three studies previously cited (140-142), the lack of experimental details is particularly significant since such additional sources of noise as laser intensity instabilities may be of special concern to intercavity techniques such as these. Therefore, it is doubtful that practical detectabilities will ever approach the theoretical limits described in these three references.

A completely theoretical treatment of a polarimeter based on a ring gyro arrangement has recently been presented (143). This proposal suggests that the presence of circularly polarized eigenmodes in a ring resonator may be exploited for enhanced optical rotation measurements. If a passively stabilized cavity is used, the difference in paths for the opposite circularly polarized modes manifests itself as a beat, or modulated difference frequency at the detector. Sample rotations result in a shift in this difference frequency. Current technology is capable of measuring frequency shifts with excellent sensitivity. For example, the authors suggest that rotations of the order of 10^{-10} radians would result in a frequency shift of approximately 1000 Hz, which should be measurable. However, the authors acknowledge that small scale birefringence (e.g., window birefringence) will seriously degrade this theoretical detection limit. In addition, the multipass arrangement described here is not useful for samples possessing any absorption at the probe wavelength.

A functioning laser-based optical rotation detection (ORD) system for liquid chromatography has previously been reported (67). This LC-ORD scheme has been used to study several systems including carbohydrate

levels in urine (68), and for the characterization of coal and shale oils (70,116). This system has not been interfaced to microbore LC due to the large (80 μℓ) volume of the detection cell.

Small and Miller (144) have described an indirect photometric technique utilizing an absorbing eluent to detect nonabsorbing ions eluting from an ion-exchange column. A novel concept would be to consider a system in which an optically active eluent is used with an optical rotation detector to detect optically inactive components eluting from a chromatographic column. This then converts the ORD scheme to a universal one to rival the standard refractive index (RI) detector. In the indirect photometric scheme, the absorption due to the eluent is electronically compensated for. In the indirect polarimetric technique, the rotation due to the eluent is compensated for by rotating the second polarizer (analyzer). This means that, while the absorption detector has a dynamic reserve of about 10^3, if an eluent of $[\alpha] = 100°$ were used, and if a rotation of 10^{-5} can be detected, the polarimetric system will have a dynamic reserve of 10^7. Also, in the indirect photometric scheme, there is a limit as to how highly absorbing an eluent one can use. This is determined by the point at which the number of photons reaching the photodetector is such that stray light and amplifier bias current become significant and the detector becomes unstable. In the indirect polarimetric scheme, no similar limit exists. For an eluent with a large $[\alpha]$, the analyzer is simply rotated an amount equal to the eluent's rotation. Therefore, the point of maximum extinction for the polarizers has changed due to the optically active eluent, but the good-

ness of the extinction has been maintained. That is, the same number of photons are reaching the photodetector regardless of whether the eluent is optically active or not, preserving the signal to noise ratio.

Indirect detection schemes can be quite useful for many applications. When surveying an unknown sample, it is useful to first determine the number and amount of different components present. Since the ideal indirect detection scheme is universal in nature, that is, it provides the same instrumental response regardless of the species, a valid determination of each component can be made. Another use of indirect detection is in size exclusion chromatography (SEC). In SEC, species elute based on their respective exclusion from pores in the chromatographic stationary phase. That is, size is the determining factor. Therefore, since the useful information is when the species elutes (i.e., molecular weight information) rather than the identity of the species, indirect detection would have much applicability. Only with a universal detector can one be sure all of the components (which may have widely differing properties) will be detected.

To qualify as an 'ideal' universal detection scheme, the property of the eluent being monitored should be unique. For example, if an absorbing eluent is used, there is a good possibility that some of the components in the sample will absorb at the detection wavelength. This would limit the usefulness of this detection scheme except in very specific cases. However, because most compounds are not optically active, a universal detection scheme based on this property would come very close to the ideal situation.

Recently, several schemes have been described (119,145,146) which allow quantitative information to be obtained for an analyte without standards, that is, without analyte identification. It is significant to note that a similar scheme can be proposed for LC with optical rotation detection. In this scheme, one eluent would be optically active and the second eluent could be either the enantiomeric isomer of the first eluent or a racemic mixture of the two.

Figure 10 illustrates this concept. In the top half of the figure, an unknown compound, x, has been introduced into a flowing stream with a detector monitoring some property of the solvent. Any signal observed at the detector represents a change in the magnitude of the property monitored by the detector. For example, if the detector is monitoring the refractive index (RI) of the flowing stream, any change in RI will register as a signal at the detector. Since no signal is seen for the injection of x into solvent 1, one can assume that both solvent 1 and compound x have identical magnitudes of the property being monitored by the detector. This is useful information.

If x is now introduced into a second flowing stream with a much different magnitude of the detection property, a signal is assured for x in this second solvent. Usually, it is very rare to find the case represented by the top portion of Fig. 10 and some signal will be observed for x in each of the two solvents. However, if as specified previously, solvents 1 and 2 differ greatly in the magnitude of the detection property, it is possible to use the signals obtained for x in the two solvents to quantify x without the necessity to identify the species.

Figure 10. Illustration of the basis for the concept of quantitative analysis without identification

TOP: Detector response, S1, to unknown species x in flowing stream 1.

BOTTOM: Detector response, S2, in solvent stream 2, where the magnitude of the detection property of solvent 2 is much different than solvent 1

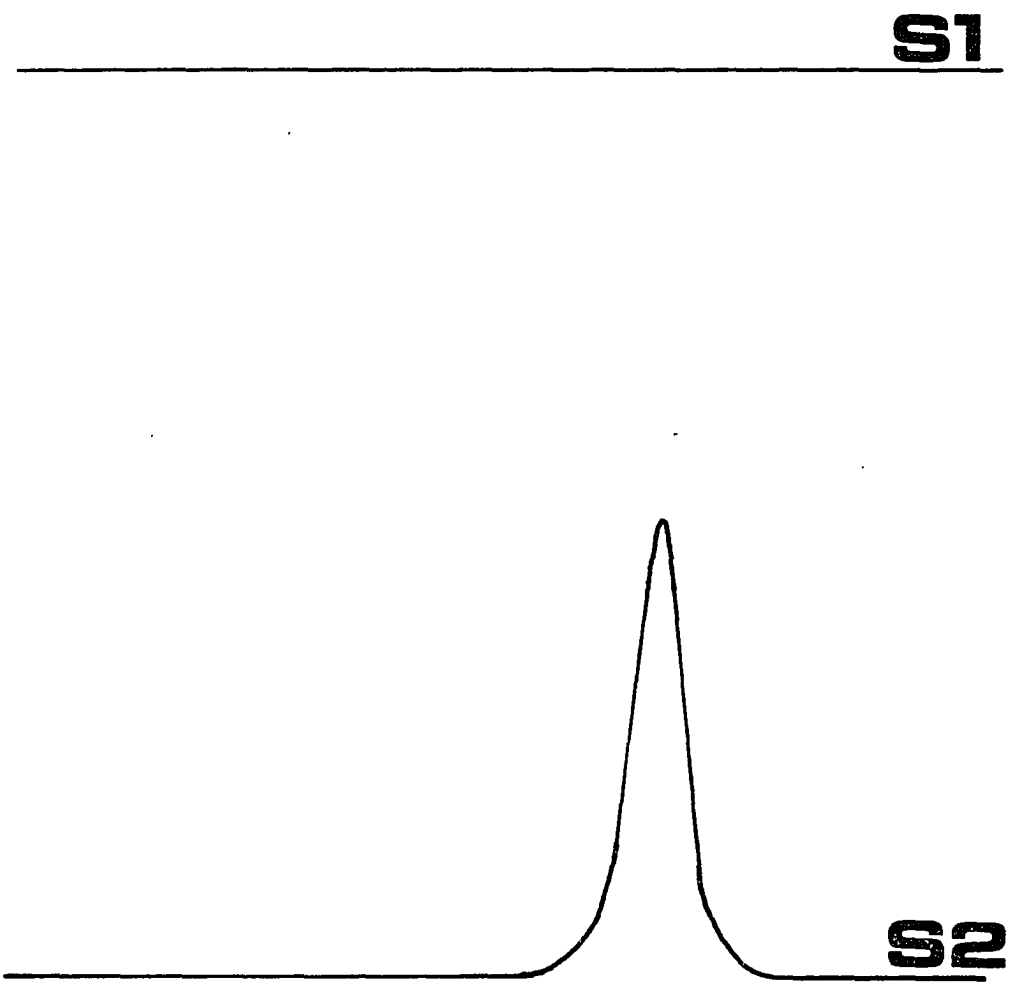
S1
S2

The following section will show in more detail how the differing response of an analyte in two eluents can be used to obtain quantitative information.

Theory

The rotation α observed for a given substance is related to the specific rotation $[\alpha]$, such that

$$\alpha = [\alpha]\ell c \tag{20}$$

and

$$\alpha = [\alpha]\ell\rho V \tag{21}$$

where ℓ is the pathlength (dm), c is the concentration (g/mL), ρ is the density (g/mL), and V is the volume fraction of the material at the detector. Since volume is additive, assuming ideal solutions, one can obtain the detector response for a chromatographic peak containing an analyte x and the eluent E. We note that the volume fractions of the two are V_x and $(1 - V_x)$, respectively. So

$$\alpha = \ell\{[\alpha_x]\rho_x V_x + (1 - V_x)[\alpha_E]\rho_E\} \quad . \tag{22}$$

In practice, one observes a peak area as determined from the base line established by having pure eluent in the cell. This base line rotation

corresponds to $\alpha_0 = [\alpha_E]\ell\rho_E$. The differential response is, thus,

$$\Delta\alpha = \ell V_x\{[\alpha_x]\rho_x - [\alpha_E]\rho_E\} \quad . \tag{23}$$

Equation (23) has the same form as Eq. (8) in reference 119 and, therefore, the optical rotation detector is useful for the quantitative method described in detail in reference 119.

In this method, one obtains two chromatograms for the same sample eluted with, e.g., an optically active eluent and then its racemic counterpart. When an analyte is detected in a particular eluent, the signal observed, S_i, is the integrated chromatographic peak area for the analyte. Two equations of the form of Eq. (23) can be obtained for the analyte detected in eluents 1 and 2, such that

$$S_1K = C_x(F_x - F_1) \tag{24}$$

$$S_2K = C_x(F_x - F_2) \tag{25}$$

where $[\alpha_i]\rho_i$ is redefined as F_i with the subscripts x, 1, 2 denoting the unknown, and eluents 1 and 2, respectively. K is a proportionality constant, and C_x is the volume fraction of the analyte injected. In contrast to reference 119, K is the same for both eluents as long as the flow rate, etc. is maintained. The reason is that the only difference between the two eluents is one of differing chirality. One can then calibrate the response of the detector by the injection of a single

calibrating substance into each eluent. By calibrating the system response, one does not need to determine K, or any physical properties of the unknown, or the two eluents (F_x,F_1,F_2) in order to calculate the concentration of an analyte injected onto the column.

The calibrating substance provides two additional relationships

$$S_3K = C(F_c - F_1) \tag{26}$$

$$S_4K = C(F_c - F_2) \tag{27}$$

where C is the injected volume fraction of the calibrating substance. Equations (24)-(27) can be solved to arrive at an expression for C_x

$$C_x = C\left(\frac{S_1 - S_2}{S_3 - S_4}\right) \quad . \tag{28}$$

It should be noted that no information is needed to solve for C_x except for the signal responses measured for the unknown and for the calibrating substance.

For the situation where the chromatographic properties of the two eluents are different, the proportionality constant, K, in Eqs. (24) and (25) will be different for each eluent. In this situation, a second calibrating substance can be used to generate two more equations which can then be solved to eliminate the different K's. Another solution to this problem is to elute each eluent with the other, if possible. This

also generates two equations which can be used to eliminate the proportionality constants. Both these methods are described in detail in reference 147. However, since by definition, enantiomers have identical physical properties, chromatographically each enantiomer will behave similarly and the simple equation listed above (Eq. (28)) will be applicable for any achiral separation. This is the unique advantage inherent to indirect polarimetry over all other detection modes for use with this quantitation scheme.

Similar to reference 119, one may solve for the specific rotation of the unknown. A simple expression can be derived if the specific rotations of the calibrating substance and one of the eluents are known. Using Eqs. (24) and (26) and eliminating K, one can derive

$$F_x = F_1 + \frac{S_1 C}{S_3 C_x} (F_c - F_1) \quad . \tag{29}$$

Again, in order to maintain significance, F_c and F_1 should be very different.

If the specific rotation of the eluent is not known, as in, for example, a binary or ternary solvent system, a second calibrating substance of known specific rotation can be used to determine the specific rotation for the unknown. This calibrating substance, D, gives

$$S_5 K = C_D (F_D - F_1) \tag{30}$$

where C_D is the volume fraction of calibrant D. It is not a necessary condition, but the algebra can be simplified if the calibrants are prepared at equal concentrations, that is, $C_D = C_c = C$.

Continuing, Eqs. (24) and (26) can be combined, yielding

$$F_x = F_c - K\left(\frac{S_3}{C} - \frac{S_1}{C_x}\right) \quad . \tag{31}$$

Equations (26) and (30), along with Eq. (31), can now be manipulated to give

$$F_x = F_c - \left(\frac{F_D - F_c}{\frac{S_5 - S_3}{C}}\right)\left(\frac{S_3}{C} - \frac{S_1}{C_x}\right) \quad . \tag{32}$$

A determination of C_x using Eq. (28), knowledge of F_D and F_c and application of Eq. (32) will allow one to determine F_x. As previously mentioned, F_D must be much different than F_c to maintain significance.

In this chapter, an optical rotation detector suitable for microbore liquid chromatography will be described. This system can be used to detect nonoptically active material in an indirect polarimetric mode. In addition, a method will be demonstrated using this detection system whereby quantitative information can be obtained without analyte identification.

Experimental

The reagents used in this study were reagent grade materials and no further purification was necessary. The ℓ-2-octanol (Aldrich Chemical Co., Inc., Milwaukee, WI) has an $[\alpha]^{17} = -9°$ (neat). (±)-2-Methyl-1-butanol (Eastman Kodak Co., Rochester, NY) was used without purification. The (-)-2-methyl-1-butanol (Eastman Kodak Co., Rochester, NY) has a listed purity of 83% minimum (by NMR) and was further purified by two treatments with decolorizing carbon followed by passage through a 2-in. silica column. Water was deionized in a conventional system.

The mobile phase was a 50:50 mixture of acetonitrile with either the (±)-2-methyl-1-butanol or the (-) isomer. All eluents were degassed under vacuum using ultrasonic agitation to minimize degassing in the cell. The chromatographic system consists of a syringe pump (ISCO, Lincoln, NE, model 314), a 25 cm x 1.0 mm 5-μm microsphere C18 chromatography column (Alltech Associates, Inc., Deerfield, IL), and a 0.5-μL sample loop coupled to an internal loop injection valve (Rheodyne, Berkeley, CA, model 7410). The flow rate used in this study was 20 μL/min.

The arrangement of an optical rotation detector for LC has been reported earlier (67,68). Several modifications necessary to adapt the system to microbore LC were made. A 33-cm lens was used to focus 20 mW of 488-nm radiation from an argon ion laser through the detector microcell. The previously reported detection/modulation cell (68) was used in the static mode (CH_3CN as the medium) and modulated at a frequency of 1 kHz. Figure 11 is a schematic representation of the laser-based mi-

Figure 11. Schematic of laser-based micropolarimeter

LASER	Argon ion laser
L	Lense; 33 cm
P	Polarizer
DC	DC solenoid and power supply
CL	Detection cell, 1 μℓ
MD	Modulation solenoid
A	Analyzer
AP	Aperture
F	Line filter
PMT	Photomultiplier tube
SG	Signal generator
LIA	Lock-in amplifier
CH	Chart recorder
IF	Computer interface
PDP/11	Computer
PU	Pump

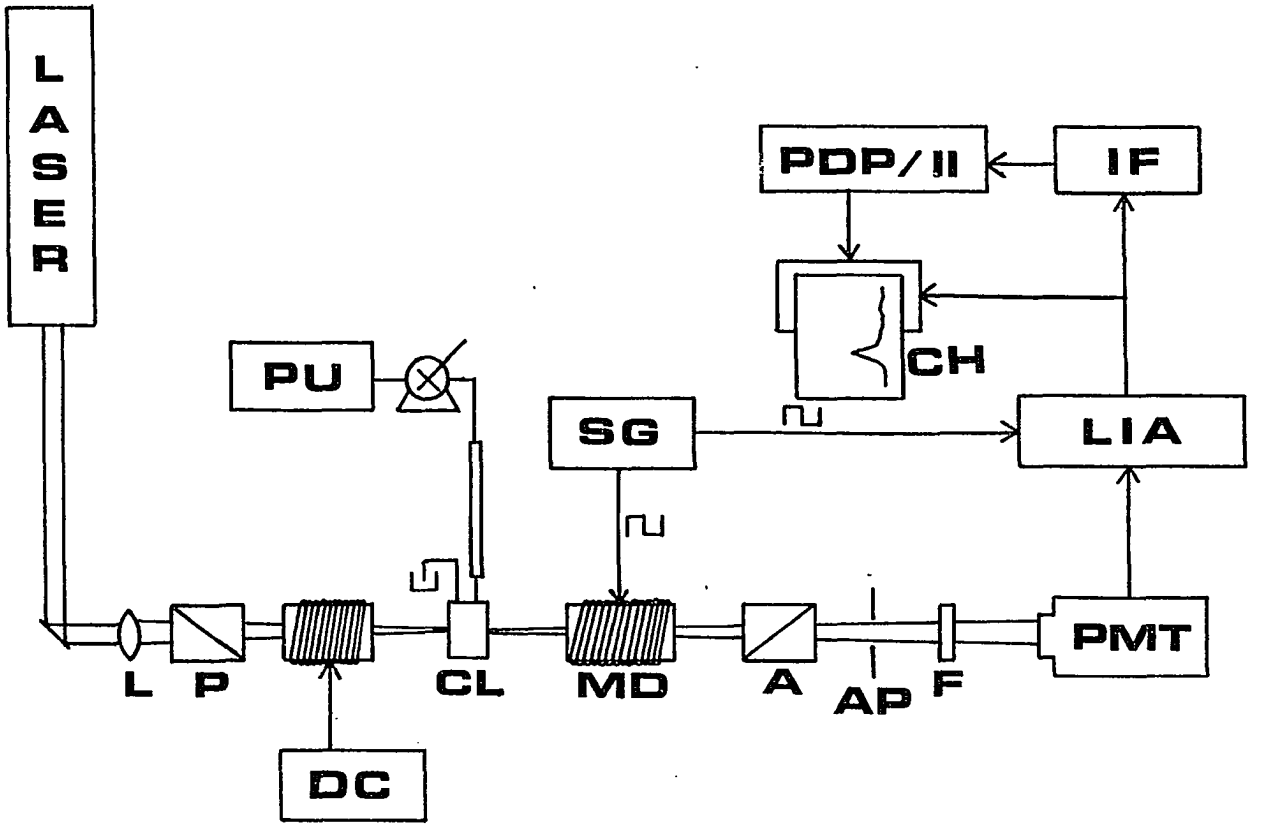
LASER
PDP/11
IF
CH
PU
SG
LIA
L
P
CL
MD
A
AP
F
PMT
DC

crovolume polarimeter. The same care (67) needed to choose windows for the detection cell was applied to the modulation cell. It was found that with proper care, the modulation cell did not degrade the favorable extinction ratio. The microcell was constructed in-house (Fig. 12) and has a volume of 1 μL for a 1-cm path. Using an independent air-based Faraday rotator to provide a standard optical rotation, laser power drift and overall system performance can be monitored. Comparing the signal produced by this DC coil with the base line noise when CH_3CN is flowing at 20 μL/min, we have determined that the detectability of the system is 1.5×10^{-5}° (S/N = 3) for a time constant of 3 s.

The output of the detector was connected to a digital voltmeter (Keithley, Cleveland, OH, model 160B), the analog output of which was in turn connected to a computer (Digital Equipment, Maynard, MA, model PDP 11/10 with LPS-11 laboratory interface). The computer takes a reading every 0.05 s and averages a set of five before storing the information. An analyte peak may be defined by 150-200 of these averaged data values. The area is determined by summation of adjusted values above a chosen baseline for each peak. These areas are then normalized against the signal obtained from the DC coil for each chromatographic trial.

Results and Discussion

Microbore LC-ORD

To evaluate the performance of the microbore LC optical rotation detection system, fructose was eluted from a C18 microbore column with deionized water. The limit of detection (LOD) for fructose was deter-

Figure 12. Microcell for ORD measurements in microbore LC: diameter, 2.54 cm; pathlength, 1 cm

(B) Bore, 0.034 cm
(E) Entrance port, o.d. 0.16 cm, i.d. 0.013 cm
(X) Exit port, o.d. 0.16 cm, i.d. 0.025 cm
(C) LC column

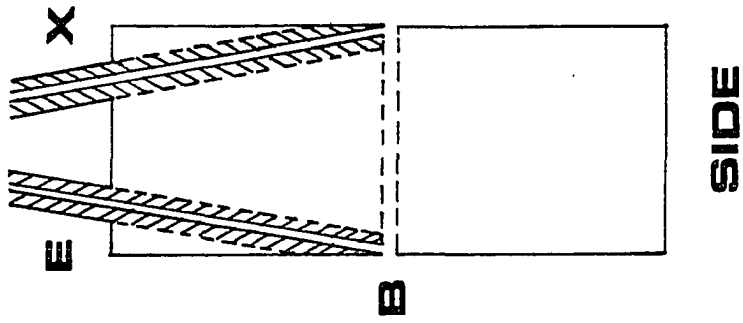
X
E
B
SIDE

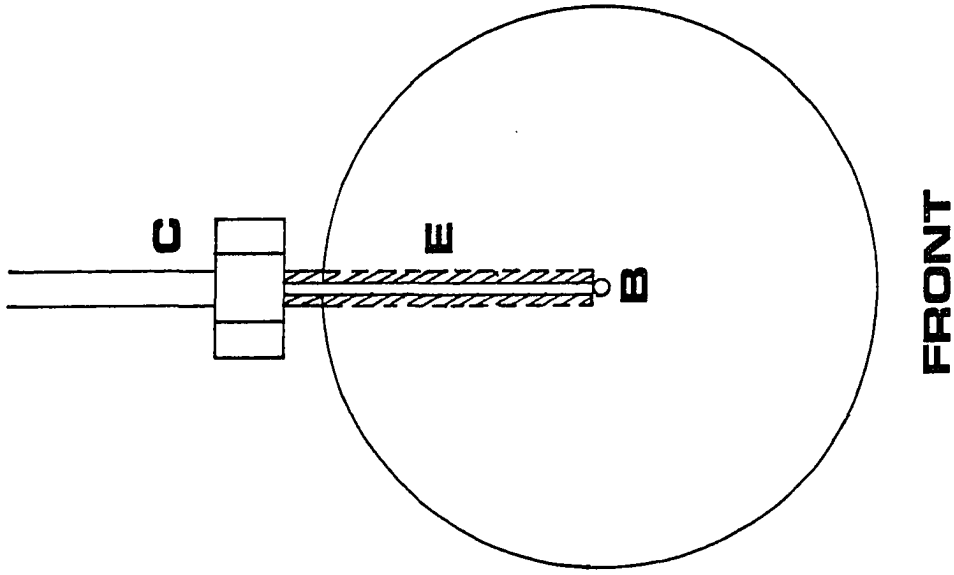
C
E
B
FRONT

mined to be 11 ng of injected material (S/N = 3). This can be compared to the conventional LC-ORD system which had a limit of detection for fructose of 100 ng (68). The improvement in the LOD despite the shorter path length is a result of increased sensitivity due to the high efficiency of the microbore column. The microcell and microbore column are better matched for maximum performance than the conventional size column/cell combination of reference 68. It should be noted that a reverse-phase C18 column with water as the eluent is not the most efficient system for the evaluation and separation of carbohydrates. Analysis of the fructose peak width at half height showed this column to have approximately 13000 plates/m for this eluent. This is a factor of 7 less than the manufacturer's specifications. Therefore, the limit of detection could be lowered by improving the column performance.

To assure that the microcell was not causing any postcolumn broadening, ℓ-2-octanol was injected with CH_3CN as the eluent. This system is better suited to the C18 column. Again, by use of the peak half-width and the retention time, the microbore column was shown to possess approximately 100,000 plates/m for a solute with k' = 2.1. This agrees well with the manufacturer's specifications. This shows that the microcell is of sufficiently small volume to maintain the efficiency of the 1-mm column.

To facilitate alignment of the microcell, the cell was mounted on a positioner which enabled the cell to be translated in the plane perpendicular to the direction of propagation of the argon ion laser. Also, the cell was first flushed with methanol to wet the channel and windows,

and then the chosen eluent was pumped through. With degassed eluents, the system operated with only minor optical adjustments for a period of over 1 month.

It is interesting to consider what is the smallest volume cell that can be built, because this will determine the size of the column this ORD system would be compatible with. The path could be made shorter to decrease the volume, but this would result in a decreased detection limit. It is better to consider the diameter of the argon ion laser beam ω_0, after being focused by a 25-cm lens. Actually, $2\omega_0$ is necessary to pass most of the energy in the laser beam. A 25-cm focal length lens will give a beam diameter ($2\omega_0$) of 0.12 mm. Therefore, it should be possible to construct a cell which would be compatible with a microbore column of 200 μm i.d. The cell inner diameter used here was limited by the smallest drill bit available to us. A 25-cm focal length lens would make possible a cavity (polarizer to polarizer) of 50 cm. There is then sufficient space for the DC coil and the modulation cell.

Indirect polarimetry

The concept of indirect polarimetry can best be visualized by inspection of Fig. 13. When a cuvette containing an optically active substance is placed in the cavity of a polarimeter operating at the point of maximum extinction, the sample induced rotation will cause light to pass through the analyzer. This situation is represented by the cuvette with the open circles and is analogous to a flowing stream of some optically active compound. The analyzer can now be rotated so that a new point of maximum extinction will be obtained.

Figure 13. Representation of indirect polarimetry: open circles, optically active species; closed circles, nonoptically active species engaged in equal volume displacement

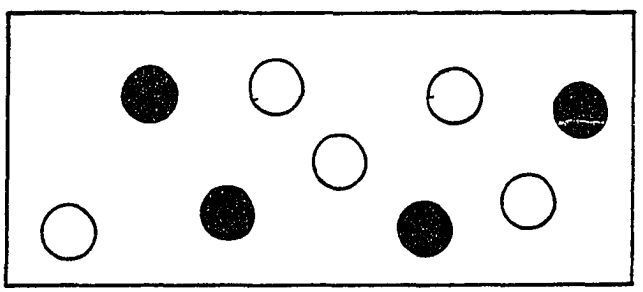

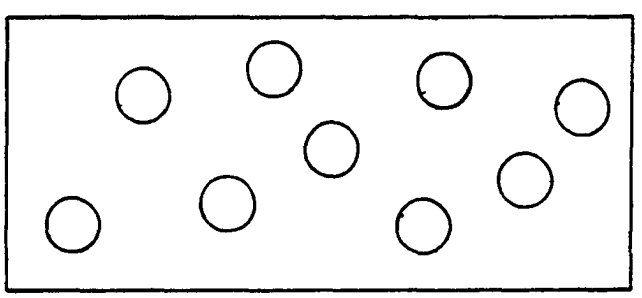

Now, if some of the optically active molecules in the cuvette are replaced by optically inactive molecules, the net rotation will no longer be the same and the plane of polarization of the light leaving the cuvette will no longer be parallel to the axis of minimum transmission defined by the analyzer. Therefore, light will pass the analyzer and reach the photodetector. This case is represented by the second cuvette where some optically active molecules have been replaced by optically inactive ones (filled circles). This, naturally, is analogous to the elution of an optically inactive compound in a flowing optically active stream and is the basis for the concept of indirect polarimetry.

Figure 14A shows the first reported detection of optically inactive materials by indirect polarimetry. This scheme utilizes an optically active eluent, in this case (-)-2-methyl-1-butanol in CH_3CN. The use of exotic solvent systems is possible with microbore LC. For example, a conventional 4.6-mm column operated at 0.75 mL/min for 8 hours would use the equivalent of $1.30 of reagent grade CH_3CN. In comparison, a microbore column operated at 30 µL/min with an eluent composed of 50:50 CH_3CN:(-)-2-methyl-1-butanol would use $0.83 of eluent. The difference would be about five times greater for HPLC grade acetonitrile.

The key to this indirect polarimetric scheme is the ability to null out the rotation due to the eluent without electronic suppression. This results in constant sensitivity in going from an optically inactive eluent to one possessing an optical rotation. Specifically, the detectability was determined to be $1.5 \times 10^{-5}°$ (S/N = 3) in pure acetonitrile and $1.5 \times 10^{-5}°$ (S/N = 3) in 50:50 acetonitrile:(-)-2-methyl-1-butanol.

Figure 14. Chromatograms of mixture one in two eluents of differing optical activity. Flow rate: 26 μℓ min^{-1}, Eluent A: (-)-2-methyl-1-butanol, B: (±)-2-methyl-1-butanol. Each eluent is a 50:50 mixture with CH_3CN

(1) injection peak
(2) ℓ-2-octanol
(3) decane
(4) tetradecane
(5) hexadecane

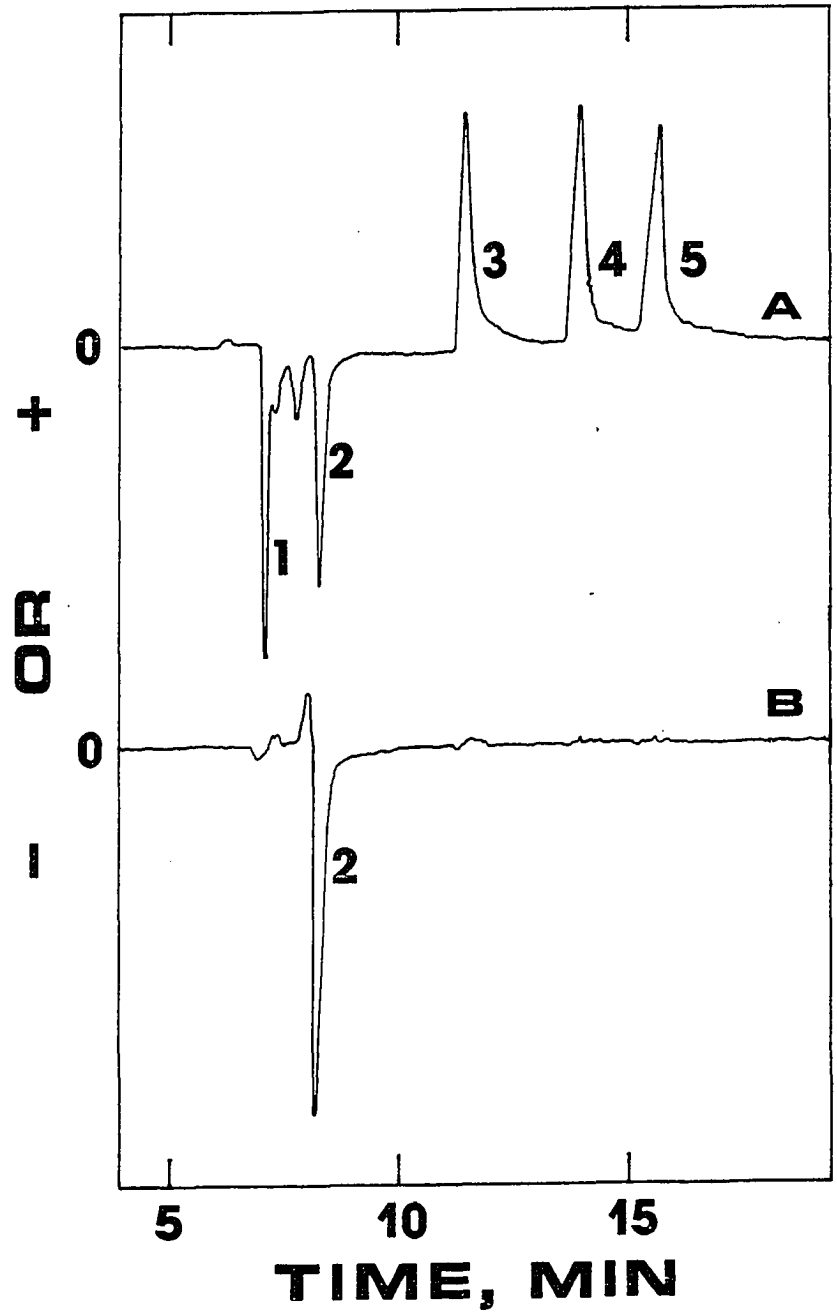
3
4
5
A
0
+
2
1
OR
B
0
I
2
5
10
15
TIME, MIN

In order for the detectability to remain the same, the base line noise must be constant in going from the optically inactive to the optically active eluent. Since optical activity is a number density effect, pump pulsations could cause severe noise problems. However, by using a syringe pump and microbore LC, we found that the base line noise did not increase with the optically active eluent.

A 50:50 solution of acetonitrile and (-)-2-methyl-1-butanol has an $[\alpha]$ of -2.95°. The detection limit for dodecane in this eluent was 390 ng (S/N = 3,3 s time constant). It should be possible to choose an eluent with an $[\alpha]$ of 100°. In this eluent, assuming that the base line noise does not increase, a detection limit of 12 ng of optically inactive material (S/N = 3) could be realized.

In evaluation of the detector system for quantitative analysis, it is not a necessary prerequisite that the detector response be linear with concentration. However, to determine quantitative information without bracketing standards as proposed in this paper, it is critical that the detector response be linear with concentration. To test the microcell-optical rotation detection system, varying quantities of dodecane were injected into an eluent stream composed of a 50:50 mixture of CH_3CN and (-)-2-methyl-1-butanol. The injected amounts spanned the concentration range covered in this study. The result is a straight line with a slope of 0.96 and a correlation coefficient of 0.9999 when the normalized area, S_i, is plotted against the normalized concentration.

The detector response in this indirect polarimetric scheme is a result of the analyte displacing a corresponding amount (volume) of the eluent at the detector when the analyte elutes. The response is, thus, universal. This then is an alternative to the RI detector for LC applications. In fact, the potential to achieve a detectability of 12 ng in the small volumes achieved here makes indirect polarimetry much more attractive.

Quantitation without analyte identification

In this quantitation scheme, the sensitivity is dependent on the difference in optical rotation between the two eluents. This is because a large difference assures that the analyte will produce a signal in at least one eluent, and the differences $S_1 - S_2$ or $S_3 - S_4$ in Eq. (28) will be significant. It is useful to compare this to the absorption (147) and refractive index detectors (119). In absorption, as mentioned before, there is a limit as to how highly absorbing an eluent one can use. In a previous study (147), it was found that an eluent with an absorbance of 1.0 was the limit if one wants to maintain the sensitivity of the detector. For a detector that can measure an absorbance change of 2×10^{-4}, the system will have a dynamic reserve of 5×10^3. In refractive index detection (119), it is typical to use two eluents that differ in refractive index by 0.1 unit. If it is assumed that a typical RI detector can measure a change of 10^{-7} RI units, this system would have a dynamic reserve of 10^6. In comparison, the optical rotation detection system has a dynamic reserve of 10^7. Among all these detectors, ORD should then provide the best detectability.

Another clear advantage to this optical rotation detection scheme is in the chromatography. For reverse-phase separations, no difference would be expected in the chromatograms obtained in either eluent. This is due to the fact that one eluent is the racemic analogue of the other. Therefore, one will not observe changes in elution order with the result that each peak can be accounted for without the need for a time-consuming consistency test (148).

The system was calibrated for detector response by multiple injections of dodecane in each eluent. It should be noted that for any particular eluent and set of chromatographic conditions (flow rate, temperature, etc.), the calibrations need only be performed once. The results of the experiments are summarized in Table 7. S_1 and S_2 are the areas measured (three or more injections) by the computer for the two mixtures in each eluent. The elution times in each eluent are approximately the same, reflecting the similar chromatography in each eluent. The A/D interface used provides a value of 2048 for full-scale deflection, and the area of each peak for each chromatographic trial has been normalized against the signal from the DC coil, which produces an absolute rotation calibration. Also listed in the table are the true volume fractions and specific rotations. The value for the specific rotation of ℓ-2-octanol was given by the manufacturer. The errors associated with the calculated values are determined by standard procedures for propagation of errors.

From inspection of Table 7, several key points can be made. First, Eq. (28) predicts the true volume fraction with good accuracy, i.e.,

Table 7. Quantitation of sample components in two different mixtures[a]

		ℓ-2-octanol	$C_{10}H_{22}$	$C_{14}H_{30}$	$C_{16}H_{34}$
S_1[b]	(1)	-74105 ± 4818	120017 ± 4669	119664 ± 4872	127339 ± 3297
	(2)	-36386 ± 2314	59448 ± 3280	59389 ± 2563	62107 ± 3114
S_2[c]	(1)	-132644 ± 2863	4888 ± 812	3171 ± 1566	2939 ± 1623
	(2)	-65818 ± 2610	1712 ± 486	1870 ± 633	1735 ± 610
true C_x ($\times 10^{-2}$)	(1)	4.00	8.00	8.00	8.00
	(2)	2.00	4.00	4.00	4.00
true $[\alpha_x]^{20}_{590}$	(1)	-9°	0	0	0
	(2)	-9°	0	0	0
calcd C_x ($\times 10^{-2}$)	(1)	3.93 ± 0.38	7.74 ± 0.34	7.83 ± 0.36	8.36 ± 0.27
	(2)	1.98 ± 0.24	3.88 ± 0.23	3.87 ± 0.19	4.06 ± 0.22
calcd $[\alpha_x]^{27}_{488}$[d]	(1)	-8.0° ± 2.8	0.07 ± 0.2	0.01 ± 0.2	0.01 ± 0.1
	(2)	-7.9° ± 3.0	0.02 ± 0.3	0.02 ± 0.2	0.01 ± 0.2

[a]Normalized area when $C_{12}H_{26}$ is used as calibrant: eluent b = 91527 ± 696, eluent c = 2250 ± 556.

[b]Eluent (-)-2-methyl-1-butanol.

[c]Eluent (±)-2-methyl-1-butanol.

[d]Calculated using Eq. (29); $C_{12}H_{26}$ as calibrant.

with errors of approximately 4% or less. This is true for the optically inactive hydrocarbons as well as the ℓ-2-octanol. The largest error was seen in the determination of $C_{16}H_{34}$, which was 4.5% high for the more concentrated mixture. At this concentration, the analyte was present in quantities approaching the limit where the column starts to show decreased efficiency. The separation of $C_{14}H_{30}$ from $C_{16}H_{34}$ was such that the latter probably experienced a small contribution from the $C_{14}H_{30}$ peak. This could explain the high result. In support of this argument, one finds that the calculated volume fraction for this compound was only 1.5% high for the less concentrated mixture.

The largest source of uncertainty in the calculation of C_x is in the determination of S_1 and S_2. There are two ways to improve this. First, by use of more injections of each mixture, the precision in measuring the areas will improve. Second, by choosing an eluent with a larger rotation, the difference in the areas determined in each eluent will be large (i.e., $S_1 - S_2$ will be larger). This will reduce the uncertainty in the difference and result in a substantial reduction in the uncertainty in C_x.

If the $[\alpha]$ for the CH_3CN:(-)-2-methyl-1-butanol mixture is assumed to be -2.95°, Eq. (29) can be used to calculate F_x for all four analytes. The results are presented in Table 7 along with their respective uncertainties. The values for the hydrocarbons are again, within experimental uncertainties, equal to zero. The specific rotation for ℓ-2-octanol was calculated to be -8°, which is different from the manufacturer's stated value of -9°. This may be due to several reasons.

First, it is difficult to assess the relationship between the specific rotation determined at 17°C and 590 nm and the value from this experiment determined at 27°C and 488 nm. Second, to apply Eq. (29), the specific rotation of the eluent must be known. However, the (-)-2-methyl-1-butanol, as obtained from the manufacturer, had a purity of between 83% and 100%. Therefore, one of the major sources of uncertainty in the determination of F_x here was the uncertainty in the value for F_1. Since in LC, solvent mixtures are frequently used as eluents, Eq. (29) will be difficult to use if F_1 has a large uncertainty associated with it. It would be better, if an accurate value for F_x is needed (e.g., drug analysis, vida infra) to measure F_1 independently at the operating conditions. Third, error analysis shows that if F_1 is larger, F_x can be determined with more certainty.

Figure 14B shows a curious result: there are very small peaks visible for the hydrocarbons C10, C14 and C16 in the racemic eluent, i.e., at 11 min, 14 min and 16 min. This is due to the change in RI which occurs as the sample elutes. The peak concentration is large enough, and the RI change great enough to cause a slight disturbance. It should be noted that no change in beam position or shape could be visually detected as the analyte passes through the cell. These areas, however, do not significantly affect the calculated values since $S_1 - S_2$ is dominated by the areas in the optically active eluent.

Figure 14 also shows that the chromatographic behavior, as expected, is the same for each eluent. This should always be the case for reverse-phase chromatography. However, it has been found (149) that

this may not be always true for normal-phase separations with optically active mobile phases. In reference 149, it was found that by modifying the mobile phase with a large chiral molecule, diastereomeric chelate-like solvates are formed between the additive and enantiomeric pair in an equilibrium relationship, leading to their separation. In the quantitation scheme presented here, this would lead to different chromatography when going from the optically active to the racemic eluent. However, if the eluent molecule is small, such as the ones used here, this behavior will not occur and both eluents will give similar retention behavior. Two other examples of suitable eluents are ℓ-2-butanol ($[\alpha]_D^{20}$ = 14°) and d-3-methylcyclohexanone ($[\alpha]_D^{25}$ = +143.7°). The use of either compound should not be cost prohibitive for microbore chromatography. Further, the d-3-methylcyclohexanone should show a large dynamic range even when diluted 50% with a suitable modifier such as cyclohexane.

Finally, a useful application of this quantitation scheme would be in drug purity testing. In biological systems, usually only one enantiomeric form of a compound will show activity. The scheme presented here will provide quantitative information on the major components of a drug mixture. Quantitative information can be also obtained on any contaminants without the need to identify them. And, if the specific rotation of the pure active component is known, a determination of F_x by this method will give the enantiomeric purity of the drug.

Conclusions

An optical rotation detection system has been constructed that is compatible with microbore liquid chromatography. This detection system

can be used to detect optically active, as well as optically inactive materials. In the indirect polarimetric mode, the uniqueness of optical activity assures that this scheme approaches the ideal universal detector. Finally, by proper choice of two eluents with differing optical rotations, and the application of a simple equation, quantitative information can be obtained without the need for analyte identification.

CHAPTER IV. ABSORPTION DETECTION IN MICROCOLUMN LIQUID CHROMATOGRAPHY VIA INDIRECT POLARIMETRY

Introduction

Liquid chromatography (LC) using microcolumns has progressed such that new detection schemes are necessary to be compatible with elution volumes in the microliter to nanoliter range. The increased demands for high sensitivity due to the smaller injection volumes have made simple modifications of detectors suitable for standard LC columns unacceptable. On the other hand, those detection schemes that are inherently suitable for small elution volumes, or are cost-prohibitive because of the specialized mobile phase or stationary phase, have benefited from the development of microcolumns. Recent work in adapting electrochemical (150) and mass spectrometric (151) detection schemes to microcolumn LC have been reported. For optical detectors, the laser has received much interest as a light source. The pertinent properties of the laser which make it useful as a source in microcolumn LC have been described in detail (63). Recent work (53,152,153) with laser-excited fluorescence detection for microbore and open tubular LC demonstrates the utility of the laser. Also, a laser-based optical rotation detection system for microbore chromatography (146) has been shown to be both very sensitive and selective.

The unique selectivity of the polarimetric detector for LC is due to the fact that optical activity is normally a characteristic of biological activity. As such, it is a rare property. As shown in Chapter III, it is also possible (146) to convert this very selective detector

to a universal detector as an alternative to the common refractive index detector for LC. In this scheme, an optically active eluent is used in conjunction with a laser-based micropolarimeter. The signal due to the eluent can be nulled out optically by rotating the analyzer an amount equivalent to the rotation of the eluent. Since the signal due to the eluent is optically, rather than electronically compensated for, the signal to noise ratio (S/N) of the system is preserved. As an optically inactive compound elutes, it replaces an equal amount of the eluent in the detector cell, and a decrease in optical rotation will be observed. A signal will be obtained as long as the analyte has a specific rotation different from that of the eluent. This then is the basis for indirect polarimetry (146). Its success naturally depends on the reduced solvent cost when interfaced to microcolumns.

Absorption detection for LC remains one of the most used methods. Routine miniaturization of conventional absorption detectors sacrifices detectability because of the shorter pathlength and the reduced light throughput. The usual transmission mode of absorption detection is being supplanted by various calorimetric methods which probe the absorption indirectly (154,155). Principal among these has been thermal lens calorimetry (153,156-158). A critical consideration there is the laser beam profile, which must be reproducible in its cross-sectional intensity distribution. Lasers in the UV region and high power lasers usually do not meet this criterion. A more general approach is to probe the bulk number density change in the optical region after heat is produced from the absorption process.

For example, the bulk density change can be monitored by detecting the change in the refractive index of the medium using a Fabry-Perot interferometer (155). The refractive index change can then be related to the amount of light absorbed by a simple expression. For a polarimetric detection scheme, if an optically active eluent is used, the heating effect produces an expansion in the liquid. This results in fewer molecules in the detection region and a decrease in optical rotation is detected.

This concept can best be illustrated by inspection of Fig. 15. Cell A is filled with an optically active substance and the analyzer is rotated an amount equal to the solvent induced rotation. Therefore, as discussed in Chapter III, the extinction ratio of the polarimetric system will be preserved. In cell B, some of the optically active solvent molecules have been replaced by optically inactive ones. The net rotation is now different than for cell A, and the amount of difference is detected by the technique of indirect polarimetry. Cell C contains some substance that absorbs at the detection wavelength. The absorption induced expansion, as mentioned previously, results in less molecules in the detection cell. This decrease in rotation can be detected by the polarimetric system, and serves as the basis for the technique of absorption detection via indirect polarimetry.

Theory

To determine the relationship between the amount of light absorbed and the observed rotation, two assumptions are necessary. First, the

Figure 15. Representation of the concept of absorption detection via indirect polarimetry. Cell A contains an optically active species (open circles). Cell B illustrates the equal volume displacement of optically active molecules with optically inactive ones (closed circles). In Cell A, absorption induced expansion results in fewer molecules in the detection volume

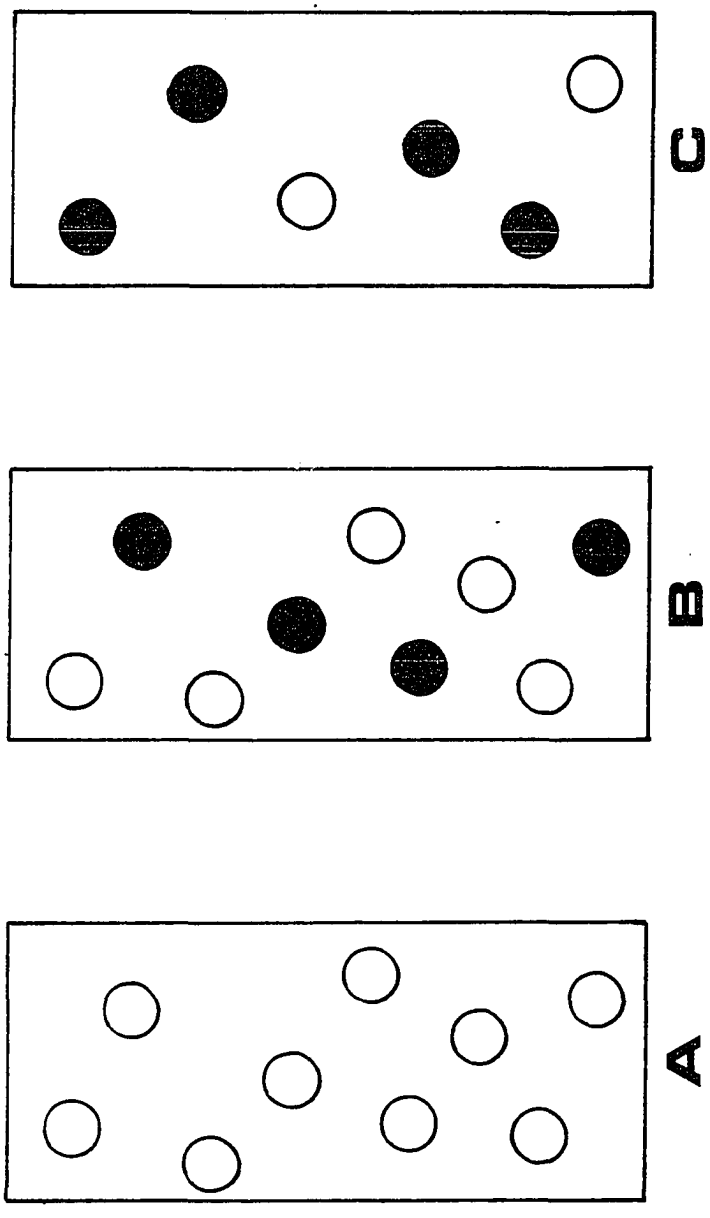
C
B
A

amount of light absorbed is equal to 2.303 AI, where A is the absorbance of the sample and I is the intensity of the source in joules. This is true only for small absorptions, but this covers most of the interesting cases in LC. Second, it is assumed that all the light absorbed eventually becomes heat. With these two conditions met, the temperature increase, $\Delta T(K)$, in the interaction region of cross-sectional area a cm^2, and unit length is

$$\Delta T = \frac{2.303\ AI}{C_p \rho a} \tag{33}$$

where C_p is the specific heat of the solvent in J $g^{-1}K^{-1}$ and ρ is the density of the medium in g cm^{-3}.

The rotation α observed for a mixture is related to the individual specific rotations $[\alpha]_i$, such that (146)

$$\alpha = \Sigma[\alpha]_i \ell \rho_i V_i \tag{34}$$

where ℓ is the pathlength (dm) and V is the volume fraction of the material at the detector. For low solute concentrations (which is the more interesting case), one can assume that the absorption-induced rotation is entirely due to the eluent, so that $\alpha = [\alpha]\ell\rho$. This can be expanded to give

$$\alpha = [\alpha]\ell \frac{\rho}{V_{SOL}} \cdot V_{SOL} \tag{35}$$

where V_{SOL} is the volume of the solution. Application of simple differential calculus to Eq. (35), and making use of the relation dV = dT • dV/dT produces Eq. (36)

$$d\alpha = [\alpha]\ell \frac{\rho}{V_{SOL}} dT\left(\frac{dV_{SOL}}{dT}\right) \quad . \tag{36}$$

The change in volume with temperature is equal to the coefficient of expansion, B, times the solution volume (159), or

$$\frac{dV}{dT} = BV_{SOL} \quad . \tag{37}$$

Substitution of Eq. (37) into (36), and noting that the case of small absorptions is being considered here, gives

$$\Delta\alpha = [\alpha]\ell\rho B\Delta T \quad . \tag{38}$$

Finally, substituting into Eq. (33), one obtains an explicit relation between the absorbance of the solution and the observed rotation

$$A = \frac{\Delta\alpha a C_p}{2.303[\alpha]\ell IB} \quad . \tag{39}$$

To assess the potential of measuring absorption via indirect polarimetry, Eq. (39) can be used to estimate the minimum detectable absorb-

ance. The micropolarimeter of reference 146 has a detectability of 1 x 10^{-5} degree (S/N = 3). Using typical values for the other parameters, a = 9 x 10^{-4} cm^2, C_p = 1.8 J $g^{-1}K^{-1}$, $[\alpha]$ = 192.0 degree cm^3 g^{-1} dm^{-1}, ℓ = 0.1 dm, J = 8.0 x 10^{-2} J and B = 1.24 x 10^{-3} K^{-1}, one finds that the minimum detectable absorbance is 3 x 10^{-6}. This is superior to conventional absorption detectors in LC.

This chapter will report improvements in detectability for indirect polarimetry (146), and show how one can use this concept as either a universal or absorption detector for LC.

Experimental

All reagents and eluents were reagent grade and used without further purification. (R)-(+)-Limonene (97%, $[\alpha]_D^{24}$ = +106°: c = 1, CH_3OH), (+)-α-pinene (98%, $[\alpha]_D^{22}$ = 47.1°), and N-methyl-o-nitroaniline were obtained from the Aldrich Chemical Company. Limonene and pinene were used either undiluted, or diluted with 5% iso-octane (UV grade), as eluents. All eluents were degassed under vacuum using ultrasonic agitation to minimize degassing in the cell. Dioctyl-, dibutyl-, diethyl- and dimethyl-phthalate were obtained as part of a phthalate ester kit (Supelco, Inc., Bellefonte, PA #4-8762).

Absorptivity data for N-methyl-o-nitroaniline were measured in a spectrophotometer (Shimadzu Corp., Kyoto, Japan, model UV-240). A 2.3 x 10^{-2} mg/mL solution of N-methyl-o-nitroaniline in cyclohexene produced an absorbance of 0.157 at 458 nm, and 0.017 at 488 nm (1 cm path). This

corresponds to molar absorptivities (L/mol. cm) of 1040 and 112 at 458 and 488 nm, respectively.

The chromatographic system consists of a syringe pump (ISCO, Lincoln, NE, model 314), a 25 cm x 1.0 mm 10-μm silica chromatography column (Alltech Associates, Inc., Deerfield, IL), and a 0.5 μL sample loop coupled to an internal loop injection valve (Rheodyne, Berkeley, CA, model 7410). Flow rates used in this study ranged from 20 to 30 μL/min.

A laser-based optical rotation detection (ORD) system suitable for use with microbore chromatography has previously been described (67,146). Briefly, this system utilizes an argon ion laser (Control Laser Corp., Orlando, FL, model 553A) focused through a 1 μL detection cell. For this study, the laser was operated at either 458 nm or 488 nm, with powers ranging from 20 to 75 mW. To function with normal-phase eluents, the cell windows are attached using a different adhesive (Balkamp High Tack Adhesive, #765-1217, Permatex Co., Kansas City, KS). The adhesive has a very fast setting time which makes it difficult to work with. However, it could be diluted with small amounts of a solvent such as 2-butanone. This enabled careful adhesive placement without affecting the properties of the set glue.

Results and Discussion

Figure 16 shows the detection of a phthalate mixture separated on a 10-μm silica column using an eluent composed of 95:5 limonene and iso-octane. The first peak is an injection peak, while peaks 2-4 represent

Figure 16. Detection by indirect polarimetry. Eluent, 95:5 (R)-(+)-limonene:isooctane; flow rate, 24 µL/min; column, 25 cm x 1 mm i.d. 10-µm silica

(1) injection peak
(2) dioctyl phthalate
(3) dibutyl phthalate
(4) diethyl phthalate

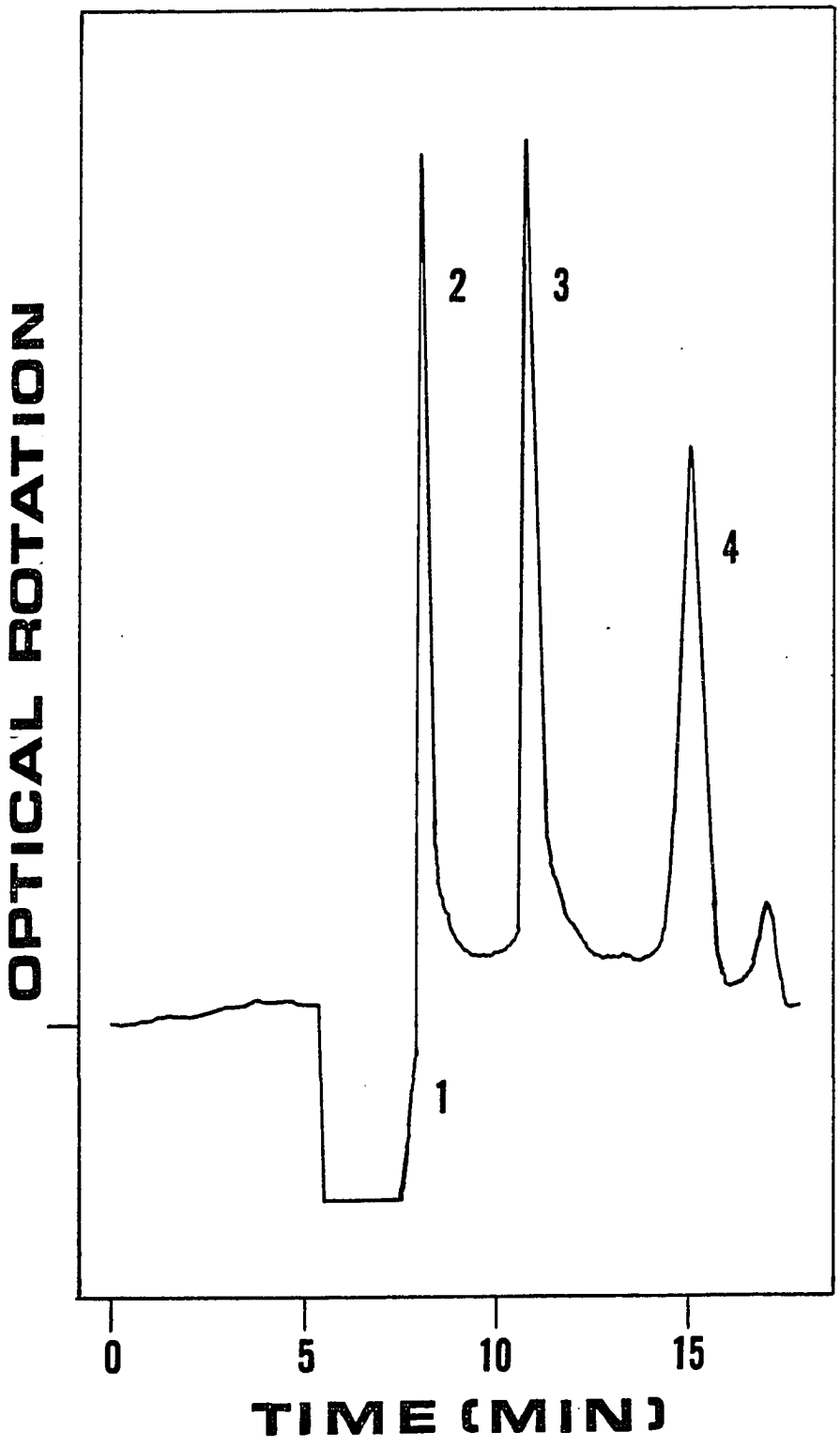
OPTICAL ROTATION
1
2
3
4
0
5
10
15
TIME (MIN)

dioctyl, dibutyl and diethyl phthalate, respectively. The injection peak is a result of the displacement of solvent molecules from the surface of the silica as solute molecules are adsorbed. A small impurity peak is evident after peak number 4, signifying a contaminant in one of the phthalate esters. Figure 16 demonstrates the universal response for this detection scheme, as it is obvious that none of the phthalate esters are optically active. Only in the unlikely case in which an eluting solute has exactly the same specific rotation at the probe wavelength as the eluent would the solute not give a response. This is actually even more uncommon than the case for refractive index (RI) detection when a solute and the eluent have the same RI. From Fig. 16, we find that the detector used in this mode has a limit of detection for dibutyl phthalate ($k' = 1.2$) of 12 ng ($S/N = 3$) of injected material. This is superior to RI detectors, especially considering the small cell volume.

These results can be compared to those presented in Chapter III. The detectability is comparable to that obtained previously by polarimetry for optically active materials (146), and is better than that obtained previously by indirect polarimetry for optically inactive materials (146) by a factor of 33. The improvement is due to the use of the highly optically-active eluent ($[\alpha]_{488} = 166$ cm^3/g dm measured). We have found the main sources of noise for these optically active eluents to be either acoustical or thermal in nature. Thermal fluctuations are a serious problem since optical activity is a number density effect. Heating or cooling of the laboratory causes baseline drifts very much

like those in RI detectors. The slower eluent flow rates and the smaller cross-sectional areas of the tubings in microcolumns actually allow better thermal equilibration compared to the larger columns. Thermal drifts were further minimized by enclosing the microbore column in a cloth sheath. Additional improvement would be expected if the entire chromatographic setup (injector, column, connecting tubing, etc.) could be contained in a thermostat-controlled enclosure.

Figure 17 demonstrates the use of the indirect polarimetric scheme as an absorption detector. The three chromatograms represent data taken at three different laser powers, and have each been normalized against the standard rotation produced by a DC solenoid (67) to maintain constant sensitivity. Peak #2 is the indirect polarimetric signal resulting from the elution of dimethyl phthalate, and the peak height is approximately equal in the three chromatograms. Peak #1 is the signal for N-methyl-o-nitroaniline by the method of absorption via indirect polarimetry. The peak height increases linearly with increasing laser power as predicted by Eq. (39). The result is a linear calibration plot corresponding to laser powers from 31 to 55 mW with a correlation coefficient of 0.994. Figure 17 shows that one can use the same experimental setup for universal detection and for absorption detection by simply changing the laser power. Peaks that do not change with laser power correspond to indirect polarimetry, and peaks that vary with laser power are due to absorption processes.

N-methyl-o-nitroaniline has a small absorption at 488 nm (ε = 112). Even so, the limit of detection (LOD) with 32 mW of 488 nm radiation is

Figure 17. Normal-phase separation of N-methyl-o-nitroaniline and dimethyl phthalate. Chromatographic conditions were identical to those in Figure 15, except that 100% limonene was used. λ = 488.0 nm

(1) injection peak
(2) absorption detection of 890 ng of N-methyl-o-nitroaniline
(3) indirect polarimetric signal from 2 µg of dimethyl phthalate, A - 31 mW, B - 48 mW, C - 55 mW

OPTICAL ROTATION
TIME (MIN)
0
10
0
10
0
10
A
B
C
1
2
3
1
2
3
1
2
3

7 ng (S/N = 3) of injected material. This is better than the LOD for the indirect polarimetric detector. To really take advantage of the absorption process, one must use higher laser powers or rely on larger absorptivities. To better match the absorption profile of N-methyl-o-nitroaniline, the experiment was repeated at 458 nm. At this wavelength, N-methyl-o-nitroaniline has a molar absorptivity of 1040. The mass detectability, as determined from Fig. 18 using 73 mW of power, was found to be 36 ng (S/N = 3) of injected material. This corresponds to an absorbance LOD of 1.8×10^{-6} absorbance units (peak volume 28 μL, S/N = 3). In Fig. 18, the baseline shift early in the chromatogram is an artifact due to the torque produced while switching the injection valve. This stabilizes after 9 min and does not affect the analyte peak. The improved LOD is also aided by a larger $[\alpha]$ for limonene at 458 nm (= 192 cm^3/g dm, measured) and a lower amount of solvent absorption at this wavelength. The observed detectability is in excellent agreement with that predicted in the theory section. α-Pinene was also investigated as an optically active eluent. The LOD for N-methyl-o-nitroaniline in this system was 17 ng of injected material (S/N = 3, 488 nm, 30 mW). This result is consistent with the limonene results, after correction for laser power and differences in eluent optical activity.

At higher laser powers, misalignment of the beam due to thermal lensing (i.e., clipping in passage through the cell, etc.) would become more critical. It should be noted that thermal lensing does not affect our signal at moderate laser powers because the entire laser beam is sent to the phototube. Since this work is performed using a continuous

Figure 18. Absorption detection based on indirect polarimetry. λ = 457.9 nm, laser power = 73 mW. Chromatographic conditions were identical to those in Figure 16

(1) injection peak
(2) 940 pg of N-methyl-o-nitroaniline

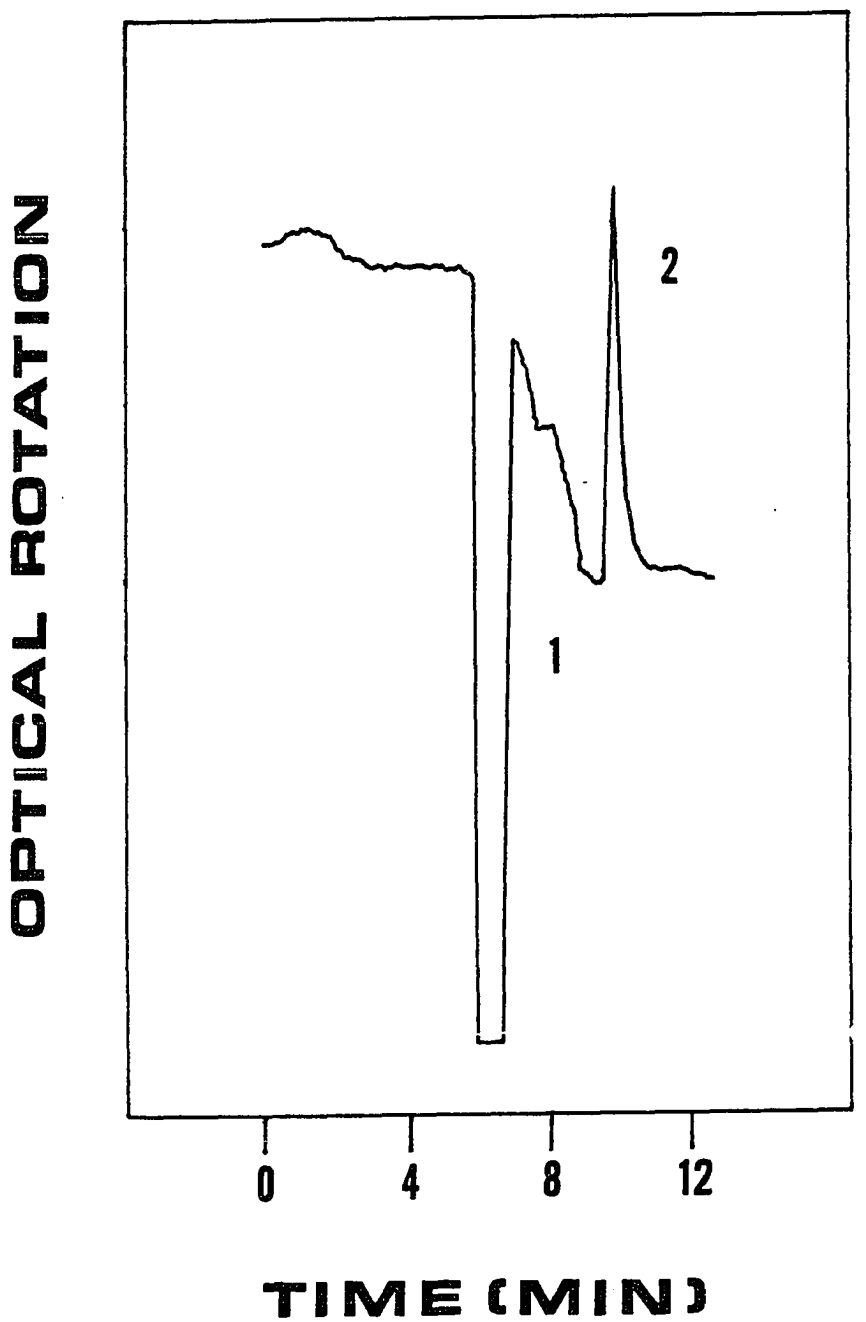
OPTICAL ROTATION
2
1
0
4
8
12
TIME (MIN)

wave laser (1 s time constant), the appropriate volume to consider in Eq. (33) is the volume of the cell, even though the volume illuminated by the laser may be much smaller. In principle, it should be possible to reduce the cell volume to match the optical region. If one assumes that the beam waist of a focused laser beam is 0.10 mm for a laser power of 100 mW, it should be possible to detect absorptions of the order of 8×10^{-8} cm^{-1}. It may also be possible to introduce the same energy in a much shorter period of time using a second pulsed laser. The instantaneous signal should be larger than the thermally-equilibrated signal. Temporal dependence (160) can also be used to distinguish the absorption process from other optical rotation processes.

It may be useful to compare this absorption detector with the thermal lens absorption detector of reference 153. Both detectors have been shown to be compatible with microcolumn chromatography. Although a smaller volume was demonstrated in reference 153, one should be able to reduce our cell volume to 100 nL by shortening the pathlength to 1 mm. Then, our absorbance LOD will become 1.8×10^{-5} absorbance units, which is still slightly better than the 4.5×10^{-5} value (S/N = 3) reported in reference 153. Furthermore, the laser power used here is only 1/10 of that in reference 153, and this can potentially result in additional enhancements. The mass LOD is comparable to that in reference 153, but since the injection volume used in this work is 100 times larger, our concentration LOD is substantially better. As discussed previously (153,161), absorption methods cannot compete with fluorescence methods, but then most molecules do not fluoresce.

The strict dependence of the thermal lens experiment on the cross-sectional intensity distribution of the absorbed laser beam can be a disadvantage in many situations. This is due to the fact that many lasers which lase in the ultraviolet region do not possess good spatial beam qualities. However, since most organic molecules absorb at wavelengths below the visible region, this can limit the usefulness of the technique. In comparison, absorption via indirect polarimetry is not dependent on the spatial characteristics of the absorbed laser beam. Therefore, its potential usefulness is greater than the thermal lens technique given the current state of laser technology.

Conclusions

The concept of indirect polarimetry has been shown to be a very sensitive detector for microbore chromatography. The uniqueness of optical activity assures the universal response of this detection scheme which is capable of detecting optically inactive materials at the 10 ng level. For an eluting solute that absorbs at the probe wavelength, picogram detection limits are possible. The combination of a microvolume detection cell with simultaneous polarimetric, indirect polarimetric, and absorption detection make this system unique.

CHAPTER V. ANALYTICAL APPLICATIONS OF THE RAMAN INDUCED KERR EFFECT

Introduction

The Raman effect was experimentally verified in 1928 by C. V. Raman (162,163). Over the past thirty years, Raman spectroscopy has been an important tool in the field of biological analysis. The use of the laser as the excitation source in Raman spectroscopy, and improvements in photon detection have shortened the time needed for analysis from days to seconds, or fractions of a second (164). Raman spectroscopy has several unique advantages (165) which make it useful for the analysis of chemically interesting systems, specifically biomolecular species. These advantages include the ability to analyze aqueous samples, and the amount and type of structural information obtainable. Additionally, since the entire spectrum is obtained in the same instrument and cell, more information can be obtained in a shorter time frame than in, for example, infrared spectroscopy. Raman methods are also excellent for the analysis of low frequency modes where other methods present serious experimental difficulties.

One disadvantage inherent to Raman spectroscopic techniques is the low efficiency of the Raman scattering process. Only about 10^{-8} of the photons incident on the sample are inelastically scattered. If the properties of the species of interest permit, the resonance Raman enhancement can account for improvements of 10 - 1000 times the normal Raman scattering cross section. A good example of the usefulness of Raman spectroscopy in bioanalysis is in binding studies of DNA to sev-

eral medically significant drugs to ascertain the mechanism of action. Raman and resonance Raman excitation profiles of DNA complexes of adriamycin (166) and actinomycin (167) have been reported. The Raman spectra of these complexes allowed these researchers to determine the vibrational structure of the lowest excited electronic state of the complex, and this information was useful in determining the interaction mechanism between the nucleic acid and these drugs. For dynamic processes, time-resolved Raman spectroscopy has been used to follow the photochemical cycle of bacteriorhodopsin (168). A recent review has an extensive listing of biological investigations made possible by the information available from a Raman spectral analysis (169).

If a Raman spectrum is obtained for molecules adsorbed on or near the slightly roughened surface of certain metals, enhancements of as much as 10^6 can be realized over normal Raman. This phenomenon, named surface enhanced Raman (SER) has proven very useful for investigations into the processes occurring at surfaces (170). However, only recently has the analytical capabilities of the technique been investigated (171), and present work is involved with extending the phenomenon to surfaces other than the few it has been observed with now (172).

From the above survey, and from recent reviews (173), it is clear that the type of information available from the Raman technique is quite useful for answering a variety of chemical questions. However, a major disadvantage of Raman spectroscopy is the difficulty in analyzing fluorescing samples because the fluorescence signal can completely overwhelm the Raman spectrum. A variety of experimental techniques have been

devised to minimize this problem including modulating the polarization of the laser (174), modulation of the laser frequency (175), and using gated detection to effect time discrimination of the luminescence background (176). Modulation of the source polarization takes advantage of the fact that some Raman transitions are strongly polarized, while frequency modulation exploits the narrow spectral characteristics of Raman lines compared to the generally broad nature of fluorescence. Additionally, since Raman signals are coincident with the excitation, gated detection can help minimize the contribution from the longer lived fluorescence.

Coherent Raman techniques were developed, in part to overcome the fluorescence limitation of spontaneous Raman spectroscopy. Fluorescence rejection can be accomplished either spatially (signals are either laser-like or encoded on a laser beam), or spectrally (the signal is obtained at a higher frequency). Of the many coherent techniques now discovered, coherent anti-stokes Raman spectroscopy (CARS) is the most used, especially for biological investigations (177,178). CARS is a wave-mixing technique and the resultant signal is superimposed on a broad, nonresonant background. This can lead to high limits of detection restricting the usefulness of CARS in many applications.

In 1964, a new coherent Raman technique, spectroscopy by inverse Raman scattering (SIRS) was first observed by Jones and Stoicheff (179). Inverse Raman spectroscopy probes the changes in molecular energy states directly without mixing the signal with a nonresonant background. In inverse Raman, the depletion of a probe beam is induced by a more in-

tense pump field such that the difference in frequency for the two fields corresponds to a Raman active transition. Figure 19 depicts the transition scheme for both conventional Raman scattering and SIRS, and it is evident that only the mode of observation is different. In SIRS, a strong pump field at ω_S induces a molecule to exist in the stimulated regime. To do so, the molecule must absorb a photon from the field at ω_L. Standard methods for absorption detection can then be used to obtain the inverse Raman spectrum (180,181).

The previously mentioned advantages of coherent Raman methods apply to inverse Raman spectroscopy. That is, fluorescence rejection is easily accomplished by proper experimental design since the signal can be encoded on a spatially coherent laser beam on the anti-stokes (high energy) side of the system. An additional advantage to SIRS is in the ability to measure the signal in a forward (0°) geometry. The Doppler broadening of a Raman line can be expressed as $\Delta\omega_D = C\omega$, where C depends only on the molecular weight and temperature of the scattering species. For a forward geometric arrangement, a reduction in the Doppler broadening contribution to the line width by the factor $(\omega_L - \omega_S)/\omega_S$ should be possible over the 90° geometry of conventional Raman spectroscopy.

A disadvantage to measuring Raman events by SIRS is that one must measure a small change (the absorption at ω_L) on top of a relatively large background (the field at ω_L). One way to improve the inverse Raman technique is to use AC-coupled detection (182). In AC-coupled inverse Raman spectroscopy, the inverse Raman signal induced on a continuous wave laser beam by a pulsed laser field at ω_S is observed by a

Figure 19. Transition schemes for normal Raman scattering (RS) and inverse Raman scattering (SIRS): straight arrow, excitation; wavy arrow, spontaneous scattering; double arrow, stimulated scattering; hatched double arrow, absorption. |a> and |b> are real vibrational levels

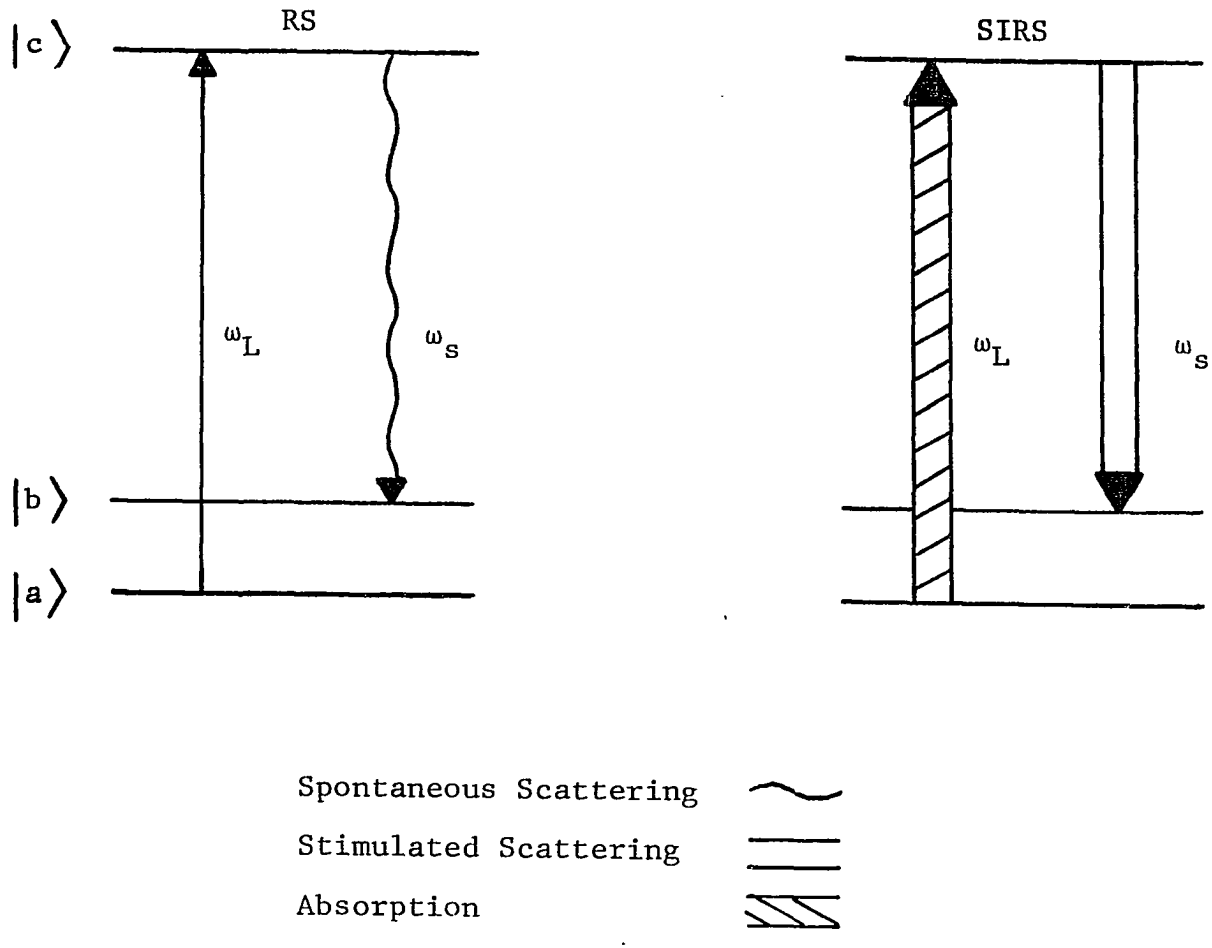
RS
SIRS
|c⟩
|b⟩
|a⟩
ωL
ωs
ωL
ωs
Spontaneous Scattering
Stimulated Scattering
Absorption

fast photodiode. The output of the photodiode is fed to capacitively coupled amplifiers which amplify the short pulse Raman signal while rejecting the constant (DC) signal on which it is encoded. The detection limits are within a factor of 2.5 of spontaneous Raman spectroscopy which enabled the Raman spectra of various biological molecules, including a proflavin-DNA complex (183) to be obtained.

The Raman induced Kerr effect (RIKE) is an intensity-dependent birefringence which manifests itself as a change in rotation of a probe beam due to the presence of a pump field which is shifted in frequency an amount equal to a Raman active band (184). RIKES is analogous to inverse Raman spectroscopy and is capable of providing all the advantages inherent to SIRS. In addition, since the measurement is made on a much smaller background than inverse Raman, the potential detectability should be much better.

The Raman induced Kerr effect will occur as long as the pump and probe fields are not oriented orthogonally to each other. Figure 20 describes the polarization conditions necessary to observe RIKES. The probe beam at ω_L is plane polarized 45° to a vertical reference plane, and is extinguished between two crossed polarizers. The pump field at ω_S, for the sake of clarity, will be considered to be plane polarized in the horizontal plane. As mentioned previously, RIKES will be observed as long as the pump and probe fields are not orthogonal. However, the maximum effect will be seen when the pump and probe fields are 45° to each other, vida infra. One can decompose the probe field into two electric fields with vectors either in the plane of the pump field or

Figure 20. Polarization scheme for observing the RIKE with a plane polarized pump field. Top, plane polarized pump field. Top, probe polarized 45° to the pump field; middle, preferential absorption from probe component parallel to pump field; bottom, rotated probe field

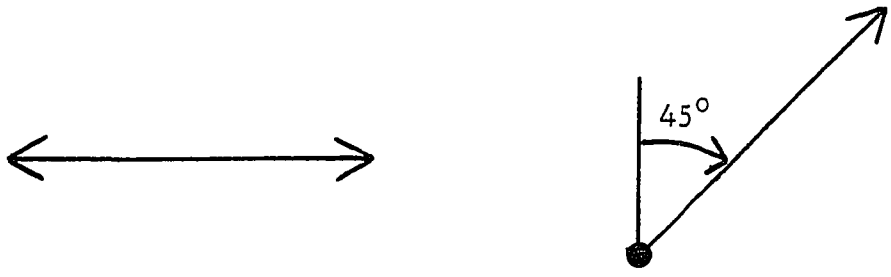

PUMP PROBE

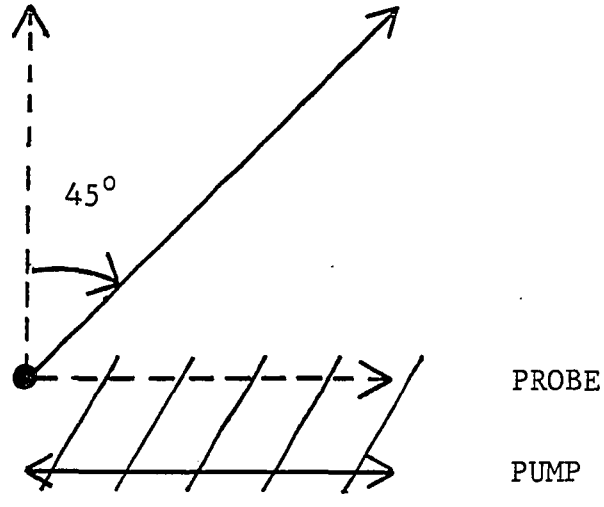

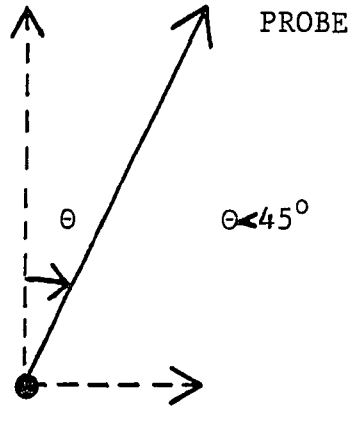

perpendicular to it. Since Raman transition probabilities are generally different for parallel (in the pump polarization plane) and perpendicular photons, the inverse Raman absorption will be of a different magnitude for each of these electric fields. After interaction with the pump field, the resultant electric field for the probe will be rotated in its direction of polarization. This rotation can be conveniently detected as an increase in the transmitted intensity of the probe field passing through the second polarizer.

One problem with the RIKE experiment as just presented is the presence of a background signal from the optical or normal Kerr effect (185). The normal Kerr effect is also an intensity-dependent birefringence caused by the intense plane polarized pump field at one frequency which manifests itself as a rotation in the probe beam. As before, the two fields must not be orthogonal. However, the frequency difference between the two fields is immaterial, and the broad background due to the normal Kerr effect can make the RIKE measurement difficult.

If, instead of a plane polarized pump field a circularly polarized field is used, there will be no normal Kerr effect (186). This is because the circularly polarized pump field will not, in contrast to a plane polarized field, induce an anisotropic environment for the probe field to interact with. The treatment for the RIKE signal resulting from a circularly polarized pump field is similar to the plane polarized case. The probe field at ω_L can be thought of as being composed of equal amounts of left- and right circularly polarized light propagating in phase. Since Raman transitions generally exhibit different probabil-

ities for same-sense versus opposite-sense circularly polarized photons (186), the magnitudes of the two circular fields comprising the probe beam will no longer be equal after interaction with the circularly polarized pump field. The resultant probe field will now have an elliptical component, and as before, this will be detected as increased transmission through the second polarizer.

The first experimental verification of the RIKE demonstrated the possible multiplex nature of this technique (184). In this work, a broad-band dye laser was used as the probe in conjunction with a spectrograph and photographic detection to simultaneously monitor a relatively broad spectral region. In this manner, the Raman spectra of cyclohexane, and benzene in the region 992 to 3062 cm^{-1} was recorded in four laser pulses. A recent review summarizes RIKE spectra obtained for a variety of materials including gas phase samples, organic and aqueous solutions, and crystalline solids such as diamond and calcite (187).

Levenson and Song (188) investigated the RIKE lineshape resulting from an elliptically polarized pump field. The lineshape was found to be a function of the interference of the Raman contributions to the intensity-dependent birefringence. Analysis of the lineshape can then provide a way to obtain a measure of the ratio of the optical Kerr coefficient to the Raman tensor element. In similar fashion, refinement of the technique has enabled these workers to determine accurate ratios of the electronic, orientational and Raman contributions to the third-order susceptibility (189). These parameters describe the nonlinear behavior of a system in the presence of a strong laser field.

Optical heterodyne detected-RIKE (OHD-RIKE) was devised to improve the signal to noise limits of the intensity detected RIKE experiment. In OHD-RIKE, the probe laser is continuous wave and the experimental parameters arranged so that a portion of the field passes through the analyzer at all times. This local oscillator field results from a slight ellipticity in the probe field. The heterodyne signal, resulting from the interaction of the probe and pump, can be extracted from background and noise signals by means of electronic filters or phase sensitive detection (190).

The first experimental example of OHD-RIKES used a pulsed pump field (191). The output from the AC amplifier was sent to a boxcar integrator to average many laser pulses. This reduces noise due to shot to shot intensity fluctuations in the pump field. In reference 191, a detectability of 0.05% of sodium benzoate in water was realized at a S/N = 5. Improved experimental design (i.e., modulation of the pump laser at 25 kHz) resulted in the detection of 0.02% of benzene in CCl_4 at a S/N = 5 (192). For gaseous samples (193), the detection of 3 Torr of H_2 is possible. One subtle advantage to OHD-RIKES is that the observed signal depends linearly on the Raman scattering cross section. This is in contrast to intensity detected RIKES where there is a squared relationship. Theoretically then, OHD-RIKES, when properly arranged should give better detection limits than either normal RIKES or CARS (190). However, the experimental results have not shown this yet. It has been pointed out (194) that the lower the background radiation due to system birefringence, the lower the heterodyne power needed to obtain the maxi-

mum signal to noise ratio (providing the system is not shot or electronic noise limited). Therefore, optimum OHD-RIKE detection limits may be possible by application of some of the techniques discussed in Chapters I-IV for reducing background birefringence.

The preceding section has demonstrated the usefulness of the RIKE experiment as a way to obtain Raman information on a variety of different samples. Another advantage, although at present unexplored, is the ease of obtaining quantitative information using the RIKE over conventional Raman methods. Therefore, this chapter will present results from an investigation of the quantitative nature of RIKES. Particular attention will be given to those factors which affect the analytical usefulness of the RIKE signal, and a unique optical null will be discussed as a way to minimize the nonresonant background.

Theory

A thorough treatment of the theoretical aspects of the RIKE has been reported (186,195). This section will briefly review the pertinent details which relate experimental parameters to the observed signal.

Since the RIKE is analogous to the inverse Raman absorption, it is appropriate to first consider the depletion in a probe beam, $P_L(0)$ due to the presence of the pump field at ω_S.

$$P_L(\ell) = P_L(0)\exp(-g\ell) \qquad (40)$$

$P_L(\ell)$ is the intensity of the probe field after interaction with the

Stokes-shifted field, ℓ is the interaction length, and g, the inverse Raman absorption coefficient, is given by

$$g = 10^7 P_S \omega_L N(d\sigma/d\Omega)/2hc^2 n_S^2 \Delta\omega \omega_S^4 \quad . \tag{41}$$

In Eq. (41), P_S is the power density of the Stokes-shifted field (W cm^{-2}), ω_L and ω_S are the probe and pump field frequencies, respectively (cm^{-1}), N is the number density of scattering molecules (molecules cm^{-3}), $d\sigma/d\Omega$ is the absolute Raman scattering cross section per polarization (cm^2 sr^{-1}), n_S is the refractive index of the medium at the Stokes frequency, $\Delta\omega$ is the width of the Raman transition, and all physical constants are in cgs units.

For the situation with a plane polarized pump field, the probe field can be resolved into two orthogonal electric fields. After interaction with the pump field in the sample, the inverse Raman absorption will be different for each of these fields. Therefore,

$$P_{L1}(\ell) = P_{L1}(0)\exp(-g_1 \ell) \tag{42}$$

and

$$P_{L2}(\ell) = P_{L2}(0)\exp(-g_2 \ell) \tag{43}$$

where

$$g_1 = g/(1 + \rho)$$
$$g_2 = g\rho(1 + \rho) \qquad (44)$$

and ρ is the depolarization ratio for linearly polarized light for the specific Raman transition. Recombining Eqs. (42) and (43), consideration of the crossed nature of the polarizers (i.e., $\hat{p}_1 \cdot \hat{p}_2 = 0$), and making use of the substitutions

$$\alpha = g_1 \ell/2$$
$$\beta = g_2 \ell/2 \qquad (45)$$

allows one to derive an expression for the field passed by the second polarizer, P_L''.

$$P_L'' = P_L(0)(e^{-\alpha} - e^{-\beta})^2 \sin^2\theta \cos^2\theta \qquad (46)$$

Here, θ is the angle between the pump and probe polarization vectors. For low absorptions, Eq. (46) simplifies to

$$P_L'' = P_L(0)(g\ell/4)^2\{(1 - \rho)/(1 + \rho)\}^2 \sin^2 2\theta \quad . \qquad (47)$$

The second derivative of Eq. (47) shows that the maximum effect will occur when $\theta = 45°$. Additionally, the presence of the normal Kerr

effect background interferes with the resonant Raman susceptibility resulting in a dispersion-like lineshape (190).

A similar treatment can be applied to the RIKE experiment when a circularly polarized pump field is used. In analogous fashion to Eqs. (42) and (43), the probe field can be resolved into two equal circularly polarized fields of identical frequency and phase, and the different attenuation of each after interaction with the pump field in the sample is

$$(\vec{E}_y')_1 = \vec{E}_x \exp\left(\frac{-i\pi}{2} - \alpha\right) \tag{48}$$

$$(\vec{E}_y')_2 = \vec{E}_x \exp\left(\frac{i\pi}{2} - \beta\right) \tag{49}$$

α and β are given by Eq. (45).

Squaring the vector sum of Eqs. (48) and (49), and simplification for the case of small absorptions gives

$$P_L'' = P_L(0)(g\ell/4)^2\{(1 - \rho)/(1 + \rho)\}^2 \quad . \tag{50}$$

As mentioned previously, the contribution from the normal Kerr effect is absent and the lineshape shows the predictable dependence on the Raman scattering cross section.

From a quantitative perspective, several key points can be made from consideration of either Eq. (47) or (50). First, the observed

signal will show a linear dependence on the intensity of the probe field. Therefore, one can increase the RIKE signal as much as needed by increasing $P_L(0)$, until the point where heating effects in the polarizers degrade their performance. Second, the RIKE signal shows a squared dependence on interaction length. This underscores the quantitative reliability of the inverse Raman and, therefore, RIKE experiments (186). Since the interaction region is defined by the intersection of two spatially coherent laser beams, the interaction length can be determined more reliably than in conventional Raman techniques. Third, because Eqs. (47) and (50) show a squared dependence on g, the RIKE signal will vary as the square of both the Stokes-field power density and number density of scattering molecules. Although it is true that a doubling of P_S will result in a factor of four increase in the observed RIKE signal; fluctuations in the pump field will also cause similar increases in the signal fluctuations. Additionally, the quantitative attractiveness of the RIKE experiment is diminished somewhat by the fact that when the concentration is halved, the signal will fall off by a factor of four. A theoretical investigation of the effect of these parameters on the S/N of the intensity detected RIKE will be presented in the results and discussion section.

The normal Kerr effect (NKE) can be a major source of background in the RIKE experiment. Since this effect is nonresonant, it appears as a broad and usually featureless signal. As such, it should be possible to electronically suppress this unwanted signal. However, as the magnitude of the background increases, the fluctuations in the background may

completely obliterate the desired RIKE signal. A better way to eliminate the background would be to optically suppress it before it is observed by the detection system.

A way to accomplish this optical null is presented in Fig. 21. In this experiment, two detection cells would be used. In one would be placed the Raman active compound dissolved in the solvent which is the source of the normal Kerr effect background. The second cell would only contain solvent. The pump field would be split into two equal portions with orthogonal polarization vectors. The probe field would pass through both cells, while the split pump field would enter each cell coincident in time and polarized 45° to the probe and orthogonally to each other.

From inspection of Fig. 21, it is clear that any NKE induced rotation, due to the interaction of pump field #1 and the horizontal component of the probe in cell #1, would be exactly compensated for by a rotation in the opposite direction induced by the interaction of pump field #2 and the vertical component of the probe in cell #2. Since only one cell contains the Raman active compound of interest, no suppression of the RIKE signal would be observed. The same optical null can be envisioned where, instead of a plane polarized pump field, each portion of the pump field would be made circularly polarized. The interaction, for example, would then be between right circularly polarized light and the right circularly polarized component of the probe field in the first cell, and left circularly polarized light and the left component in cell #2. Even though the normal Kerr effect background would be suppressed

Figure 21. Polarization scheme for double beam optical null. Pump fields #1 and #2 are polarized orthogonally to each other and 45° to the probe

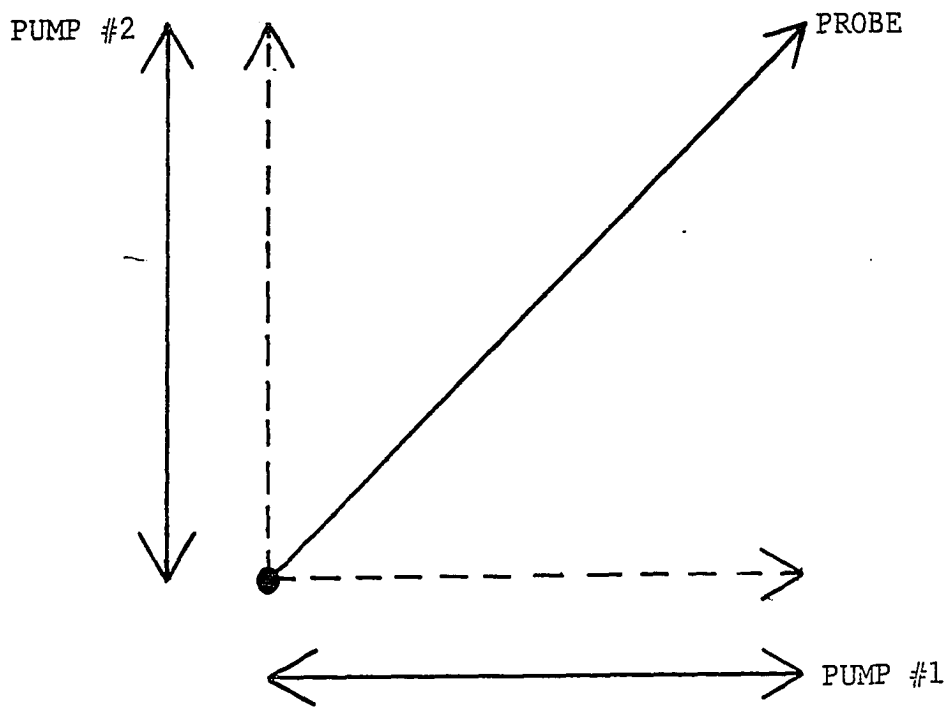
PUMP #2
PROBE
PUMP #1

without the double beam null for the circularly polarized case, this method can also serve to null out RIKE signals from the solvent which might interfere with the band(s) of interest. This unique optical null concept can, therefore, improve both the detectability of the RIKE experiment by suppressing background signal, and the selectivity by suppressing interfering Raman bands.

Experimental

The experimental arrangement used to investigate the Raman induced Kerr effect is detailed in Fig. 22. The complete experiment was assembled on a rigid optical breadboard (Newport Research Corp., Fountain Valley, CA, model XZ-24). For the first studies, the pump laser was an in-house constructed, dual flashlamp, elliptical cavity Ruby laser with a 15 cm active medium. The laser was passively Q-switched using a 1:5 dilution of a saturated benzene solution of vanadyl phthalocyacine. A 2 cm cell filled with this bleachable dye produced a single output pulse of approximately 300 mJ. The probe laser for these early studies was a linear dye laser (Spectra-Physics, Mountain View, CA, model 375) pumped by an argon ion laser (Control Laser Corp., Orlando, FL, model 554A). Other studies utilized a YAG pumped dye laser as a source of the Stokes field (YAG Laser: model 481, dye laser: model TDL III, scan controller: model ASC-2; Quantel International, Santa Clara, CA). The dye laser has a nominal linewidth of 0.1 cm^{-1}. The frequency doubled output of the YAG laser at 532 nm was used to pump either Rhodamine 560, 590 or 610, which spanned the wavelength range needed for these studies. Con-

Figure 22. Experimental arrangement for the RIKE

YDL	YAG dye laser
M	mirror
H	half-wave plate
LA	probe laser
P	polarizer
A	analyzer
R	right angle prism
L	lens
CL	detection cell
S	spatial filter
F	laser line filter
PMT	photomultiplier tube
SA	boxcar signal averager
SC	fast oscilloscope
CH	chart recorder

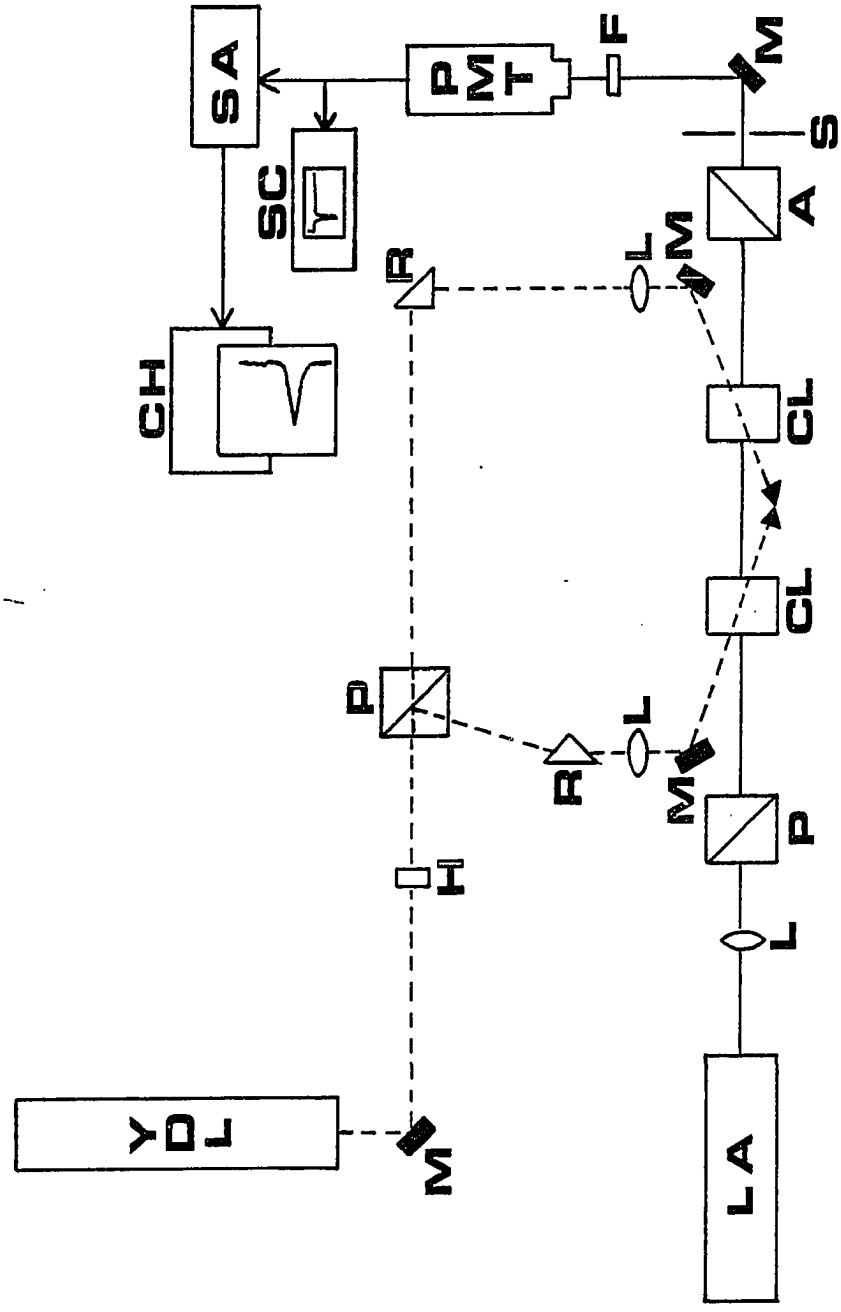
SA
PMT
F
M
S
A
SC
R
L
M
CH
CL
CL
P
L
M
R
P
I
L
YDL
M
LA

currently with the YAG system, either a helium-neon laser (Melles Griot, Irvine, CA, model 05-LHP-151), or an argon ion laser was used to probe the RIKE event. Power adjustment of the argon ion laser was effected by the placement of a low quality glan polarizing prism after the laser output aperture, but before the first steering mirror. Judicious placement of a spatial filter (diameter = 2 mm) after the first steering mirror favorably improved the extinction ratio by eliminating a halo of scatter accompanying the 1.5 mm argon ion laser beam.

The probe field was polarized and extinguished by the same pair of Karl Lambrecht, high quality calcite polarizing prisms described in earlier chapters. The analyzer was mounted in a rotational stage with 10^{-3} degree resolution (Aerotech Inc., Pittsburgh, PA, model ATS-301R), while the polarizer was placed in an in-house constructed mount of sufficient bulk to minimize vibrational disturbances. The polarizer was oriented so that the transmitted laser beam was plane polarized 45° to the optical table. By limiting the pump field to either vertical or horizontal polarization, the pump field maintained the necessary 45° relationship to the probe field at all times. Light passing through the analyzer was detected by a high gain photomultiplier tube (Products for Research, Inc., Danvers, MA, models 56TVP/252 or 56AVP/5532) operated at 1000 to 1700 volts by a regulated power supply (Keithley Instruments, Inc., Cleveland, OH, model 242). Scatter and stray light were minimized by placing a narrow band-pass laser line filter (Melles Griot, Irvine, CA, model 03-FIL-002) at the entrance to the PMT housing.

For the double beam experiment, a half-wave plate (Melles Griot, Irvine, CA, model 02-WRQ-023) and a double escape polarizing prism (Karl Lambrecht, Chicago, IL, model AGLA-CN-10) served as a variable ratio beamsplitter. Circularly polarized light was produced by either a quarter-wave plate (Melles Griot, Irvine, CA, model 02-WRQ-003) or a Fresnel rhomb prism (Karl Lambrecht, Chicago, IL, model FR4-13-580-VN). Beam steering optics consisted of either high quality metal surface mirrors (Newport Research Corp., Fountain Valley, CA, model 10D10) anti-reflection coated 90° prisms (Melles Griot, Irvine, CA, model 01-PQB-001), or 488 nm dielectric coated mirrors (CVI Laser Corp., Albuquerque, NM, model AR5015). The probe beam was brought to a focus by either a 30, 50 or 100 cm focal length plano-convex spherical lens (Melles Griot, Irvine, CA, series 01-LQF). Focusing of the pump source was effected by either a glass, plano-cylindrical lens (Melles Griot, Irvine, CA, series 01-LQC), or a 30 cm plano-convex spherical lens similar to that listed previously. An optical delay line was used in the double beam experiment. This was constructed of two 90° prisms mounted on a translational stage (Newport Research Corp., Fountain Valley, CA, model 430-1). The delay line served to change the distance one beam traveled relative to the other arm of the two beam system.

The output of the photomultiplier tube was displayed on a fast oscilloscope (Tektronix, Inc., Beaverton, OR, model 7904 with a 7B92 time base and 7A19 fast rise amplifier). The PMT signal was processed by either a sampling amplifier (Tektronix, Inc., Beaverton, OR, model 7S14) used in conjunction with the oscilloscope, or a boxcar integrator

(EG&G Princeton Applied Research, Princeton, NJ, mainframe model 162 with model 164 gated integrator processor module). The output from the boxcar was displayed on a chart recorder (Houston Instruments, Austin, TX, omniscribe series 5000 model B5117-SI).

A detection cell in which the pump and probe fields enter orthogonally to each other is depicted in Fig. 23. The cell was machined from a two inch piece of round aluminum stock through which a central 3 mm channel was drilled. Quartz tubing (i.d. 1 mm) was cemented into this channel to pass the pump beam. As is evident in Fig. 23, there are actually two independent cells constructed such that the pump field entrances are orthogonal to each other and the probe beam channel.

For the experiments involving a colinear geometry, two cells were constructed similar to the orthogonal cell but without the pump beam entrance. These cells were independently mounted and positioned to facilitate investigation of the effect of argon-ion laser beam size on the RIKE signal. All plumbing was standard 1/16 inch stainless steel HPLC tubing. Because of the variety of compounds to be tested in these studies, a thorough investigation of several potential window adhesives was undertaken. These results are summarized in Table 8.

Results and Discussion

Signal processing

To determine that the RIKE was being observed, the output from the PMT was terminated in 50 ohms and displayed on a fast oscilloscope. A peak was observed coincident with the arrival of the pump beam in the

Table 8. Effect of various Raman active liquids on potential window adhesives (NE = no effect; SS = slight swelling; SD = severe distortion)

	Armstrong A-12 Epoxy[a]	Silicone RTV[b]	Black Plastic Rubber[c]	Balkamp High Tack[d]
Acetonitrile	NE	NE	NE	NE
Water	NE	NE	NE	NE
Methanol	NE	NE	NE	NE
THF	SS	SD	SD	SD
Methylene Chloride	SS	SS	SD	SD
Benzene	SS	SD	SD	SD
CCl_4	SS	SD	SD	NE
$CHCl_3$	SD	SD	--	--
CS_2	NE	SS	--	--
Nitrobenzene	SS	SS	SD	SS
Chlorobenzene	SS	SS	SD	SS
Hexane	SS	SD	NE	NE

[a]A-12 Adhesive; Armstrong Products Co., Warsaw, IN.

[b]Silastic No. 732 RTV; Dow Corning Corp., Midland, MI.

[c]Duro Black Plastic Rubber; Loctite Corp., Cleveland, OH.

[d]Balkamp High Tack Adhesive Sealant No. 765-1217; Permatex Co. Inc., Kansas City, KS.

detection cell, corresponding to an increase in the intensity registered by the PMT. This increased intensity disappeared when either the probe or pump beam was blocked, or when the difference in ω_L and ω_S no longer corresponded to a Raman transition. When the YAG-dye laser was used as the pump source, the laser was first blocked, unblocked and then scanned over the Raman transition. This provided a measure of the probe laser background, normal Kerr effect and RIKE, respectively.

A 7S14 sampling amplifier with a fixed 350 picosecond gate was used to sample the RIKE signal. A problem with this method of processing was that there is a 5-7 ns jitter associated with the YAG trigger pulse. This jitter is substantially larger than the 350 ps sampling gate resulting in a widely fluctuating output. A photodiode set to sample a portion of the YAG beam was used to trigger the sampling amplifier. This provided much more reliable triggering. The gate was positioned over the peak maximum, however, the peak maximum is the portion of the peak most affected by variations in the pump field. This fact, coupled with the narrow fixed gate, resulted in an unacceptably varying output.

A boxcar integrator provided a better way to sample the RIKE signal. This system synchronously samples the PMT signal with an aperture that is adjustable both in its duration (width), and the position in time when it occurs. Successive gated signals are integrated to improve the signal to noise ratio. This is possible because, theoretically, the signal will build up as the number of scans, while the noise increases only as the square root of the number of scans.

Optimum S/N was obtained when a 10 ns gate was used. However, the 10 Hz repetition rate of the YAG system was slightly below that required by the processor module. Ideally, the output from the boxcar should approach the average value sampled at the input. At 10 Hz, the sample and hold circuitry could not maintain the voltage at this low repetition rate and this leakage decreased the signal to noise ratio. This problem was overcome by the installation of a digital storage board. The output from the sample and hold circuit was converted to a digital value, stored and the analog equivalent of the stored value fed back to the sample and hold circuit until the next event occurred. This combination provided a useful sampling system for observing the RIKE event.

Experimental observations

The first attempts to observe the RIKE utilized a ruby laser lasing at 6943 Å as the pump source, and a CW dye laser as the probe. To obtain the necessary power density, the ruby laser was passively Q-switched using a bleachable dye. In this manner, 7-10 laser shots could be obtained before the dye solution required changing. Scattered photons from the pump laser were a large source of background. In this experimental arrangement, it was not possible to use narrow bandwidth line filters to isolate the probe beam, since the wavelength of the probe field was scanned. It was found that several totally reflecting 6943 Å mirrors placed at the entrance to the PMT, in conjunction with a light tunnel to isolate the probe path, eliminated this problem

In this first experiment, the dye laser was tuned to 6496 Å and the ruby beam brought in 90° to it. At this wavelength, $\omega_L - \omega_S = 992\ cm^{-1}$,

which corresponds to a benzene transition. With benzene in the detection cell, upon firing of the ruby laser, the intensity recorded by the PMT increased by a factor of 2-3 over that when the dye laser was positioned off resonance. However, it was difficult to unambiguously attribute the observed signal to the RIKE. Shot to shot variations were severe, and the limitation imposed by the ruby laser of only being able to make a measurement once per minute meant it was possible other effects could be causing the observed signal.

An improved experimental arrangement used a YAG pumped dye laser as the pump field, and an argon ion laser as the probe. As before, a 90° geometry was used, and a schematic of the detection cell can be seen in Fig. 23. The second half of the cell in Fig. 23 is necessary for the double beam experiment to be described shortly.

The first use of this arrangement was to generate normal Kerr effect signal. With a 1:3 V:V solution of benzene in CH_3CN, and the dye laser tuned off the benzene 3065 cm^{-1} transition, substantial (intensity increases greater than 100 times) NKE signal was observed. When a half-wave plate was used to render the polarization of the pump field parallel to the probe, the NKE signal disappeared. This demonstrated that the proper polarization conditions were available to observe the RIKE.

The advantage of tuning the pump versus the probe laser became clear in this study. The narrow bandwidth laser line filters mentioned previously effectively removed all of the scattered pump field radiation without the need for additional optics. With this arrangement, the 3065

Figure 23. 90° detection cell for the RIKE experiment

PR probe
P1 pump beam #1
P2 pump beam #2

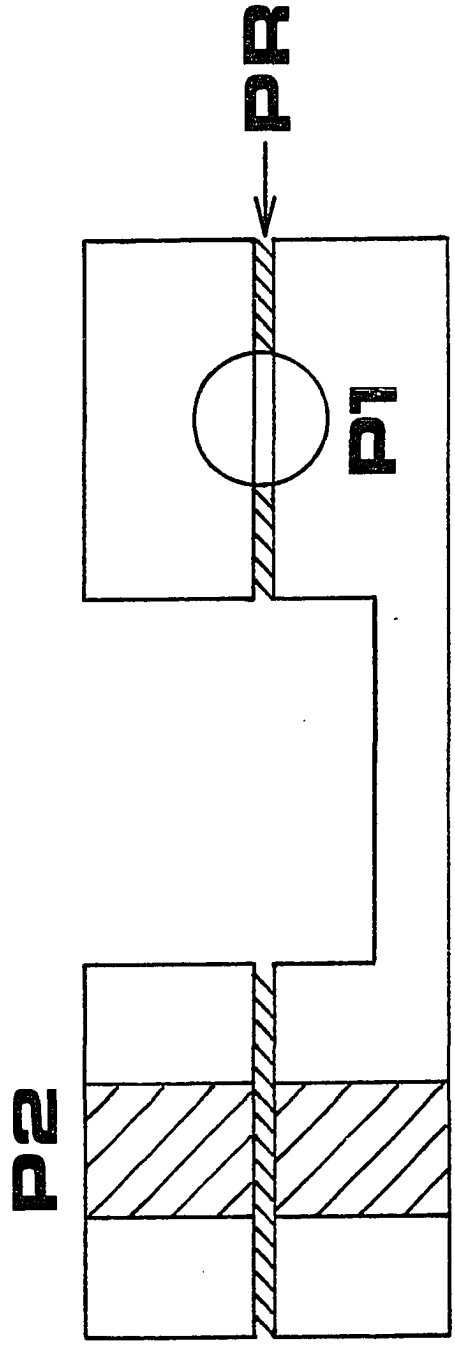
PR
P1
P2

cm^{-1} transition of benzene, and the 2977 cm^{-1} transition of CH_3CN was recorded. CH_3CN does not affect the window adhesive as does the benzene, and so it provided a more suitable system to study during these preliminary experiments. However, several disadvantages to the 90° experimental arrangement became apparent during these first investigations. First, the 90° geometry does not take full advantage of the resolution obtainable with the RIKE technique. Second, it was difficult to control the focusing of the pump laser. To overlap the probe laser properly, the pump beam was focused to a "line" with a cylindrical lens. However, the quartz tube channel necessary to pass the pump radiation also acted as a short focal-length cylindrical lens. The combination focusing of these two elements was difficult to control. Third, and most important, is the fact that with the 90° arrangement there is no means for background suppression.

With the colinear geometry schematically depicted in Fig. 22, the crossing angle is estimated to be approximately 1°. This provides effective overlap of the pump and probe beams for almost the entire length of the 5 cm detection cell. To produce the circularly polarized light necessary for background suppression, two methods were tried. First, a quarter-wave plate was used to render the pump field elliptically polarized to such an extent that when reflected once at 45°, the resulting field was circularly polarized. A simple way to check this was to monitor the NKE while rotating the quarter-wave plate to minimize the nonresonant signal. Wave plates, however, are constructed to operate at a particular wavelength. This can cause problems when wavelength scanning

of the pump field is necessary. A better way to produce a circularly polarized pump beam is to pass a linearly polarized field through a Fresnel rhomb prism. Again, by monitoring the NKE, it was possible to adjust the optics to maximize the degree of circular polarization. In this manner, the pump field could be made approximately 90% circularly polarized, effectively suppressing the nonresonant background.

Figure 24 is a scan over the 2977 cm^{-1} C-H transition of CH_3CN. The spectrum was obtained using a 10% V:V solution of CH_3CN in water. Figure 24 unambiguously demonstrates that the RIKE is being observed, and it is evident that the full width at half maximum (FWHM) is approximately 10 cm^{-1}. This demonstrates the high resolution obtainable with the RIKE technique.

The principal impetus behind these experiments was to investigate the analytical aspects of the RIKE. As such, it was important to verify the results predicted by Eqs. (47) and (50). Figures 25 and 26 show the dependence of the RIKE signal on the intensity of the probe and pump fields, respectively. As predicted, the signal shows a linear dependence on the power of the probe field. The extinction ratio increased linearly with increased probe power up to approximately 100 mW. At greater powers, heating of the polarizer housing caused slight degradations in the extinction reading. Therefore, the S/N should be maintained at a probe beam power of 100 mW, and the RIKE signal would be maximized. The squared dependence on the pump field power is verified in Fig. 26. The slight leveling at powers greater than approximately 5

Figure 24. 2977 cm^{-1} transition of CH_3CN; 1 s time constant, scan rate: 0.2 Å s^{-1}, scale: 17 Å cm^{-1}

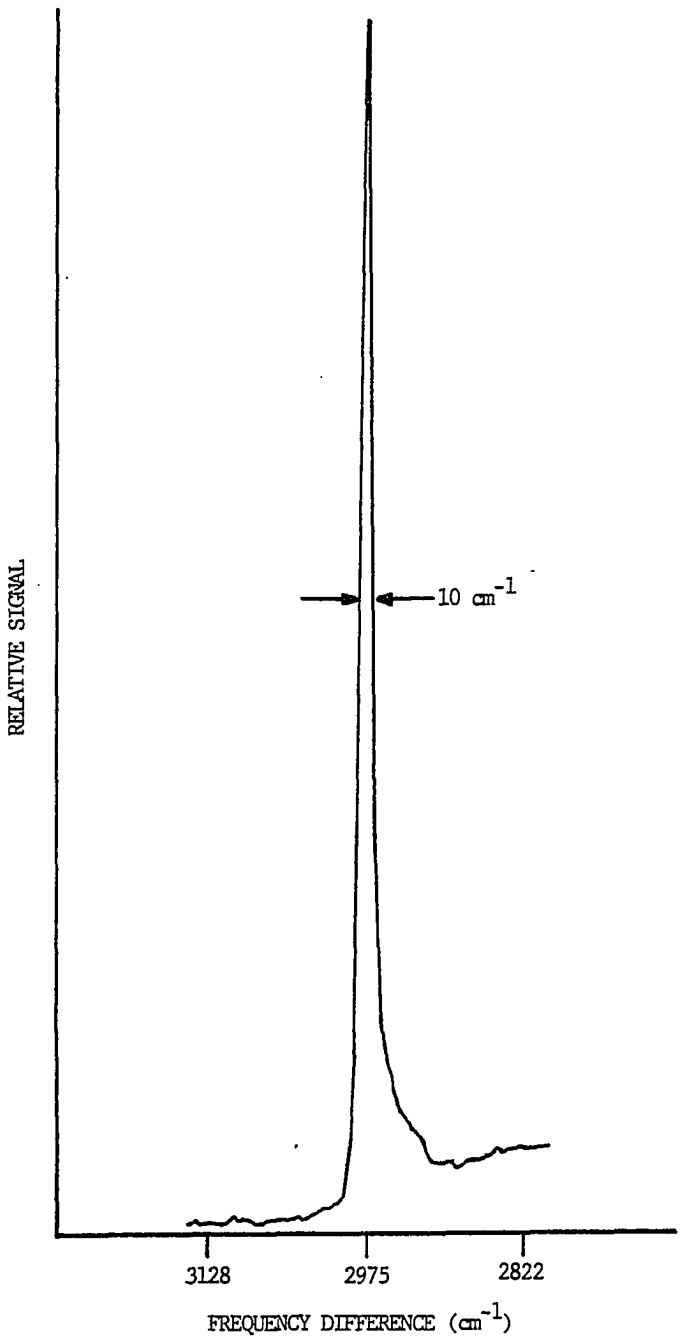
RELATIVE SIGNAL
10 cm-1
3128
2975
2822
FREQUENCY DIFFERENCE (cm-1)

Figure 25. Dependence of the RIKE signal on probe field power

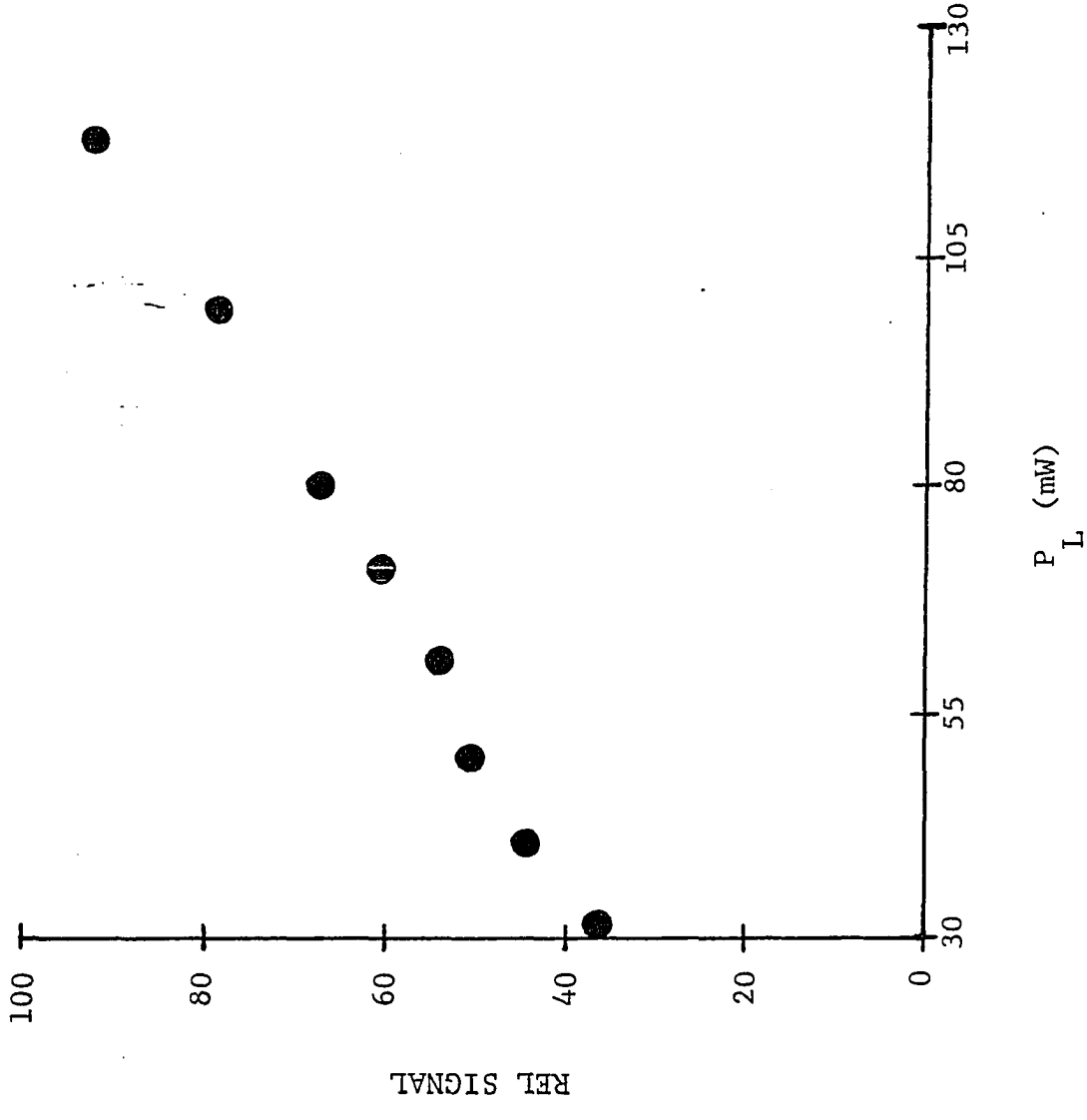
REL SIGNAL
100
80
60
40
20
0
30
55
80
105
130
P_L (mW)

Figure 26. Dependence of the RIKE signal on the square of the pump field power

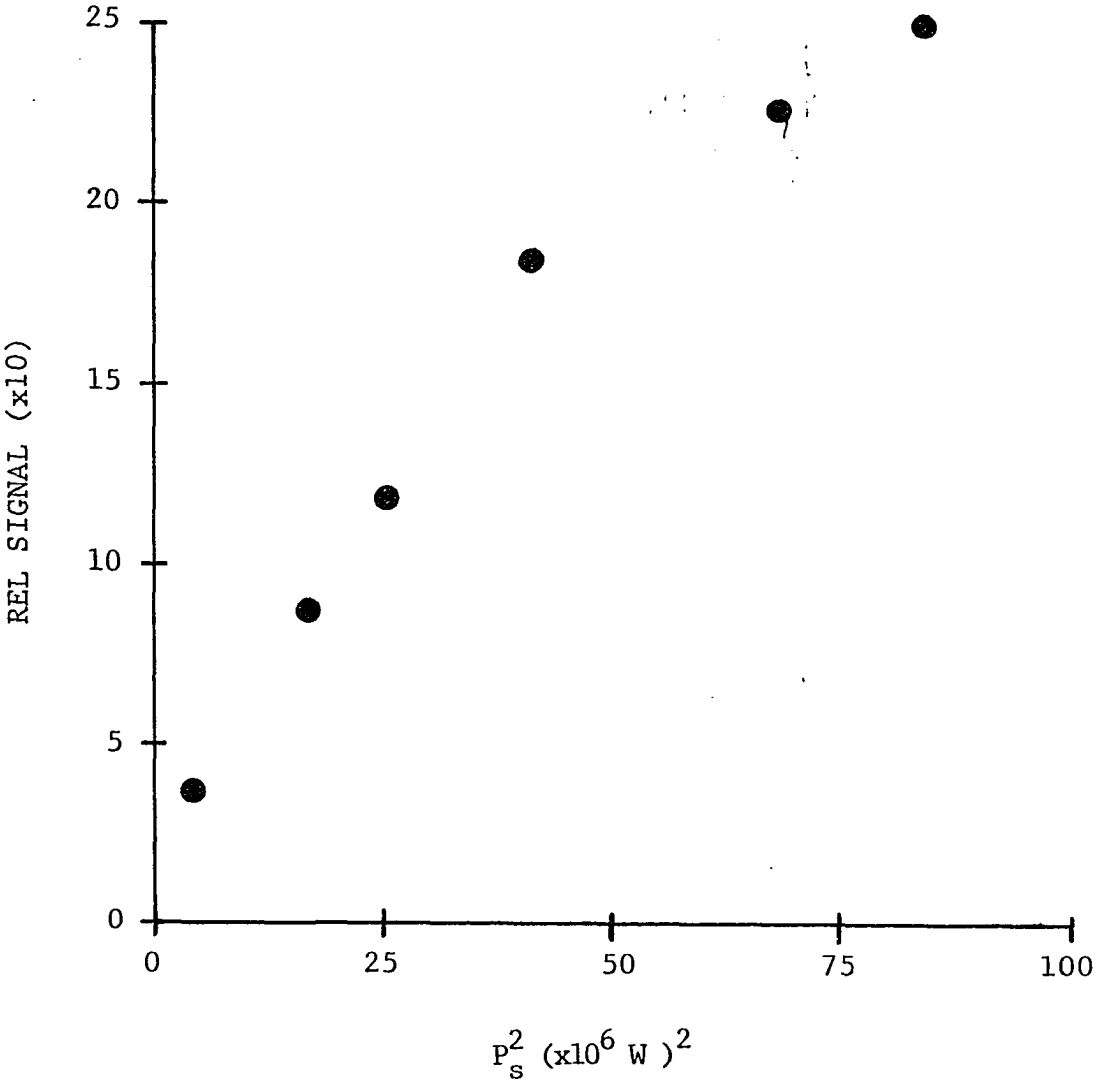
25
20
15
10
5
0
REL SIGNAL (x10)
0
25
50
75
100
P_s^2 (x10^6 W)^2

MW is probably due to slight position changes in the YAG output at higher power settings.

Figure 27 shows the expected squared dependence of the RIKE signal on the number density of scattering molecules. It should be noted that the signal for each of these three studies was obtained by scanning over the CH_3CN transition. This provided a convenient way to determine the magnitude of the NKE for each experiment, so that the data could be corrected to account for the background. The limit of detection for CH_3CN in water was determined to be 0.4% V:V at a S/N of 3. The sources of background included residual NKE signal plus Raman scattering from the solvent. D_2O was used next as the solvent since its Raman lines are spectrally shifted relative to H_2O. With D_2O in the detection cell, 0.2% of CH_3CN was detected at a S/N of 3. In comparison, a 0.5% solution of benzene in CCL_4 was detected at a S/N of 5 for a similar intensity detected RIKE experiment (196). However, the detected species in that work was benzene which has a cross section at least twice that of CH_3CN. Therefore, since the RIKE signal depends on the square of the cross section, the results of reference 196 should be multiplied by a factor of 4 to put the results on the same scale. Therefore, the LOD reported here is at least an order of magnitude better than previously reported results.

Theoretical signal to noise ratio limits

It has been stated that the success of the intensity detected RIKE experiment depends on the efficiency of the laser polarization and how

Figure 27. Dependence of the RIKE signal on the square of the number density of scattering molecules

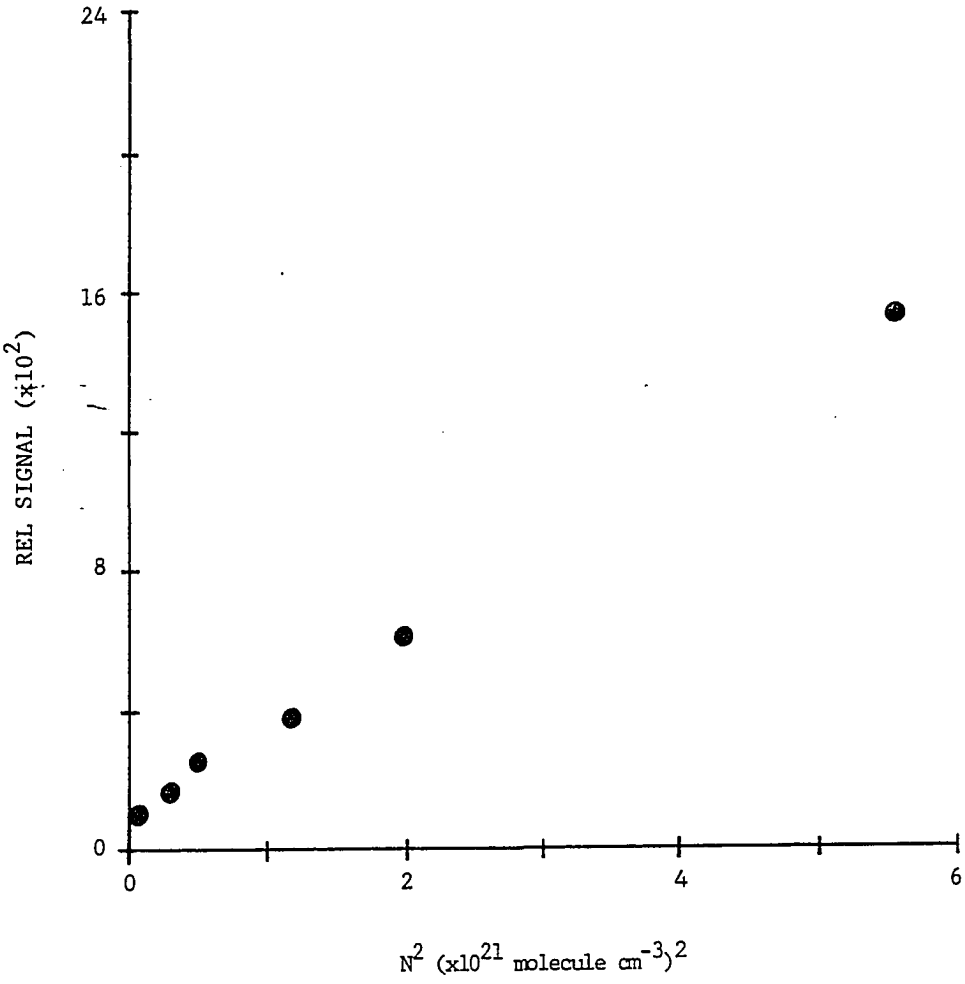
24
16
8
0
REL SIGNAL (x10^2)
0
2
4
6
N^2 (x10^21 molecule cm^-3)^2

high the rejection ratio is for the polarizers (197). However, from the results presented in the previous section, it is clear that the four orders of magnitude improvement in the extinction ratio (10^{-10} vs. 10^{-6}) reported here has not benefited the RIKE experiment as much as expected. To provide an explanation for this fact, a study of the sources of noise affecting the RIKE experiment was undertaken. The results, it is hoped, will not only identify the sources of noise and provide some insight into the limits obtainable in this experiment as it is now conducted, but it should also point to those parameters which must be changed to improve the S/N capabilities of the technique.

The model for this study is as follows. Three assumptions were made for the sake of clarity and simplification. First, the polarizers are operated in a crossed configuration (i.e., $\hat{p}_1 \cdot \hat{p}_2 = 0$). Since one aim of this study is to correlate results obtained for extinction ratios of 10^{-10} versus 10^{-6} for polarizers with orthogonal transmission axes, this is a reasonable assumption. Second, the pump field will be assumed to be circularly polarized and $(1 - \rho)/(1 + \rho) \sim 1$. By utilizing a circularly polarized pump field, the lineshape will be symmetrical and the RIKE signal can be obtained from the height of the peak maximum relative to the baseline. Third, signal averaging will cause the signal to increase as the number of events sampled, while the noise will increase only as the square root of the number of sampled events.

With these conditions met, the RIKE signal, in photons, can be represented by

$$\text{Signal} = SI_L(0)(g\ell/4)^2 \tag{51}$$

where S is the number of events sampled, $I_L(0)$ is the number of probe photons available during the duration of the pump pulse, and g and ℓ have the same meaning as defined earlier. The shot noise of the system is a function of the number of photons arriving at the detector, or

$$\text{Shot Noise} = (S\varepsilon I_L(0))^{1/2} \quad . \tag{52}$$

Here, ε is the extinction ratio of the polarizer/analyzer pair. The noise due to the fluctuations in the pump field, P_S is given by

$$\text{Pump Noise} = S^{1/2}CI_L(0)(g\ell/4)^2 \tag{53}$$

where C is the rms fluctuations in the pump field intensity. Finally, fluctuations in the probe field, or flicker noise can be represented by

$$\text{Flicker Noise} = S^{1/2}DI_L(0) \tag{54}$$

and D is the rms fluctuations in the probe intensity at frequency, ω_L. The total noise of the system is, therefore, the sum of Eqs. (52)-(54), and the signal to noise ratio of the system is then obtained by dividing Eq. (51) by the total noise.

$$S/N = \frac{SI_L(0)(g\ell/4)^2}{(S\varepsilon I_L(0))^{1/2} + S^{1/2}CI_L(0)(g\ell/4)^2 + S^{1/2}DI_L(0)\varepsilon} \qquad (55)$$

Equation (55) was investigated using a small PC computer. Each experimental variable was in turn varied, and the effect on the S/N determined. Table 9 summarizes some of the results of this study. For ease of comparison, Table 9 was prepared with a constant N = 1.5×10^{20} molecules cm^{-3} (1% V:V), $I_L(0) = 7.5 \times 10^8$ photons (30 mW, 10 ns), and the rms fluctuations in the probe were set at 1%.

Section A shows the effect of increasing P_S on the S/N. At larger P_S, the signal increases as predicted by Eq. (47) and experimentally verified earlier, however, the noise in the signal due to fluctuations in P_S also increases proportionally. Therefore, when the total noise is dominated by the noise due to P_S, the S/N should remain constant even as P_S is increased. This is illustrated in A. The S/N at P_S = 1 MW cm^{-2} is low because at this pump field power density, there is so little RIKE signal being generated that other sources of noise dominate. The entries for P_S equal to 30 and 100 MW cm^{-2}, respectively, better illustrate this point. Even when P_S is increased by a factor of 3.3, the S/N remains virtually constant. In fact, the S/N is equal to 99 at P_S = 25 MW cm^{-2}, and 99.99 at 1000 MW cm^{-2}, respectively. Therefore, it is useless to operate under these experimental conditions at pump powers greater than approximately 25 MW cm^{-2} unless the fluctuation in P_S can be reduced.

Table 9. Effect of experimental parameters on the S/N of the intensity-detected RIKE

	P_S(MW cm^{-2})	ϵ	Boxcar Time Const. (s)[a]	rms Pump Fluctuations	S/N[b]
A.	1	10^{-10}	10	0.10	10.1
	30	10^{-10}	10	0.10	99.0
	100	10^{-10}	10	0.10	99.9
B.	30	10^{-10}	10	0.10	99.0
	30	10^{-8}	10	0.10	91.0
	30	10^{-6}	10	0.10	44.3
C.	30	10^{-10}	10	0.01	910
	30	10^{-8}	10	0.01	497
	30	10^{-6}	10	0.01	73.7
D.	30	10^{-10}	0.1	0.10	9.90
	30	10^{-10}	1.0	0.10	31.3
	30	10^{-10}	10	0.10	99.0
E.	30	10^{-10}	10	0.01	910
	30	10^{-10}	10	0.05	196
	30	10^{-10}	10	0.10	99.0

[a]Number of samples = boxcar time constant x rep rate laser.

[b]For N = 1.5×10^{20} molecules cm^{-3} (1% V:V), $I_L(0) = 7.5 \times 10^8$ photons (30 mW), and D = 1% (1% rms fluctuations in probe).

Section B shows the effect of increasing extinction ratio on the RIKE S/N. As is clearly evident, a four orders of magnitude improvement in the extinction ratio only produces a factor of 2 improvement in the S/N. Again, this underscores the fact that the dominant source of noise is due to the fluctuations in P_S, and the RIKE experiment is not shot noise limited. In entry C, the rms fluctuations in P_S have been reduced to 1%, and the same improvement in the extinction ratio now results in more than an order of magnitude increase in the S/N. Clearly, to approach the shot noise limit for the RIKE experiment, it will be necessary to reduce the fluctuations in the field at ω_S. This may be possible by careful normalization of each RIKE event with respect to laser power. By applying the proper function, it should be possible to correct each data point in a scan, thereby reducing the influence of the variations in P_S. Another way is to use a laser that produces more pulses per unit time to improve the averaging. A copper vapor laser (CVL) pulses at 5 kilohertz with an output composed of 510 nm (67%) and 578 nm (33%) light. A preliminary experiment to generate the normal Kerr effect showed almost an order of magnitude improvement in the NKE S/N compared to previous trials with the YAG system. Attempts to locate compounds with Raman transitions corresponding to the difference in frequency of the copper vapor laser and an argon ion line were unsuccessful. However, the NKE results suggest that a similar improvement in the RIKE S/N may be possible using the CVL as the pump source and a CW dye laser as the probe.

Sections D and E of Table 9 demonstrate the points mode above. In D, the number of samples has been increased from one (t.c. = 0.1) to one-hundred (t.c. = 10) with the concomitant increase of 10 in the S/N. Since the CVL is capable of generating power densities greater than 20 MW cm^{-2}; improvements in the RIKE S/N of at least 20 should be attainable considering the 5 kHz sampling rate. In E, the rms fluctuations in the pump field have been reduced from 10% to 1% with almost an order of magnitude improvement in the S/N. It seems conceivable that proper normalization should be able to reduce the fluctuation from 10% to 5% which would result in a factor of two improvement in the S/N.

Several other experimental parameters were neglected for clarity, including noise associated with the electronics, the influence of the purity of the circularly polarized field at ω_S, operation at polarizer positions away from the minimum, and sources of background (NKE and Raman scattering from the solvent). However, even so, the results presented here are useful for understanding the intensity detected RIKE experiment. Equation (55) can also be solved to determine what concentration is detectable at a signal to noise ratio of three. Using values for the experimental parameters similar to those when the LOD of 0.2% was determined (P_S = 30 MW cm^{-2}, $I_L(0)$ = 7.8 x 10^8 photons, ω_S = 1.75 x 10^4 cm^{-1}, ω_L = 2.05 x 10^4 cm^{-1}, ε = 10^{-10}, S = 10 sec., D = 190, C = 10% and ℓ = 5 cm), a theoretical detection limit of 0.02% should be attainable. In fact, the optimum and experimental values are probably closer because the interaction length was overestimated, and the assumption $(1 - \rho)/(1 - \rho) \sim 1$ may be in error. If the power density at ω_S can be

increased to 100 MW cm^{-2}, $I_L(0)$ increased to 100 mW, and if the fluctuations in P_S can be reduced to 5%, a volume fraction of 4 x 10^{-3}% would be detectable.

A theoretical investigation of the limits of detection for several nonlinear Raman techniques has been reported (198). The results, in ppm, along with the LOD for spontaneous Raman scattering are listed below.

CARS	11,000
SRS	4,000
Spont. Raman	300
OHD-RIKES	110

In these calculations, the rms fluctuations in the pump and probe fields were 5% and 0.5%, respectively, with a P_S of 50 kW and no averaging. In comparison, the experimentally determined LOD of 2000 ppm reported here for 100 averaged laser pulses falls in the middle of the listed values. In addition, the theoretical LOD for the intensity detected RIKE is at least as good as that obtainable from the best of the other nonlinear Raman methods. This should provide the impetus for further research on the RIKE technique.

Double beam RIKE as a means for background suppression

As discussed previously, a major source of background is the nonresonant normal Kerr effect. Conceptually, it should be possible to subtract out the background by the use of a sample/reference cell configuration. However, as the RIKE signal decreases in magnitude, a point is reached where the background is a substantial portion of the total signal. At this point, two large signals must be differenced to obtain

the small RIKE signal. The uncertainty in such a procedure is always large. A better method would be to suppress the background before the photodetector. In this manner, the RIKE signal would be observed on top of a small background and no differencing procedure would be necessary. In addition, saturation of the photodetector with a large background signal would no longer be a consideration.

The first demonstration of the double beam optical null used a 90° geometry and the cell diagramed in Fig. 23. The experiment was performed in the following manner. First, the RIKE signal was maximized for each cell by blocking one cell at a time and adjusting the pump beam to facilitate maximum overlap with the probe. Next, both cells were unblocked to obtain a measure of the amount of cancellation. Finally, the pump beam position into the second cell was adjusted to maximize the cancellation (i.e., minimize the total signal). In this manner, approximately 25-30% of the maximum signal in one cell could be cancelled out of the total. When the 25 cm focal length spherical lenses used to focus the pump beams for the first trials were replaced with cylindrical lenses, the magnitude of the signal in each cell was increased substantially (more overlap with the probe), but the efficiency of the cancellation did not improve.

The problem is in the size mismatch of the pump and probe beams in the cell, and the situation is illustrated in Fig. 28. Since the pump beam must pass through a cylindrical glass tube before entering the sample chamber, it is difficult to control the degree of focusing. In effect, the glass tube acts as a short focal length cylindrical lens.

Figure 28. Overlap of the two pump beams with the probe (outer circle) for the double beam experiment with a 90° geometry: left, spherical focusing; right, cylindrical focusing. Solid: overlap (cancellation) region; hatched: RIKE signal, no cancellation

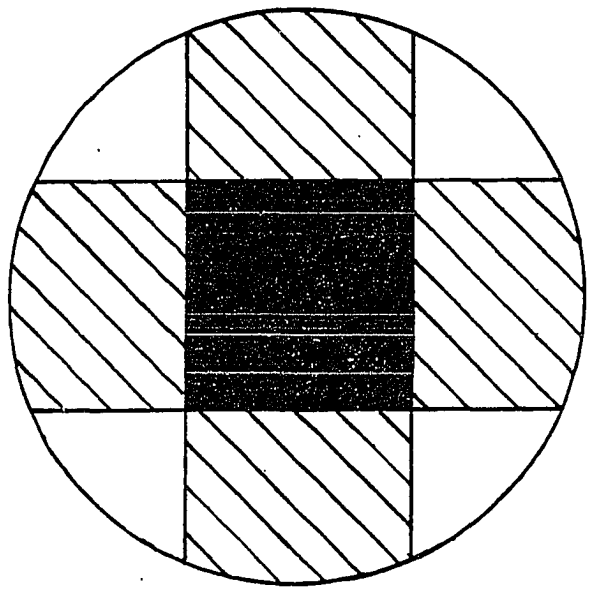

R

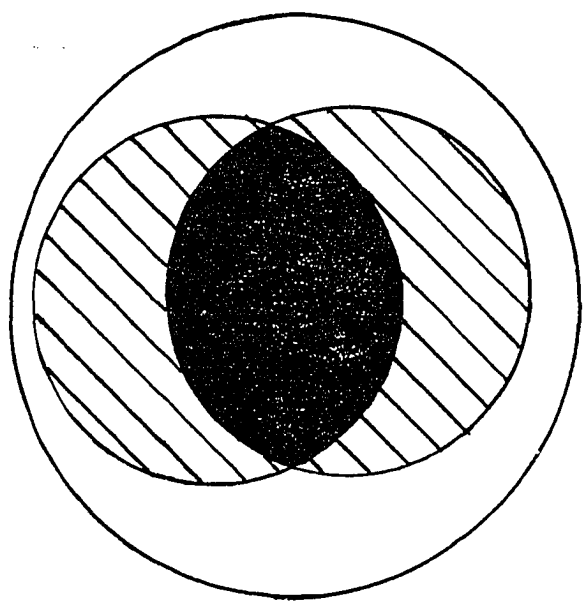

L

In the left portion of Fig. 28, the situation for spherical focusing is depicted. Only in those regions in space where the two pump beams overlap the probe and each other, would cancellation take place. Nonoverlapped regions produce noncancellable signal. On the right of Fig. 28, the analogous situation for cylindrical focusing is diagramed. Again, it is very difficult to provide total spatial overlap of the three beams.

Another consideration was that the two pump beams arrive in the detection cell at approximately the same time. To assure this, an optical delay line was put in one arm and scanned to produce a varying time delay. However, no further cancellation was evident. This was not unexpected since in 10 ns, light travels approximately 3 meters. Therefore, slight mismatches of a few centimeters are inconsequential compared to the 3 meters light travels during the duration of the YAG pulse. Only when cancellation can be made close to 99% will distance considerations for the two beams be important.

Even with adjustment of the degree of focusing of the probe and pump beams, no further cancellation was possible. Since it was very difficult to control the effect of the glass tube, a colinear geometry was utilized next. The colinear arrangement eliminated the need for a separate entrance for the pump beams and overlap was made much easier.

The first experiments used Fresnel rhomb prisms to produce a circularly polarized pump field, and cancellation of the benzyl alcohol RIKE signal was observed. Later, in order to simplify the experiment as much as possible, the rhombs were removed and a plane polarized pump field

used. First, the polarization of the two pump fields were made parallel, and addition was observed. That is, if the signal was 50 units in each cell separately, when both cells were unblocked, a signal of 100 relative units was recorded. Next, the polarization of the two fields was made orthogonal, the signal maximized in each cell separately, and then both cells were unblocked to give the cancelled signal. Figure 29 shows the best cancellation trial. In Fig. 29, the pump laser was positioned 2960 cm^{-1} from the 488 nm probe, and the total signal is, therefore, composed of a contribution from the NKE of CH_3CN, and the RIKE of benzyl alcohol. With the pump beams orthogonally polarized and balanced in power, the signals due to the two detection cells are 52 and 51 units, respectively. When the pump beam was introduced into both cells simultaneously, the signal was reduced to 11 units. Therefore, cancellation of approximately 80% of the signal was observed.

The limitation to the double beam technique is due to the inhomogeneous nature of the pump beam, and the unequal degree of overlap in the two cells. Future work should involve eliminating these two problems to expand the utility of the double beam null. Even with its present capability, the double beam null may have use in minimizing spectral overlap between closely spaced solvent and analyte Raman transitions. For even severely overlapping peaks, an 80% reduction in the interferent contribution should allow peak location and half-width information to be obtained.

Figure 29. Cancellation results for the double beam null. Cancelled signal measured with both cells unblocked

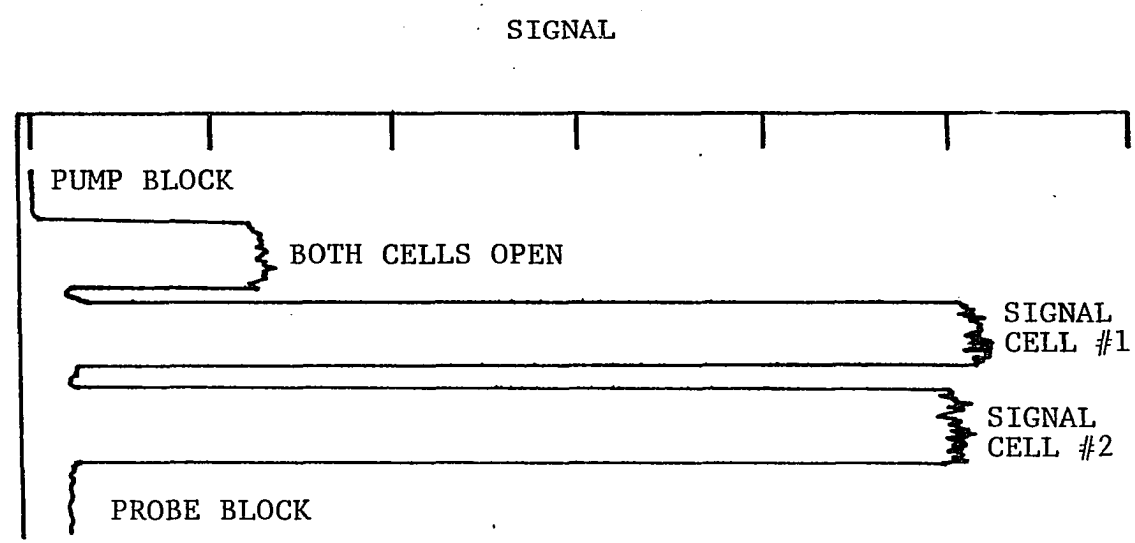
SIGNAL
PUMP BLOCK
BOTH CELLS OPEN
SIGNAL
CELL #1
SIGNAL
CELL #2
PROBE BLOCK

Conclusions

In summary, the RIKE has been shown to be a useful nonlinear Raman technique with analytical capabilities as good as most existing Raman techniques. The advantages common to other nonlinear Raman methods are maintained in the RIKE, but with a simpler experimental arrangement than, for example, CARS. In this chapter, the experimental parameters affecting the RIKE were experimentally verified, and a theoretical investigation of the S/N capabilities of this technique isolated those variables which limit it now. Solutions to these limitations were proposed. In addition, a unique optical null has been demonstrated for the suppression of nonresonant background or solvent RIKE signals. The utility of this double beam optical null will have to await the development of high power pulsed lasers with more homogeneous beam profiles.

REFERENCES

1. Hecht, E.; Zajac, A. "Optics", Addison-Wesley Publishing Company: Reading, MA, 1974; Chapter 1.

2. Brown, J. C.; Duncanson, J. A., Jr.; Small, G. J. Anal. Chem. 1980, 52, 1711.

3. Maple, J. R.; Wehry, E. L.; Mamantov, G. Anal. Chem. 1980, 52, 920.

4. Yang, Y.; D'Silva, A. P.; Fassel, V. A. Anal. Chem. 1981, 53, 894.

5. Young, M. "Optics and Lasers", Springer-Verlag: Berlin, 1977; Chapter 8.

6. Hecht, E.; Zajac, A. "Optics", Addison-Wesley Publishing Company: Reading, MA, 1974; Chapter 8.

7. Young, M. "Optics and Lasers", Springer-Verlag: Berlin, 1977; Chapter 4.

8. Fowles, G. R. "Introduction to Modern Optics", Holt, Rinehart and Winston, Inc.: New York, 1968; Chapter 2.

9. Born, W.; Wolf, E. "Principles of Optics", Pergamon Press: New York, 1959; Chapter 14.

10. Clark, D.; Grainger, J. F. "Polarized Light and Optical Measurements", Pergamon Press: Oxford, 1971; Chapter 3.

11. Tinoco, I., Jr.; Bustamente, C.; Maestre, M. F. NATO Adv. Study Inst. Ser., Ser. C 1979, 48, 57.

12. Abu-Shumays, A.; Duffield, J. J. Anal. Chem. 1966, 38, 29A.

13. Maestre, M. F.; Katz, J. E. Biopolymers 1982, 21, 1899.

14. Madison, V.; Schellman, J. Biopolymers 1972, 11, 1041.

15. Woody, R. W. Biopolymers 1969, 8, 669.

16. Woody, R. W. "Peptides, Polypeptides and Proteins", Blout, E. R.; Bovey, F. A.; Goodman, M.; Lotan, N., Eds.; Wiley-Interscience: New York, 1974; p. 338.

17. Johnson, W. C.; Tinoco, I., Jr. Biopolymers 1969, 8, 715.

18. Atkinson, W. M.; Han, S. M.; Purdie, N. Anal. Chem. 1984, 56, 1947.

19. Bowen, J. M.; Purdie, N. Anal. Chem. 1981, 53, 2237.

20. Bowen, J. M.; Crone, T. A.; Kennedy, R. K.; Purdie, N. Anal. Chem. 1982, 54, 66.

21. Bowen, J. M.; Purdie, N. Anal. Chem. 1980, 52, 573.

22. Bowen, J. M.; Crone, T. A.; Hermann, A. O.; Purdie, N. Anal. Chem. 1980, 52, 2436.

23. Crone, T. A.; Purdie, N. Anal. Chem. 1981, 53, 17.

24. Drake, A. F.; Gould, J. M.; Mason, S. F. J. Chromatogr. 1980, 202, 239.

25. Westwood, S. A.; Games, D. E.; Sheen, L. J. Chromatogr. 1981, 204, 103.

26. Gaffney, J. S.; Premuzic, E. T.; Orlando, T.; Ellis, S.; Snyder, P. J. Chromatogr. 1983, 262, 321.

27. McClain, W. M. J. Chem. Phys. 1973, 58, 324.

28. Wirth, M. J.; Kaskelo, A.; Sanders, M. J. Appl. Spectrosc. 1981, 35, 14.

29. Liao, P. F.; Bjorklund, G. C. Phys. Rev. Lett. 1976, 36, 584.

30. Wieman, C.; Hansch, T. W. Phys. Rev. Lett. 1976, 36, 1170.

31. Tong, W. G.; Yeung, E. S. Anal. Chem. 1985, 57, 70.

32. Teets, R.; Feinberg, R.; Hansch, T. W.; Schawlow, A. L. Phys. Rev. Lett. 1976, 37, 683.

33. Shalagin, A. M. Sov. Phys. JETP 1977, 46, 50.

34. Song, J. J.; Lee, J. H.; Levenson, M. D. Phys. Rev. A 1978, 17. 1439.

35. Levenson, M. D.; Eesley, G. L. Appl. Phys. 1979, 19, 1.

36. Ovdar, J.; Minot, C.; Garetz, B. A. J. Chem. Phys. 1982, 76, 2227.

37. Werncke, W.; Klein, J.; Lav, A.; Lenz, K.; Hunsalz, G. Opt. Comm. 1974, 11, 159.

38. Jorgenson, J. W.; Smith, S. L.; Novotny, M. J. Chromatogr. 1977, 142, 233.

39. Yeung, E. S. In "Lasers in Chemical Analysis", Hieftje, G. M.; Travis, J. C.; Lytle, F. E., Eds.; The Humana Press: Clifton, NJ, 1981; Chapter 14.

40. Grasselli, J. G.; Snavely, M. K.; Bulkin, B. J. "Chemical Applications of Raman Spectroscopy", John Wiley & Sons: New York, 1981; Chapter 4.

41. Koenig, J. L. Appl. Spectrosc. Rev. 1971, 4, 223.

42. Koenig, J. L.; Angood, A. C. J. Polym. Sci., Polym. Phys. Ed. 1970, 8, 1787.

43. Purvis, J.; Bower, D. I. Polymer 1974, 15, 645.

44. Purvis, J.; Bower, D. I. J. Polym. Sci., Polym. Sci. Ed. 1976, 14, 1461.

45. Laitirew, H.; Ewing, G. "A History of Analytical Chemistry", Maple Press: York, PA, 1977; p. 165.

46. Morrison, R. T.; Boyd, R. N. "Organic Chemistry", 3rd Ed.; Allyn and Bacon: Boston, 1973; p. 120.

47. O'Loane, J. K. Chem. Rev. 1980, 80, 41.

48. Buckingham, A. D.; Stiles, P. J. Acct. Chem. Res. 1974, 7, 258.

49. Rosenfeld, L. Z. Phys. 1928, 52, 161.

50. Kirkwood, J. G. J. Chem. Phys. 1937, 5, 479; 1939, 7, 139.

51. Condon, E. V.; Altar, W.; Eyring, H. J. Chem. Phys. 1937, 5, 753.

52. Mason, S. F. Contemp. Phys. 1968, 9, 239.

53. Caldwell, D. J.; Eyring, H. "The Theory of Optical Activity", Wiley-Interscience: New York, 1971.

54. Olsen, E. D. "Modern Optical Methods of Analysis", McGraw-Hill: New York, 1975; Chapter 10.

55. Heller, W.; Curme, H. G. In "Physical Methods of Chemistry", Weissberer, A.; Rossiter, B. W., Eds.; Wiley-Interscience: New York, 1972, Vol. 1, Part III.

56. Rossi, P. Analyst (London) 1975, 100, 25.

57. Collingwood, C.; Day, P.; Denning, R. G.; Quested, P. N.; Snellgrove, R. J. Phys. E: Sci. Instrum. 1974, 7, 991.

58. Willard, H. H.; Merritt, L. L., Jr.; Dean, J. A.; Settle, F. A., Jr. "Instrumental Methods of Analysis", Wadsworth Publishing Company: Belmont, CA, 1981; Chapter 14.

59. Boehme, W.; Wagner, G.; Oehme, V. Anal. Chem. 1982, 54, 709.

60. Boehme, W. Chromatogr. Newsl. 1980, 8, 38.

61. O'Shea, D. C.; Callen, W. R.; Rhodes, W. T. "An Introduction to Lasers and Their Applications", Addison-Wesley Publishing Company: Reading, MA, 1977, p. 2.

62. Cummings, A. L.; Layer, H. P.; Hocken, R. J. In "Lasers in Chemical Analysis", Hieftje, G. M.; Travis, J. C.; Lytle, F. E., Eds.; Humana Press: Clifton, NJ, 1981; Chapter 15.

63. Yeung, E. S. "Optical Detectors for Microcolumn Liquid Chromatography", Journal of Chromatography Library; Novotny, M. V.; Ishii, D., Eds.; Elsevier: New York, 1985; Vol. 50, p. 135.

64. Yeung, E. S. "Laser Spectroscopic Methods for Detection in Liquid Chromatography", Advances in Chromatography, Volume 23, Giddings, J. C.; Grushka, E.; Cases, J.; Brown, P. R., Eds.; Marcel Dekker: New York, 1984; Chapter 1.

65. Yariv, A. "Quantum Electronics", John Wiley and Sons: New York, 1975; Chapter 6.

66. Moeller, C. E.; Grieser, D. R. Appl. Opt. 1969, 8, 206.

67. Yeung, E. S.; Steenhoek, L. E.; Woodruff, S. D.; Kuo, J. C. Anal. Chem. 1980, 52, 1399.

68. Kuo, J. C.; Yeung, E. S. J. Chromatogr. 1981, 223, 321.

69. Kuo, J. C.; Yeung, E. S. J. Chromatogr. 1982, 229, 293.

70. Kuo, J. C.; Yeung, E. S. J. Chromatogr. 1982, 253, 199.

71. Kuo, J. C. Ph.D. Dissertation, Iowa State University, Ames, IA, 1982.

72. "Prism Polarizers", Karl Lambrecht Corp., Chicago, 1980.

73. Malmstadt, H. V.; Enke, C. G.; Crouch, S. R. "Electronics and Instrumentation for Scientists", Benjamin/Cummings: Reading, MA, 1981; Chapter 14.

74. Bobbitt, D. R. Ames Laboratory Research Report, Iowa State University, Ames, IA, Sept. 1984.

75. Yeung, E. S. J. Opt. Soc. Am. 1985, submitted.

76. Synovec, R. E.; Yeung, E. S. Anal. Chem, 1985, submitted.

77. Given, P. H., Workshop Report on Basic Research in Organic Geochemistry Applied to National Needs, Dec. 1980, p. B-45 to B-70 (CONF-801249, UC-11).

78. Davis, A.; Spackman, W.; Given, P. H. Energy Sources 1976, 3, 55.

79. Neavel, R. C.; Hippo, E. J.; Smith, S. E.; Miller, R. E. Am. Chem. Soc. Div. Fuel Chem. Preprints 1980, 25, 246.

80. Neavel, R. C. In "Coal Structure", Adv. Chem. Ser. 1981, No. 192; Chapter 1.

81. Mackenzie, A. S.; Brassell, S. C.; Eglinton, G.; Maxwell, J. R. Science 1982, 217, 491.

82. Eglinto, G.; Calvin, M. Sci. Am. 1967, 216, 32.

83. Patience, R. L.; Rowland, S. J.; Maxwell, J. R. Geochim. et Cosmochim. Acta 1978, 42, 1871.

84. Tissot, B. P.; Welte, D. H. "Petroleum Formation and Occurrence", Springer-Verlag: Berlin, 1978.

85. White, C. M.; Shultz, J. L.; Sharkey, A. G., Jr. Nature 1977, 620.

86. Brooks, J. D.; Gould, K.; Smith, J. W. Nature 1969, 222, 257.

87. Bartle, K. D.; Jones, D. W.; Pakdel, H.; Snape, C. E.; Calimli, A.; Olcay, A.; Tugrul, T. Nature 1979, 277, 284.

88. Mukhopadhyay, D. K.; Hagemann, H. W.; Hollerbach, A.; Welte, D. H. Energy Sources 1979, 4, 313.

89. Jones, D. W.; Pakdel, H.; Bartle, K. D. Fuel 1982, 61, 44.

90. Baset, Z. H.; Pancirov, R. J.; Ashe, T. R. In "Advances in Organic Geochemistry 1979", Douglas, A. G.; Maxwell, J. R., Eds.; Pergamon: New York, 1980; p. 619.

91. Gulyaeva, N. D.; Aref'ez, O. A.; Patrov, A. A. Khim. Tverd. Topl. 1982, 16, 30.

92. Hersch, R. E.; Fenske, M. R.; Matsun, H. J.; Koch, E. F.; Booser, E. R.; Braun, W. G. Anal. Chem. 1948, 20, 434.

93. Rosenfeld, N. D. J. Am. Oil Chem. Soc. 1967, 44, 703.

94. Lawlor, D. L. In "Oil Sands and Oil Shale", Strauz, O. P., Ed.; Verlag Chemie: New York, 1978, p. 267.

95. Zahn, C.; Langer, S. H.; Blaustein, B. D.; Wender, I. Nature 1963, 200, 53.

96. Zahn, C.; Blaustein, B. D. Pentages, G.; Wender, I. U.S. Bureau of Mines Report of Investigation 6525 1964.

97. McLean, J.; Rettie, G. H.; Spring, F. S. Chem. Ind. (London) 1958, 1515.

98. Ikan, R.; McLean, J. J. Chem. Soc. 1960, 893.

99. Ikan, R.; Kashman, J. Israel J. Chem. 1963, 4, 502.

100. Pictet, A.; Kaiser, O. Ann. Chim. (Paris) 1918, 10, 317.

101. Fischer, F.; Glund, W. Ber. 1917, 50, 111.

102. Speight, J. G. "The Chemistry and Technology of Coal", Marcel Dekker: New York, 1983.

103. Moore, E. S. "Coal", John Wiley and Sons: New York, 1922.

104. Johnson, C. R.; Asher, S. A. Anal. Chem. 1984, 56, 2258.

105. Fysh, S. A.; Swinkels, D. A.; Fredericks, P. M. Appl. Spectrosc. 1985, 39, 354.

106. Ciupek, J. D.; Zaket, D.; Cooks, R. G.; Wood, K. V. Anal. Chem. 1982, 54, 2215.

107. Selucky, M. L. Anal. Chem. 1983, 55, 141.

108. "Analytical Methods for Coal and Coal Products", Karr, C. Jr., Ed., Academic Press: New York, Vol. 1, 2, 1978; Vol. 3, 1979.

109. Whitehorst, D. D.; Butrill, S. E., Jr.; Derbyshire, F. J.; Farcasiu, M.; Odoerfere, G. A.; Rudnick, L. R. Fuel 1982, 61. 994.

110. Bartle, K. D.; Zander, M. Erdol Kohle, Erdgas, Petrochemie 1983, 36, 15.

111. "Analytical Methods for Coals, Cokes and Carbons", Society of Chemical Industry Conference-London, Fuel 1983, 62.

112. Alexander, G.; Hazai, I. J. Chromatogr. 1981, 217, 19.

113. Marsh, M. K.; Smith, C. A.; Snape, C. E.; Stokes, B. J. J. Chromatogr. 1984, 283, 173.

114. Burchill, P.; Herod, A. A.; Mahon, J. P.; Pritchard, E. J. Chromatogr. 1983, 281, 109.

115. Brown, R. S.; Hausler, D. W.; Taylor, L. T.; Carter, R. C. Anal. Chem. 1981, 53, 197.

116. Bobbitt, D. R.; Reitsma, B. H.; Rougvie, A.; Yeung, E. S.; Aida, T.; Chen, Y.; Smith, B. F.; Squires, T. G.; Venier, C. G. Fuel 1985, 64, 114.

117. Yeung, E. S.; Rougvie, A.; Bobbitt, D. R.; Venier, C. G.; Squires, T. G.; Smith, B. F. Proc. Int. Conf. Coal Science 1983, Pittsburgh, PA, p. 635.

118. Schwager, I.; Yen, T. F. Fuel 1978, 57, 100.

119. Synovec, R. E.; Yeung, E. S. Anal. Chem. 1983, 55, 1599.

120. Synovec, R. E.; Yeung, E. S. J. Chromatogr. 1984, 283, 183.

121. Eliel, E. L. "Stereochemistry of Carbon Compounds", McGraw-Hill: New York, 1962; Chapter 14.

122. Kates, M.; Joo, C. N.; Palameta, B.; Shier, T. Biochem. 1967, 6, 3329.

123. Novotny, M. Anal. Chem. 1981, 53, 1294A.

124. Tsuda, T.; Nakagawa, G. J. Chromatogr. 1983, 268, 369.

125. Takeuchi, T.; Ishii, D.; Mori, S. J. Chromatogr. 1983, 257, 327.

126. Scott, R. P. W.; Kucera, P. J. Chromatogr. 1981, 169, 327.

127. Kucera, P.; Manivs, G. J. Chromatogr. 1981, 216, 9.

128. Menet, H. G.; Gareil, P. C.; Rosset, R. H. Anal. Chem. 1984, 56, 1770.

129. Dovichi, N. J.; Harris, J. M. Anal. Chem. 1981, 53, 689.

130. Pang, T. J.; Morris, M. D. Appl. Spectrosc. 1985, 39, 90.

131. Yang, Y. Anal. Chem. 1984, 56, 2336.

132. Yeung, E. S.; Sepaniak, M. J. Anal. Chem. 1980, 52, 1465A.

133. Diebold, G. J.; Zare, R. N. Science 1977, 196, 1439.

134. Folestad, S.; Johnson, L.; Josefsson, B.; Galle, B. Anal. Chem. 1982, 54, 925.

135. Wilson, S. A.; Yeung, E. S. Anal. Chem. 1985, submitted.

136. Cox, G. B.; O'Neill, I. K. UV Spectrom. Group Bull. 1977, 5 (Suppl.), p. 64.

137. Reinecke, W.; Aden, E.; Hajdu, S. Exp. Tech. Phys. 1977, 25, 307.

138. Baumann, W. Fresenius Z. Anal. Chem. 1977, 284, 31.

139. Boehme, W. Chromatogr. Newsl. 1980, 8, 38.

140. Mak, A. A.; Orlov, O. A.; Ustyugov, V. I. Kvantovaya Elektron. 1982, 9, 2412.

141. Voitovich, A. P.; Sardyko, V. I. Opt. Spectrosc. 1982, 53, 644.

142. Zapapsskii, V. S. Opt. Spektrosk. 1982, 52, 1105.

143. Elliott, C. J.; Small, J. G. In "Physics of Ring Gyros", 1984, SPIE Vol. 487, p. 128.

144. Small, H.; Miller, T. E. Anal. Chem. 1982, 54, 462.

145. Wilson, S. A.; Yeung, E. S.; Bobbitt, D. R. Anal. Chem. 1984, 56, 1457.

146. Bobbitt, D. R.; Yeung, E. S. Anal. Chem. 1984, 56, 1577.

147. Wilson, S. A.; Yeung, E. S. Anal. Chim. Acta 1984, 157, 53.

148. Synovec, R. E.; Yeung, E. S. Anal. Chem. 1984, 56, 1452.

149. Dobashi, A.; Hara, S. Anal. Chem. 1983, 55, 1805.

150. Knecht, L. A.; Guthrie, E. J.; Jorgenson, J. W. Anal. Chem. 1984, 56, 479.

151. Tijssen, R.; Bleumer, J. P. A.; Smit, A. L. C.; Van Kreveld, M. E. J. Chromatogr. 1981, 218, 137.

152. Folestad, S.; Johnson, L.; Josefsson, B.; Galle, B. Anal. Chem. 1982, 54, 925.

153. Sepaniak, M. J.; Vargo, J. D.; Kettler, C. N. Maskarines, M. P. Anal. Chem. 1984, 56, 1252.

154. Boccara, A. C.; Fournier, D.; Jackson, W.; Amer, N. M. Opt. Lett. 1980, 5, 377.

155. Woodruff, S. D.; Yeung, E. S. Anal. Chem. 1982, 54, 1174.

156. Harris, J. M.; Dovichi, N. J. Anal. Chem. 1980, 52, 695A.

157. Buffet, C. E.; Morris, M. D. Anal. Chem. 1983, 55, 376.

158. Mori, D.; Imasaka, T.; Ishibashi, N. Anal. Chem. 1982, 54, 2034.

159. Hirschfelder, J.O.; Curtiss, C. F.; Bird, R. B. "Molecular Theory of Gases and Liquids", Mayer, M. G., Ed.; John Wiley and Sons: New York, 1954, p. 282.

160. Dovichi, N. J.; Haris, J. M. Anal. Chem. 1981, 53, 106.

161. Guthrie, E. J.; Jorgenson, J. W.; Diuzneski, P. R. J. Chromatogr. Sci. 1984, 22, 171.

162. Raman, C. V.; Krishnan, K. S. Nature 1928, 121, 501.

163. Raman, C. V. Nature 1928, 121, 619.

164. Carey, P. Tr. Anal. Chem. 1983, 2, 175.

165. Sloane, H. Appl. Spectrosc. 1971, 25, 430.

166. Angeloni, L.; Smulevich, G.; Marzocchi, M. P. Spectrochim. Acta 1982, 38A, 213.

167. Smulevich, G.; Angeloni, L.; Marzocchi, M. P. Spectrochim. Acta 1982, 28A, 219.

168. Campion, A.; Terner, J.; El-Sayed, M. A. Nature 1977, 265, 659.

169. Carey, P. R. "Biochemical Applications of Raman and Resonance Raman Spectroscopies", Academic Press: New York, 1982.

170. Jeanmaire, D. J.; Van Duyne, R. P. J. Electroanal. Chem. 1977, 84, 1.

171. Vo-Dinh, T.; Hiromoto, M. Y. K.; Begun, G. M.; Moody, R. L. Anal. Chem. 1984, 56, 1667.

172. Van Duyne, R. P.; Haushalter, J. P. J. Phys. Chem. 1983, 87, 2999.

173. Gardiner, D. J. Anal. Chem. 1980, 52, 96R.

174. Arguello, C. A.; Mendes, G. F.; Leite, R. C. C. Appl. Optics 1974, 13, 1731.

175. Galeener, F. L. Chem. Phys. Lett. 1977, 48, 7.

176. Van Duyne, R. P.; Jeanmaire, D. L.; Shriver, D. F. Anal. Chem. 1974, 46, 213.

177. Kubota, K. Spectrochim. Acta 1982, 38A, 617.

178. Schneider, F. W. In "Non-Linear Raman Spectroscopy and its Chemical Applications", Kiefer, W.; Long, D. A., Eds.; D. Reidel: Holland, 1982, p. 445.

179. Jones, W. J.; Stoicheff, B. P. Phys. Rev. Lett. 1964, 13, 657.

180. Yeung, E. S. J. Molec. Spectrosc. 1974, 53, 379.

181. Hughes, L. J.; Steenhoek, L. E.; Yeung, E. S. Chem. Phys. Lett. 1978, 58, 413.

182. Haushalter, J. P.; Ritz, G. P.; Wallan, D. J.; Dien, K.; Morris, M. M. Appl. Spectrosc. 1980, 34, 144.

183. Chen, T. I.; Morris, M. M. J. Phys. Chem. 1983, 87, 2314.

184. Heiman, D.; Hellwarth, R. W.; Levenson, M. D.; Martin, G. Phys. Rev. Lett. 1976, 36, 189.

185. Mayer, G.; Gires, F. Comp. Rend. 1964, 25, 2039.

186. Yeung, E. S. "Raman and Related Methods in Chemical Analysis" In "Analytical Applications of Lasers", Piepmeier, E. H., Ed.; Wiley: New York, 1985, in press.

187. Schrotter, H. W. In "Non-Linear Raman Spectroscopy and its Chemical Applications", Kiefer, W.; Long, D. A., Eds.; D. Reidel: Holland, 1982, p. 603.

188. Levenson, M. D.; Song, J. J. J. Opt. Soc. Am. 1976, 66, 641.

189. Song, J. J.; Levenson, M. D. J. Appl. Phys. 1977, 48, 3496.

190. Levenson, M. D. In "Chemical Applications of Nonlinear Raman Spectroscopy", Harvey, A. B., Ed.; Academic Press: New York, 1981, p. 227.

191. Eesley, G. L.; Levenson, M. D.; Tolles, W. M. IEEE J. Quant. Electron. 1978, 14, 45.

192. Owyoung, A. IEEE J. Quant. Electron. 1978, 14, 192.

193. Owyoung, A. Opt. Lett. 1978, 2, 91.

194. Levenson, M. D.; Eesley, G. L. Appl. Phys. 1979, 19, 1.

195. Hughes, L. J. Ph.D. Dissertation, Iowa State University, Ames, IA, 1980.

196. Eesley, G. L. "Coherent Raman Spectroscopy", Pergamon Press: New York, 1980, p. 45.

197. Omenetto, N.; Winefordner, J. D. CRC Crit. Rev. Anal. Chem. 1981, 13, p. 59.

198. Levenson, M. D.; Song, J. J. In "Coherent Nonlinear Optics", Feld, M. S.; Letokhov, V. S., Eds.; Springer-Verlag: Berlin, 1980, p. 293.

ACKNOWLEDGEMENTS

One does not reach this point in one's graduate career without being indebted to many people for their help and encouragement. As such, I would like to use this opportunity to thank these people for their contributions.

To Professor Edward S. Yeung, I am sincerely thankful to have been a member of his research group. My development as a scientific researcher is due, in entirety, to the stimulating atmosphere provided in Professor Yeung's group. I hope that I will be able to treat my graduate students with the same compassion, enthusiasm and fairness shown to me during my tenure here. My family and I are also indebted to the Yeung family for their kind hospitality which made our sojourn in Ames so memorable. I would also like to thank my committee members, Dr. Dennis Johnson, Dr. Rodney Walters, Dr. Walter Struve and Dr. Donald Beitz for their time, advice, and many helpful discussions.

I am grateful to my office mate, Steve, for teaching me that there is room for each of us to be good, to Kristy and Rob, for good times and friendship, and to Bernie, Carmen, Barb, and all my other friends, past and present, who took this trek with me. I would like to thank four people for their help with this thesis work: Dr. Clifford Venier for his patient explanations and collaboration with the coal investigations, Gary Wells for advice on microcell construction techniques, Dr. Steve Woodruff for technical advice, and Lesley Swope for the masterful typing of this manuscript.

My heartfelt thanks go to my second family, Mom, Dad and Pam for always being there to help. I am thankful to my brother, Bill, and sister, Diane, for their support, and to my parents, Marion and Bill, for their love and encouragement during the difficult times. For my father, who taught me never to give up, I would like to dedicate this thesis in the name of his late brother, my namesake, Bobby.

Finally, to my wife Susan, and buddy, Justin, I am thankful for your patience. Your love, encouragement and understanding was so much more than I deserved.